PROPERTIES OF SECONDARY ORGANIC AEROSOL IN THE AMBIENT ATMOSPHERE: SOURCES, FORMATION, AND PARTITIONING

A Dissertation
Presented to
The Academic Faculty

By

Christopher J. Hennigan

In Partial Fulfillment
Of the Requirements for the Degree
Doctor of Philosophy
In the School of Civil and Environmental Engineering

Georgia Institute of Technology

December, 2008

PROPERTIES OF SECONDARY ORGANIC AEROSOL IN THE AMBIENT ATMOSPHERE: SOURCES, FORMATION, AND PARTITIONING

Approved by:

Dr. Rodney J. Weber
School of Earth and Atmospheric Sciences
Georgia Institute of Technology

Dr. Michael H. Bergin
School of Civil and Environmental Engineering and School of Earth and Atmospheric Sciences
Georgia Institute of Technology

Dr. James A. Mulholland
School of Civil and Environmental Engineering
Georgia Institute of Technology

Dr. Athanasios Nenes
School of Earth and Atmospheric Sciences and School of Chemical And Biomolecular Engineering
Georgia Institute of Technology

Dr. Armistead G. Russell
School of Civil and Environmental Engineering
Georgia Institute of Technology

Date Approved:

ACKNOWLEDGEMENTS

I would like to start by thanking my advisor, Dr. Rodney Weber, for helping to guide and shape my graduate experience. I am truly grateful for the opportunity to have worked with Rodney. I have learned so much in working with him, and my development as a scientist is due in large part to his influence. I am also thankful for his willingness to conduct research that was not funded and for his belief in this work. It was this effort which led to a large portion of my dissertation.

I would like to acknowledge my committee, Drs. Michael Bergin, James Mulholland, Athanasios Nenes, and Armistead Russell, for their scientific insight and for their career advice. I have been fortunate to work individually with three of the committee members, whose expertise has helped me tremendously. Athanasios Nenes has provided help and advice with the ISORROPIA model and with the interpretation of the Mexico City data set. Armistead Russell has provided modeling help along with unique perspective and insight into many of our analyses. Michael Bergin helped to obtain a Mist Chamber, and has been an integral part of its deployment and in subsequent analyses of MC data.

Several people contributed additional assistance with the Mexico City study. Dr. Greg Huey provided data (O_3, OH, RO_2, and NO) and invaluable manuscript comments, Dr. Anne Case Hanks provided nitric acid predictions, and Dr. Barry Lefer provided photolysis rate data. Also, Janet Aldridge, from the Georgia Department of Natural Resources, has been very helpful in retrieving NO_x, O_3, and PM data from the Atlanta monitoring network.

Dr. Amy Sullivan provided enormous help with analytical techniques, and made the $WSOC_p$ and nitrate measurements in Mexico City. Dr. Rick Peltier provided computer/tech assistance, and was a mentor and a friend. I would also like to acknowledge current Weber group members Arsineh Hecobian, Dr. Neeraj Rastogi, Xiaolu Zhang, and Michelle Oakes.

Finally, my family has provided me with unending support that has made this all possible. In particular, my wife, Audra, has been wonderful, possessing an abundance of patience throughout this journey. I am grateful for her sacrifice and for her encouragement. Without her, this work would not have been possible.

TABLE OF CONTENTS

LIST OF TABLES

LIST OF FIGURES

LIST OF ABBREVIATIONS

BB: Biomass Burning

BL: Boundary Layer

C-130: National Science Foundation C-130 Research Aircraft

CI: Confidence Interval

Cl^-: Chloride ion

Ca^{2+}: Calcium ion

CIMS: Chemical Ionization Mass Spectrometer

CO: Carbon monoxide

CST: Central Standard Time

EC: Elemental Carbon

EPA: Environmental Protection Agency

ES&T: Environmental Science & Technology Building

FID: Flame Ionization Detection

HCl: Hydrochloric acid

HNO_3: Nitric acid

IC: Ion Chromatograph

J: Photolysis rate

k: Temperature-dependent kinetic rate constant

LiF: Lithium Fluoride

LOD: Limit Of Detection

MC: Mist Chamber

MCMA: Mexico City Metropolitan Area

Mg^{2+}: Magnesium ion

MILAGRO: Megacity Initiative: Local and Global Research Objectives

MW: Molecular Weight

m/z: Mass-to-charge ratio

Na^{+}: Sodium ion

Na_2CO_3: Sodium carbonate

$NaHCO_3$: Sodium bicarbonate

NH_3: Ammonia

NH_4^{+}: Ammonium ion

NH_4NO_3: Ammonium nitrate

NO: Nitric Oxide

NO_2: Nitrogen Dioxide

NO_2^{-}: Nitrite ion

NO_3: Nitrate Radical

NO_3^{-}: Nitrate ion

NO_x: Nitric Oxide + Nitrogen Dioxide

O_3: Ozone

OC: Organic Carbon

OH: Hydroxyl Radical

OOA: Oxygenated Organic Aerosol

PAH: Polycyclic Aromatic Hydrocarbon

PILS: Particle-into-Liquid Sampler

PM: Particulate Matter

PM_{10}: Particulate matter with aerodynamic diameter less than 10 μm

$PM_{2.5}$: Particulate matter with aerodynamic diameter less than 2.5 μm

POA: Primary Organic Aerosol

RH: Relative Humidity

RO_2: Peroxy radical

SO_2: Sulfur dioxide

SO_4^{2-}: Sulfate ion

SOA: Secondary Organic Aerosol

SVOC: Semi-Volatile Organic Compound

T: Temperature

TOC: Total Organic Carbon

TOT: Thermal Optical Transmittance

UTC: Coordinated Universal Time

UV: Ultraviolet light

VOC: Volatile Organic Compound

WSOC: Water Soluble Organic Carbon

$WSOC_g$: Gas-phase Water-Soluble Organic Carbon

$WSOC_p$: Particulate Water-Soluble Organic Carbon

SUMMARY

This thesis characterizes several properties of ambient secondary organic aerosol (SOA), an important and abundant component of particulate matter. The research utilized the fraction of particulate organic carbon that was soluble in water ($WSOC_p$) to approximate SOA concentrations in two largely different urban environments, Mexico City and Atlanta. Among the properties investigated were SOA sources, formation, volatility, and gas/particle partitioning. The findings presented in this thesis are significant because they represent results from ambient measurements, which are relatively scarce, and because they report on properties of SOA that, until now, were highly uncertain.

Measurements of atmospheric gases and fine particle chemistry were made in the Mexico City Metropolitan Area (MCMA) at a site ~ 30 km down wind of the city center. Ammonium nitrate (NH_4NO_3) dominated the inorganic aerosol fraction and showed a distinct diurnal signature characterized by rapid morning production and a rapid mid-day concentration decrease. Between the hours of 08:00-12:45, $WSOC_p$ concentrations increased and decreased in a manner consistent with that of NO_3^-, and the two were highly correlated ($R^2 = 0.88$) during this time. A box model was used to analyze these behaviors and showed that, for both NO_3^- and $WSOC_p$, the concentration increase was caused primarily (~75-85%) by secondary formation, with a smaller contribution (~15-25%) from the entrainment of air from the free troposphere. For NO_3^-, a majority (~60%) of the midday concentration decrease was caused by dilution from boundary layer expansion, though a significant fraction (~40%) of the NO_3^- loss was due to particle

evaporation. The $WSOC_p$ concentration decrease was due largely to dilution (~75%), but volatilization did have a meaningful impact (~25%) on the decrease, as well. The results provide an estimate of ambient SOA evaporation losses and suggest that a significant fraction (~35%) of the fresh MCMA secondary organic aerosol measured at the surface volatilized.

Measurements of $WSOC_p$ and gas-phase water-soluble organic carbon ($WSOC_g$) were made in Atlanta for an entire summer. The $WSOC_g$ measurement was the first in Atlanta, and the measurement showed unique properties of $WSOC_g$, and also similarities with $WSOC_p$. Concentrations of $WSOC_g$ (mean $WSOC_g$ concentration = 13.7 μg C m^{-3}) were higher throughout the summer than those of $WSOC_p$ (mean $WSOC_p$ concentration = 3.3 μg C m^{-3}). Both showed mid-day concentration peaks in their diurnal averages that suggested photochemical formation, however the diurnal profile of $WSOC_g$ also exhibited a nighttime peak, attributed to nighttime biogenic VOC emissions, that was not present for $WSOC_p$. Gas phase formic and acetic acid together were moderately correlated with $WSOC_g$, and together accounted for approximately 20% of $WSOC_g$ on a carbon mass basis. $WSOC_g$ concentrations in biomass burning (BB) events were consistent with the highest $WSOC_g$ concentrations observed throughout the remainder of the summer, but concentrations of $WSOC_p$ in the same BB events were higher by a factor of 2-5 than those observed throughout the remainder of the summer. Overall, the fraction of particle-phase WSOC was significantly higher in the BB events than it was in non-BB airmasses, which supports previous findings of high BB emissions of $WSOC_p$.

Fourteen separate events were observed throughout the summer in which $WSOC_p$ and water vapor concentrations were highly correlated (average $WSOC_p$-water vapor r =

0.92), however, for the entire summer, no well-defined relationship existed between the two. The correlation events, which lasted an average of 19 hours, were characterized by a wide range of $WSOC_p$ and water vapor concentrations. Several hypotheses for the correlation are explored, including heterogeneous liquid phase SOA formation and the co-emission of biogenic VOCs and water vapor. The data provide supporting evidence for contributions from both, and suggest the possibility of a synergistic effect between the co-emission of water vapor and VOCs from biogenic sources on SOA formation. Median $WSOC_p$ concentrations were also correlated with elemental carbon (EC), though this correlation extended over the entire summer. Despite the emission of water vapor from anthropogenic mobile sources and the $WSOC_p$-EC correlation, mobile sources were not considered a potential cause for the $WSOC_p$-water vapor correlations due to their low contribution to the water vapor budget. Meteorology could perhaps have influenced the $WSOC_p$-EC correlation, but other factors are implicated as well. Overall, the results suggest that the temperature-dependent co-emission of water vapor and SOA precursor-VOCs by vegetation may be an important process contributing to SOA in some environments.

Finally, the gas/particle partitioning of WSOC in Atlanta was investigated. The parameter, F_p, represented the fraction of total WSOC ($WSOC_p$ + $WSOC_g$) in the particle phase and was used extensively in the partitioning analyses. In a somewhat surprising result, WSOC partitioning did not show a dependence upon temperature, though the dynamic temperature range encountered throughout the summer was significant (range > 20 °C). This was likely due to other factors, such as increased photochemistry and the temperature-dependent emission of biogenic VOCs, that confounded a true determination

of the temperature effect on WSOC partitioning. There was no observed relationship between F_p and the total organic carbon (OC) aerosol mass, though one was observed between F_p and $WSOC_p$ concentrations, suggesting that chemical similarities between the absorbing organic phase and partitioning compounds are important. During the summer in Atlanta, WSOC gas/particle partitioning showed a strong RH dependence that was attributed to particulate liquid water. At elevated RH levels (> ~70%), a significant increase in WSOC partitioning to the particle phase was observed and followed the predicted water uptake by fine particles. The enhancement in particle-phase partitioning translated to increased median particle WSOC concentrations ranging from 0.3-0.9 μg C m^{-3}. Ozone did not have an observable effect on F_p, though NO_x concentrations did, as lower NO_x levels were associated with higher values of F_p. The F_p -NO_x relationship was not likely related to the gas/particle partitioning process, but was likely a result of the influence NO_x imparts on the product distribution of VOC oxidation. The results provide a detailed overview of the WSOC partitioning behavior in the summertime in an urban region dominated by biogenic emissions, and indicate that secondary organic aerosol formation involving partitioning to liquid water may be a significant aerosol formation route that is generally not considered. They also suggest a significant role of the $WSOC_p$ concentration in the gas/particle portioning process, possibly due to heterogeneous chemical reactions occurring within the aerosol aqueous phase, and suggest that NO_x is an important factor in WSOC formation, as well.

Chapter 1

Introduction

Aerosols, also known as particulate matter (PM), are solid and liquid particles suspended in a gaseous medium. Ambient aerosols are an important and ubiquitous component of earth's atmosphere. Even at relatively low concentrations, they can impart a significant impact on physical and chemical processes occurring throughout the atmosphere, from the lower troposphere to the upper stratosphere.

1.1 Importance of Aerosols in the Ambient Atmosphere

Atmospheric particles absorb and scatter light and thus they have a direct impact on earth's radiation balance and climate. For example, particles composed of elemental carbon (EC) absorb light and have a warming effect on the climate [*Hansen et al*., 2000], while particles composed of sulfate (SO_4^{2-}) do not absorb light, but instead scatter it and thus have a cooling effect on climate [*Charlson et al*., 1992]. Ambient aerosol populations are frequently chemically complex and often have both absorptive and scattering properties. In addition to the direct impact aerosols have on the radiation balance, they also have a substantial but highly uncertain indirect effect. Particles serve as the nuclei, or seeds, upon which cloud droplets form. The size and composition of the aerosol distribution determine the size and number of cloud droplets for a given supersaturated environment [*Lohmann et al*., 1999]. These cloud properties then determine both cloud albedo, which is the degree of incident solar radiation that is reflected back into space by the cloud, and cloud lifetime [*Haywood and Boucher*, 2000].

Overall, the net climate forcing by the aerosol indirect effect is highly uncertain [*IPCC*, 2007].

Another byproduct of the interaction of radiation with aerosols is visibility reduction. Particles reduce visibility and contribute to the "haze" associated with urban pollution. Visibility reduction is an important issue in cities [*Sloane et al*., 1991], and in rural areas, especially in national parks [*Malm et al*., 1994].

In addition to impacts on climate and visibility, aerosols have an adverse effect upon human health. An increase in human mortality has been linked to ambient particles with diameter smaller than 10 μm (PM_{10}) [*Samet et al*., 2000] and 2.5 μm ($PM_{2.5}$) [*Dockery et al*., 1993]. Aerosols have also been linked to acute health effects, especially in children. Incidences of bronchitis [*Dockery et al*., 1996], decreased lung function [*Gauderman et al*., 2000], and overall hospital admissions for respiratory ailments [*Pope*, 1991] in children were all linked to PM concentrations. Though studies have shown strong evidence for negative effects of aerosols on human health, the mechanisms by which these effects occur are largely unknown.

Due to their deleterious, though somewhat uncertain effects on human health and their uncertain implication in climate change, a better characterization of their physical and chemical properties would enable a more complete understanding of atmospheric aerosols. Such an understanding is a vital step towards mitigating their effects.

1.2 Sources of Secondary Organic Aerosol

Particles that are not directly emitted, but formed in the atmosphere from various gas-phase and heterogeneous chemical and photolytic reactions, are known as secondary.

Carbonaceous particles, especially those formed from secondary processes, remain poorly characterized. Though chemically diverse, these particulate organic compounds formed through secondary processes are collectively known as secondary organic aerosol (SOA). SOA is important due to its ubiquitous and abundant presence in the atmosphere.

Natural emissions of volatile organic carbon compounds from plants and vegetation, or biogenic VOCs, are responsible for the majority of SOA formation on a global scale [*Tsigaridis and Kanakidou*, 2003]. Isoprene (2-methyl-1,3-butadiene, C_5H_8) is the most abundant biogenic VOC (excluding methane) [*Guenther et al*., 1995] and it is thought to contribute significantly to SOA formation [*Henze and Seinfeld*, 2006]. It used to be neglected in models as an SOA source due to low particle yields derived from smog chamber experiments [*Liousse et al*., 1996], however, recent field observations [*Claeys et al*., 2004] presented strong evidence for substantial SOA formation from isoprene. (The aerosol yield is defined as the total mass of secondary organic aerosol formed divided by the total mass of VOC reacted.) Subsequent smog chamber studies [e.g., *Kroll et al*., 2005] observed significant SOA yields from isoprene and indicate that it is a potentially important source of SOA, as well. SOA formation from isoprene is initiated by reaction with the hydroxyl radical (OH), and the aerosol yield and reaction products are both highly dependent upon the isoprene:NO_x concentration ratio [*Kroll et al*., 2006]. Smog chamber experiments have observed oligomer (Section 1.4) formation in the photooxidation of isoprene (i.e., reaction with OH in the presence of NO_x) [*Dommen et al*., 2006; *Surratt et al*., 2006] and this process may be enhanced by the presence of acidic seed aerosol [*Limbeck et al*., 2003].

In addition to isoprene, the class of biogenic VOCs collectively known as monoterpenes is also believed to be a major global source of SOA [*Kanakidou et al.*, 2005]. These $C_{10}H_{16}$ compounds, including α-pinene and β-pinene, have relatively high emission rates [*Guenther et al*., 1995] and high aerosol yields in smog chamber studies [e.g., *Griffin et al*., 1999]. In the oxidation of monoterpenes to form SOA, reactions initiated by OH, ozone (O_3), and the nitrate radical (NO_3) are all important, with the order of importance dependent upon the chemical structure of each parent hydrocarbon [*Griffin et al.*, 1999]. They, in general, have short atmospheric lifetimes due to chemical features that are conducive to reaction with atmospheric oxidizing agents, including carbon-carbon double bonds and often cyclic or bicyclic structures [*Atkinson and Arey*, 2003]. For example, the atmospheric lifetimes of α-pinene, a species with moderate reactivity among monoterpenes, for reaction with NO_3, O_3, and OH are 11 min, 4.6 h, and 2.6 h, respectively [*Atkinson and Arey*, 2003]. Similar to isoprene, monoterpene SOA yields are dependent on the relative VOC/NO_x ratio, with a higher ratio favoring higher aerosol yields [*Presto et al*., 2005]. Though not as abundant as the monoterpenes, other biogenic VOCs can produce SOA, as well. These include sesquiterpenes, $C_{15}H_{24}$ compounds, which are less abundant but have much higher SOA yields in smog chamber studies than monoterpenes [*Griffin et al.*, 1999].

VOCs emitted by anthropogenic sources are believed to produce a minor fraction (~10%) of global SOA [*Tsigaridis and Kanakidou*, 2003]. However, recent studies by *de Gouw et al.* [2005] and *Volkamer et al*. [2006] suggest that SOA formed from anthropogenic VOCs could be far greater than current models predict. On a regional scale, anthropogenic VOC emissions can be the dominant source of SOA (for example,

Los Angeles in the summertime) [*Hildemann et al*., 1994; *Vutukuru et al*., 2006]. The photooxidation of both diesel exhaust [*Weitkamp et al*., 2007] and unburned gasoline [*Odum et al.*, 1997] has produced high SOA concentrations in smog chamber experiments. Among anthropogenic VOCs, aromatic compounds are responsible for the majority of ambient SOA formation, followed by alkanes and alkenes [*Pandis et al.*, 1992; *Vutukuru et al.*., 2006]. For aromatic compounds, like benzene, toluene, and xylenes, the oxidation pathway, including that towards SOA formation, is initiated by reaction with OH [*Atkinson*, 2000]. Similar to biogenic VOCs, aerosol yields of SOA from aromatic compounds are highly sensitive to VOC/NO_x ratios, with higher ratios generally favoring higher aerosol yields [*Song et al.*, 2005; *Ng et al*., 2007]. Alkanes can comprise 40-50% of total VOCs in certain urban environments [*Lim and Ziemann*, 2005], yet experimental studies on SOA formation from alkanes have been limited. In smog chamber experiments, *Wang et al*. [1992] found aerosol yields from a cycloalkane, methlycyclohexane (C_7H_{14}), to be significantly higher (~9% for the cycloalkane compared to <0.001% for the n-alkane) than that of the n-alkane, n-octane (C_8H_{18}). *Lim and Ziemann* [2005] also observed a small aerosol yield from n-octane (~0.5%), but found the aerosol yields for n-alkanes to depend highly upon carbon number and observed yields of ~50% for $C \geq 13$ compounds. In all cases, the SOA formation pathway begins with the abstraction of an H atom from the VOC by OH [*Atkinson*, 1997]. Due to their carbon-carbon double bond, linear alkenes can form SOA through initial reaction with OH, O_3 [*Forstner et al*., 1997], or NO_3 [*Gong et al*., 2005]. However, due to their relatively low aerosol yields [e.g., *Wang et al*., 1992; *Forstner et al.*, 1997] and abundances [*Chamedes et al*., 1992], anthropogenic alkenes are thought to

be minor contributors to SOA in urban environments [*Pandis et al*., 1992] and negligible on global scales [*Tsigaridis and Kanakidou*, 2003].

Biomass burning is the largest global source of primary organic carbon aerosol [*Liousse et al*., 1996], however global estimates of SOA from biomass burning are highly uncertain (and, in fact, do not even exist). The emission of VOCs which are known SOA precursors, like aromatics and monoterpenes, have been observed from prescribed burning and forest fires [*Andreae and Merlet*, 2001; *Lee et al*., 2005]. *Lee et al*. [2008] inferred significant SOA formation in one event in which aged biomass burning plumes were sampled. Despite the lack of model estimates, the emissions profiles [*Andreae and Merlet*, 2001; *Lee et al*., 2005] and the results of *Lee et al.* [2008] together suggest that biomass burning could be a significant global source of SOA.

1.3 Formation of Secondary Organic Aerosol

In the classical theory of SOA formation [e.g., *Pankow*, 1994a], VOCs undergo oxidative reactions in the gas phase and form a wide range of products with varying volatilities, from highly volatile to non-volatile. The highly volatile products will remain exclusively in the gas phase (potentially undergoing further gas-phase reaction), while the non-volatile products will exist solely in the particle phase. Those products of intermediate volatility, so-called 'semi-volatiles', will establish equilibrium (i.e., partition) between the gas and particle phase. The gas/particle partitioning of semi-volatile compounds is dependent upon multiple factors, including the compound's saturation vapor pressure, ambient temperature, and the existing organic + aqueous aerosol mass into which the semi-volatiles may partition [*Pankow*, 1994a].

The reaction of organic compounds in cloud and fog droplets (cloud or fog processing) has also been suggested as a viable and potentially significant source of SOA [*Blando and Turpin*, 2000]. Organics (formic and acetic acid) were first identified as components in precipitation by *Galloway et al.* [1982]. *Chameides and Davis* [1983] first investigated in-cloud organic reactions and identified an aqueous pathway for the formation and destruction of formic acid. Recent studies suggest increasingly complex SOA formation mechanisms within clouds [e.g., *Lim et al.*, 2005; *Carleton et al.*, 2007]. It is important to note that for SOA formation mechanisms involving clouds, the major oxidant initiating reaction may be different from the gas-phase mechanisms. For example, in the formation of SOA from isoprene through a gas-phase oxidation pathway, OH is the initiating oxidant (see discussion above). However, O_3 and NO_3 also react with isoprene to form water-soluble compounds that can react in the aqueous phase, and these reactions must be accounted for in the cloud processing mechanism [*Lim et al*., 2005]. Similar to gas-phase SOA formation, the VOC/NO_x ratio may impart a significant impact on aerosol yields from cloud processing, as well [*Ervens et al.*, 2008].

In addition to aqueous phase reactions in clouds or fog, heterogeneous chemical reactions may be a significant source of SOA. Heterogeneous reactions are those which occur in the organic particulate phase or in the liquid water associated with particles. A number of smog chamber studies have observed enhancements in SOA formation from the presence of acidic seed particles, supporting the premise that heterogeneous reactions are an important mechanism in SOA formation. *Jang and Kamens* [2001] observed increased aerosol yields from six different aldehydes in the presence of acidic seed particles, compared to a non-acidic seed. *Limbeck et al*. [2003] observed a strong

positive (non-linear) correlation between aerosol yields from isoprene and the sulfuric acid seed concentration, and *Iinuma et al*. [2004] observed significantly higher yields from the ozonolysis of α-pinene in the presence of acidic seed particles compared to neutral seed. *Gao et al*. [2004] found the formation of oligomers, high molecular weight organics that have been frequently observed in ambient aerosol [*Graber and Rudich*, 2006], to be enhanced by acidic seed. In contrast to the chamber results, ambient studies by *Zhang et al*. [2004], *Gao et al*. [2006], and *Peltier et al*. [2007a] found no evidence for acid-catalyzed SOA formation in Pittsburgh, the southeastern US, and Atlanta, respectively.

Another potential source of SOA is through the oxidation of evaporated primary organic aerosol (POA) vapors [*Robinson et al.*, 2007]. The theory of *Robinson et al*. [2007] is that some fraction of POA, contrary to its traditional treatment by models, evaporates upon dilution with ambient air. These semi-volatile gases subsequently undergo oxidation and re-partition to the aerosol phase as SOA. In smog chamber experiments, *Lipsky and Robinson* [2006] observed significant evaporation of POA emissions from diesel exhaust and wood smoke. *Robinson et al*. [2007] observed significant smog chamber SOA production from diesel exhaust above that predicted by models and they attribute the additional SOA to the oxidation of low-volatility VOCs which evaporated from POA upon dilution. Additionally, their model predictions indicate that POA, which is emitted predominantly from urban centers, may be a significant SOA source on regional scales by this pathway.

1.4 Chemical Properties of Secondary Organic Aerosol

Because it consists of likely hundreds to thousands of compounds, the chemical properties of ambient SOA are highly diverse. Organic compounds with an array of functional groups, including mono- and di-carboxylic acids, carbonyls, alcohols, and organic nitrates, have been identified as components of atmospheric SOA [*Saxena and Hildemann*, 1996]. SOA consists of compounds that are both hydrophobic and hydrophilic in nature [*Sullivan and Weber*, 2006]. The molecular weight (MW) range of SOA is typically broad, and can vary widely depending on location, season, aerosol source, and age, among other factors. For example, ambient aerosol samples collected in Zurich, Switzerland, showed distinctive peaks in the MW range (based on the mass-to charge ratio in mass spectrometric analysis) of 150-550 which had a highly oligomeric character [*Kalberer et al*., 2006]. Oligomers are higher molecular weight compounds, or macromolecular compounds, that have been frequently observed in both smog chamber experiments and in ambient aerosol samples [*Graber and Rudich*, 2006]. Oligomers are also called 'Hulis' for having chemical properties similar to humic acid, which is a chemically complex mixture of high MW compounds frequently found in natural aquatic environments [*Graber and Rudich*, 2006]. It is this vast chemical complexity which has rendered its comprehensive chemical speciation unattainable, to date.

Once formed, SOA may also undergo substantial transformation, or aging, in the particle phase. This aging process likely involves oxidation of the organic compounds by either O_3 or OH [*Rudich et al*., 2007]. Studies by *Kalberer et al*. [2004] and *Baltensperger et al.* [2005] observed a decrease in SOA volatility with age in smog

chamber experiments. In addition to volatility, density and hygroscopicity are two important aerosol properties that may be altered by chemical aging [*Rudich et al*., 2007]. Chemical aging is not strictly a phenomenon that affects secondary organic compounds, though, as primary organic compounds and elemental carbon may also undergo similar processes [*Rudich et al*., 2007].

There is no direct measurement exclusively of SOA, but currently several methods are used to infer SOA concentrations. Using known emission factors of organic carbon (OC) and elemental carbon (EC), the ratio of OC to EC, known as the EC tracer method, is used to estimate SOA [*Gray et al.*, 1986; *Turpin and Huntzicker*, 1995]. An algorithm applied to measurements made with an Aerodyne Aerosol Mass Spectrometer can distinguish the oxygenated organic aerosol (OOA) fraction of organic aerosol from the hydrocarbon-like organic aerosol [*Zhang et al*., 2005a]. Under certain conditions, this OOA fraction is expected to be comprised almost entirely of secondary organic compounds [*Zhang et al*., 2005b]. In the absence of significant biomass burning emissions, the particulate water-soluble organic carbon ($WSOC_p$) measurement made via the PILS-WSOC method [*Sullivan et al.*, 2004] provides an approximate measurement of SOA, although some fraction of the SOA may not be soluble. A study by *Miyazaki et al*. [2006] found that SOA estimated by the EC tracer method was highly correlated with $WSOC_p$ ($R^2 = 0.70 – 0.79$) and observed $WSOC_p$/SOA slopes of 0.67 – 0.75. The same study also found 90% or more of primary organic aerosol to be insoluble in water. A study by *Kondo et al*. [2007] found excellent agreement ($R^2 = 0.86 – 0.93$) between OOA and $WSOC_p$ and observed that, across seasons, an average of 88% of OOA in a large urban center was water soluble.

This dissertation investigates several critical aspects of secondary organic aerosol:

- In an urban region dominated by anthropogenic emissions, the Mexico City Metropolitan Area, the formation and volatility of SOA are examined, along with their link to particle water.
- In a region dominated by biogenic VOC emissions, the gas/particle partitioning of WSOC is examined in Atlanta. This includes:
    - The effect of temperature on WSOC partitioning
    - The effect of organic aerosol mass on WSOC partitioning
    - The effect of relative humidity on WSOC partitioning
    - The effects of NO_x, O_3, and other meteorological parameters on WSOC partitioning
- Multiple summertime events were observed in Atlanta in which $WSOC_p$ and water vapor were highly correlated. The causes of these events are examined, and evidence about the sources and formation of $WSOC_p$ (SOA) are presented.

Chapter 2

Methods

Many of the analyses presented in this Dissertation are based on ambient measurements. This Chapter describes the methods and analytical techniques used to measure the major gaseous and particulate species of interest.

2.1 Particle-into-Liquid Sampler (PILS)

For many of the particle measurements used in the analyses that constitute this Dissertation data set, a particle-into-liquid sampler (PILS) was used as the particle collection method. The PILS is a device used to sample water-soluble aerosol species with fast time resolution [*Weber et al.*, 2001; *Orsini et al*., 2003]. Figure 2.1 shows a schematic of the PILS.

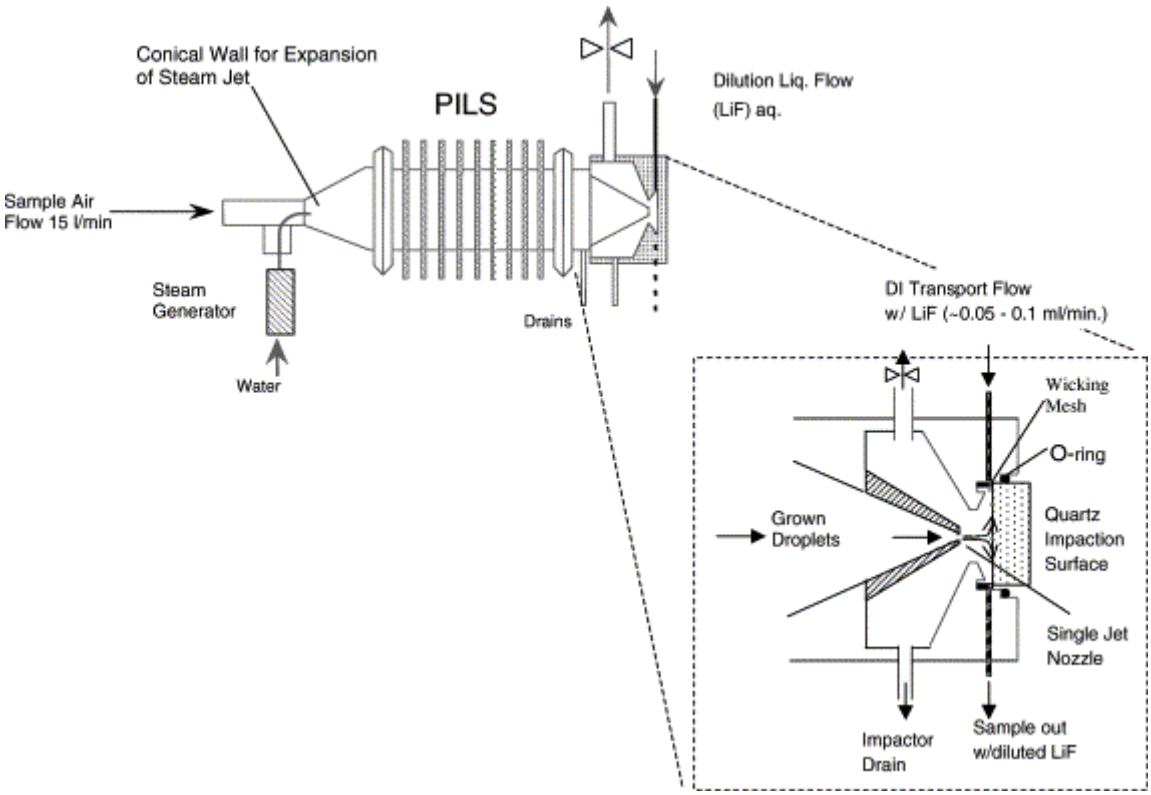

Figure 2.1 Schematic of the particle-into-liquid sampler (PILS), from *Orsini et al.* [2003].

The PILS works by mixing ambient air, sampled at 15-17 L min^{-1}, with steam generated from ultra-pure water (> 18.0 MΩ) to create an environment within the PILS body at supersaturated water vapor concentrations. The ambient particles undergo condensational growth within the PILS body, after which they are accelerated through a nozzle and impacted onto a quartz or polycarbonate disc. The PILS collects particles in the 0.03-6 μm size range with near-100% efficiency [*Orsini et al*., 2003], and is thus an excellent method to sample $PM_{2.5}$. The collection of particles smaller than 0.03 μm is not efficient; however, the analyses performed are based on mass concentrations, rendering this small size range unimportant. A continuous flow of ultra-pure water over the top of

the impaction disc then transfers the impacted particles into an aqueous phase where they can then be transported for subsequent analysis in near-real time. Because the analyses are performed on this aqueous phase, the conversion to ambient air concentrations requires the following equation

$$C_a = \frac{C_L * Q_L * R}{Q_a} \qquad \text{Equation 2.1}$$

where C_a is the ambient air concentration in μg m^{-3}, C_L is the measured liquid concentration in μg L^{-1}, Q_L is the liquid flow rate over the top of the impaction disc in mL min^{-1}, R is the sample dilution ratio, and Q_a is the flow rate of sample air through the PILS in L min^{-1}. The dilution ratio, R, is typically measured by spiking the transport water with a known concentration of an inert species not present in ambient samples (e.g., LiF).

PILS measurements generally agree quite well in comparisons to traditional filter sampling techniques [*Orsini et al.*, 2003; *Weber et al.*, 2003a; *Sullivan et al.*, 2004]. The continuous, near-real time sampling capabilities of the PILS offer substantial improvements over traditional filter-based techniques. In addition to being less labor-intensive, measurements with PILS provide greater time resolution and thus, better temporal characterization of water-soluble species. Due to the enhanced time resolution, PILS measurements have been used extensively to characterize aerosol chemical composition on aircraft studies [e.g., *Ma et al.*, 2003; *Hennigan et al.*, 2006; *Peltier et al.*, 2008], where high temporal resolution is especially critical.

2.1.1 PILS Coupled to Ion Chromatographs

In the Megacity Initiative: Local and Global Research Objectives (MILAGRO) study (results provided in Chapter 3), the PILS was coupled to dual ion chromatographs (ICs) for the determination of the ambient inorganic aerosol chemical composition (PILS-IC method) [*Orsini et al.*, 2003]. Species measured included the cations sodium (Na^+), ammonium (NH_4^+), calcium (Ca^{2+}), and magnesium (Mg^{2+}); the anions chloride (Cl^-), nitrite (NO_2^-), nitrate (NO_3^-), and sulfate (SO_4^{2-}); as well as organic acids formic acid (measured as formate ion, $HCOO^-$), acetic acid (measured as acetate ion, H_3CCOO^-), and oxalic acid (measured as oxalate ion, $C_2O_4^{2-}$). With an appropriate analytical column, the number of organic acids analyzed can be increased substantially [*Sorooshian et al*., 2007] by this method. To remove gaseous species that may interfere with the particle measurements, denuders were placed immediately upstream of the PILS in the sample configuration. Two glass honeycomb denuders were coated with a sodium carbonate solution for the removal of acidic gases (e.g., HCl, HNO_3, SO_2) and a citric acid solution for the removal of ammonia (NH_3).

Depending on field conditions and measurement objectives, a wide range of analytical columns and sample integration times can be used for the IC analyses. During the MILAGRO study (described in detail in Chapter 3), a Metrosep A-Supp 5-150 analytical column (Metrohm, Herisau, Switzerland) with 4 mM sodium carbonate (Na_2CO_3)/1 mM sodium bicarbonate ($NaHCO_3$) eluent at 0.8 mL min^{-1} flow rate was used to analyze the above anions. A Metrosep Cation 1-2 analytical column (Metrohm, Herisau, Switzerland) with 4 mM L-tartaric acid/1 mM dipicolinic acid eluent at 1.2 mL min^{-1} flow rate was used to analyze the above cations. A six-minute sample integration

time was used, followed by 11 minutes of 'off-line' time for sample analysis, resulting in one six-minute sample every 17 minutes. The uncertainty of the NO_3^- measurement using this technique was approximately 15% [*Weber et al.*, 2003a].

2.1.2 PILS coupled to a Total Organic Carbon Analyzer

In both Mexico City and Atlanta, the water-soluble organic carbon content of particles ($WSOC_p$) was measured via the PILS coupled to a Sievers 800 Total Organic Carbon (TOC) Analyzer (GE Analytical, Boulder, CO) [*Sullivan et al.*, 2004]. The PILS-WSOC method can provide measurements with 3-second time resolution however, for the ground-based measurements described here, 6-minute sample integration times were used.

Particle size selection was accomplished through the deployment of either a cyclone (URG, Chapel Hill, NC) or a non-rotating mirco-orifice impactor [*Marple et al.*, 1991]. For the $WSOC_p$ measurement, the sample air stream was passed through an activated carbon parallel-plate denuder [*Eatough et al.*, 1993] to remove VOCs that could interfere with the measurement. Once in the aqueous phase, the sample was passed through a 0.22 μm liquid filter. The organic carbon content of the sample was then quantified by the TOC Analyzer. The calibration of the TOC Analyzer occurred in the factory and was periodically verified with sucrose standards across the full range of liquid concentrations (50-2000 ppb C) encountered in ambient sampling. Twice daily, the sample air stream was directed through a HEPA filter to determine the carbon content of the ultra-pure water and any penetration of interfering VOCs through the denuder. Data were corrected based on this dynamic blank. The limit of detection for the PILS-

WSOC method is 0.1 μg C m^{-3} and the uncertainty of the $WSOC_p$ measurement was ~10% [*Sullivan et al*., 2004].

In the absence of significant biomass burning emissions, the particulate water-soluble organic carbon ($WSOC_p$) measurement provides an approximate measurement of SOA, although some fraction of the SOA may not be soluble. A study by *Miyazaki et al*. [2006] found that SOA estimated by the EC tracer method was highly correlated with $WSOC_p$ ($R^2 = 0.70 – 0.79$) and observed $WSOC_p$/SOA slopes of 0.67 – 0.75. The same study also found 90% or more of primary organic aerosol to be insoluble in water. A study by *Kondo et al*. [2007] found excellent agreement ($R^2 = 0.86 – 0.93$) between oxygenated organic aerosol (OOA) measured by an Aerodyne Aerosol Mass Spectrometer and $WSOC_p$ and observed that, across seasons, an average of 88% of OOA in a large urban center was water soluble.

2.2 Organic Carbon and Elemental Carbon Analyzer

Total particulate organic carbon (OC) and elemental carbon (EC) measurements were made with a Sunset Labs OCEC Field Analyzer (Sunset Laboratory Inc., Tigard, OR) in accordance with NIOSH method 5040 [*NIOSH*, 1996]. Ambient particles were collected onto a quartz filter downstream of an activated carbon parallel plate denuder [*Eatough et al*., 1993], in place to prevent semi-volatile organic gases from condensing onto the filter. After a collection period of 45 minutes, the filter is heated in a stepwise manner to ~800 °C in a helium atmosphere. OC on the filter volatilizes and is detected by Flame Ionization Detection (FID). After a brief cooling step, the temperature is subsequently increased to ~850 °C in a mixture of helium (~98%) and oxygen (~2%).

The carbon that evolves from the filter during this step is also detected by FID and is assumed to be EC. During the initial heating step, some fraction of the OC can char and adhere to the filter instead of volatilizing. This charred material will then volatilize in the heating step with oxygen and can negatively bias the OC measurement (positively bias the EC measurement). To correct this problem, the Analyzer uses a thermal optical transmittance (TOT) method for the determination of OC and EC [*Birch and Cary*, 1996]. This method uses the transmission of a laser through the filter to monitor the amount of light-absorbing material on the filter and to determine the delineation between 'charred' OC and EC [*Birch*, 1998]. At a sampling time of 45 minutes, the LOD is estimated to be 0.5 μg C m^{-3} and the uncertainty is estimated at 20% [*Peltier et al.*, 2007b].

2.3 Mist Chamber

A mist chamber was used for certain gas-phase measurements in the Atlanta study and the system schematic is shown in Figure 2.2. Sample air was pulled at approximately 21 L min^{-1} through a Teflon filter for complete removal of particles. The sample then entered a glass mist chamber (MC) [*Cofer and Edahl*, 1986] initially filled with 10 mL of ultra-pure water and fitted with a hydrophobic Teflon filter at the chamber exit. This mist chamber has been shown to efficiently sample gases with an effective Henry's Law constant greater than ~ 10^3 [*Spaulding et al.*, 2002]. For the present configuration, the collection efficiency was tested using nitric acid, and was found to be 95.1% ± 2.1% (mean ± 1σ). An automated valve in between the MC and the vacuum pump was programmed to collect a five-minute batch sample once every ten minutes. In the five-

minute period between samples, the MC was rinsed with 10 mL ultra-pure water while the previous sample was being analyzed. With the exception of periodically changing the Teflon filter upstream of the MC, and filling the water reservoir, the system was completely automated.

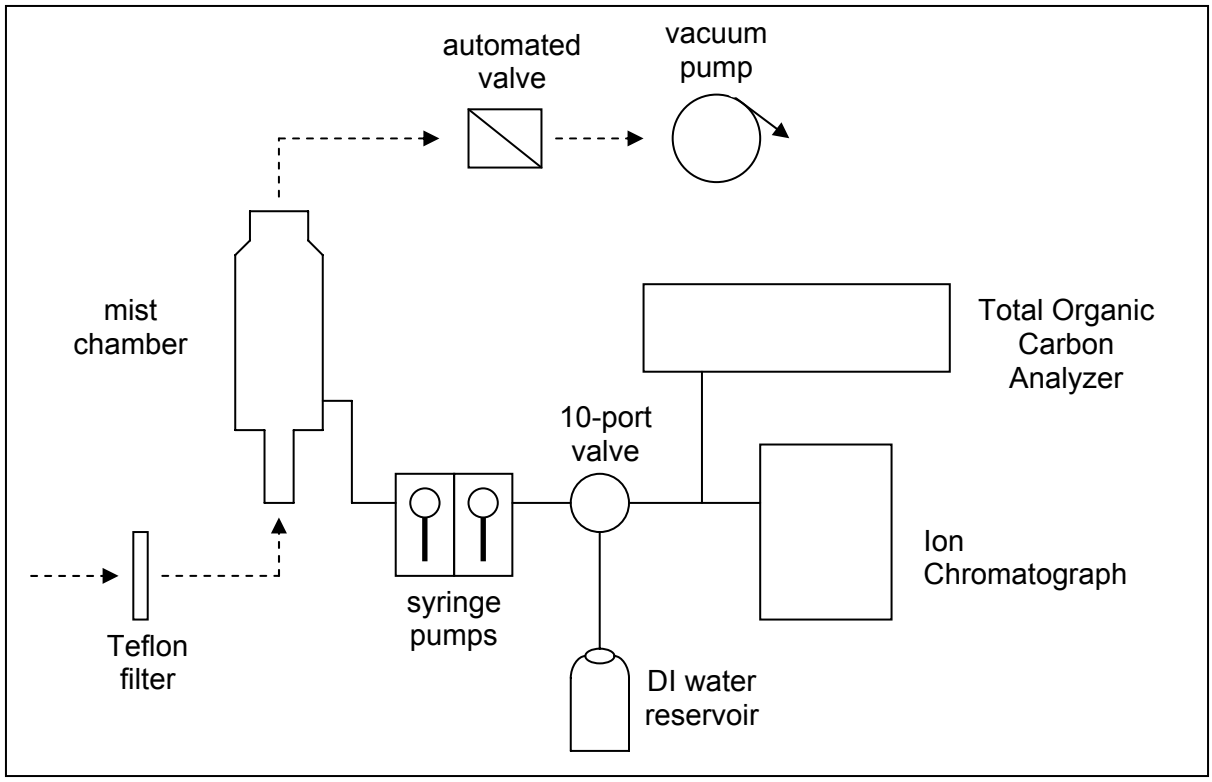

Figure 2.2 Schematic of the mist chamber sampling system.

An accurate determination of the concentrations measured with the MC depends on an accurate measure of the volume of water used to collect the sample. Consequently, one factor that had to be accounted for was water evaporation during sample collection. Calibrations of water evaporation were performed using gravimetric analysis on three separate days (n total = 56). It was found that evaporation was approximately constant,

regardless of ambient temperature and relative humidity (RH) conditions. During the calibrations, ambient temperature exhibited a range of 18.5-32.4 °C while ambient RH exhibited a range of 23-66%. With a beginning volume of 10 mL, the ending volume after five minutes of sampling was 8.75 mL, and the uncertainty was 0.12 mL (1.4%) at the 95% confidence interval. Because the ambient temperature and RH conditions encountered during calibrations covered much of the ranges observed during sampling, the assumption of a constant ending water volume was valid throughout the study period.

2.3.1 MC coupled to a Total Organic Carbon Analyzer

For measurements of bulk water-soluble organic carbon gases ($WSOC_g$), the MC was coupled to a Sievers 900 Total Organic Carbon Analyzer (GE Analytical, Boulder, CO) in a method similar to that of *Anderson et al*. [2008]. Of the 8.75 mL sample, 5 mL were sent to the TOC analyzer, which was operated in Turbo mode to provide measurements on a 4-second time interval. In this setup, the average of approximately 60 consecutive TOC measurements was used to quantify each MC sample, since the TOC liquid sample rate was 1 mL min^{-1}. While the MC was in sample collection mode, the TOC Analyzer sampled the ultra-pure water to determine the carbon concentration in the water used for sample collection. This background was subtracted from the subsequent aqueous sample concentration in order to calculate the ambient $WSOC_g$ concentration. At an air flow rate of 21 L min^{-1} and a five-minute sample integration time, the LOD for the $WSOC_g$ measurement was 0.9 μg C m^{-3}. Based on uncertainties in the airflow (± 5%), ending water volume (± 1.4%), analyzer sample concentration (± 2%), and

background concentration (± 2%), an overall uncertainty for the $WSOC_g$ measurement was estimated at 7%.

2.3.2 MC coupled to Ion Chromatographs

For measurements of gas-phase formic, acetic, and oxalic acids, the MC was coupled to an Ion Chromatograph (IC) (Metrohm, Herisau, Switzerland) for measurement of the formate, acetate, and oxalate ions, respectively. An isocratic separation was performed using an anion Metrosep A Supp 5-100 analytical column (Metrohm, Herisau, Switzerland) and 3.2 mM Na_2CO_3/1 mM $NaHCO_3$ eluent at a flow rate of 0.5 mL min^{-1}. Due to the relatively long retention times of the organic acids, IC sample analysis was performed on a 20 minute time interval. The LOD's for formic acid, acetic acid, and oxalic acid were 40 ng m^{-3}, 80 ng m^{-3}, and 80 ng m^{-3}, respectively. Based on the uncertainties in the airflow (± 5%), ending water volume (± 1.4%), and liquid sample concentration (± 10%), the overall uncertainty for the organic acids was approximately 12%.

2.4 Sampling and Analysis Methodology

The Mexico City study was part of the large, multi-national and multi-agency field study MILAGARO (Chapter 3). The ground-based measurements were made for approximately 3.5 weeks, and a three-day period from this data set was chosen for the analysis presented in Chapter 3. The Atlanta study was not performed in conjunction with any agency-sponsored field campaigns. Consequently, the measurements were carried out for approximately 4.5 months. Due to several periods of off-line analyses and

calibrations, the final data set from Atlanta was equivalent to approximately 3 months of continuous sampling. As detailed above, the measurements were carried out at a high time resolution; six minutes for the $WSOC_p$ measurement, a five-minute $WSOC_g$ sample every 10 minutes, and hourly for the OC and EC measurements. The high time resolution and extended length of the measurements resulted in the collection of extensive data sets ($n > 11000$ for $WSOC_p$ and $WSOC_g$, $n > 1400$ for OC and EC). Consequently, the analyses performed have a high statistical strength and the findings are robust, which enhances their significance.

Chapter 3

The Sources and Volatility of $WSOC_p$ and Nitrate in Mexico City

In this chapter, the semi-volatile nature of SOA measured in the Mexico City Metropolitan Area (MCMA) is examined through simple box model analyses that involve a comparison with ammonium nitrate (NH_4NO_3), a semi-volatile species whose thermodynamic properties are well understood.

3.1 Study Overview

Measurements of aerosol and gas-phase species were made in March, 2006 as part of the Megacity Initiative: Local and Global Research Objectives (MILAGRO) field campaign. The study was focused on examining the chemical nature and processing of pollution outflow from the MCMA. Data reported here are from the ground-based measurement site, T1, located approximately 30 km downwind of the MCMA city center at the Universidad Tecnológica de Tecámac (lat 19.708, lon -98.982, elevation 2.2 km). Measurements at T1 were performed from March 7-31, 2006; however the present analysis focuses only on the period of March 27-29. The selected period was characterized by consistent diurnal behavior of $PM_{2.5}$ mass and the highest daily maximum NO_3^- concentrations (Figure 3.1). It was also the period least impacted by biomass burning [*Stone et al.*, 2008], which along with SOA is a source of fine particle WSOC [*Sullivan et al*., 2006]. All concentrations are reported at ambient temperature and pressure.

Inlets for aerosol measurements were located approximately 10 m above the ground and were fitted with cyclones (URG, Chapel Hill, NC) to select particles with aerodynamic diameters less than 2.5 μm ($PM_{2.5}$). The aerosol measurements, described in detail in Chapter 2, included $WSOC_p$, and inorganic ionic components (including nitrate, NO_3^-, and ammonium, NH_4^+). Aside from the above methods that were detailed in Chapter 2, supporting measurements were made as part of the study as well. Hydroxyl (OH) and peroxy (RO_2) radical concentrations were measured with a chemical ionization mass spectrometer (CIMS) [*Sjostedt et al*., 2007]. Measurements of nitric oxide (NO) and photolysis rates (J values) were made with a chemiluminescence detector [*Ryerson et al*., 2000] and an actinic flux spectroradiometer [*Shetter and Muller,* 1999], respectively. Ozone (O_3) was measured with a commercial UV photometric O_3 analyzer (TECO, Model 49C). Although no data is presented, ammonia (NH_3 (g)) was also measured at T1 and was generally found to be plentiful, consistent with an observed neutral aerosol indicated by the simultaneous presence of significant SO_4^{2-} and NO_3^- concentrations [*Fountoukis et al.*, 2007].

Data from the National Science Foundation (NSF) C-130 aircraft also involved in this study are used in the following analysis to assess the impact of dilution due to boundary layer expansion. This includes PILS-instrumentation for measurements of inorganic ions and $WSOC_p$ using methods similar to the T1 site, but modified for aircraft operation [*Sullivan et al*., 2006; *Peltier et al*., 2008]. In contrast to the T1 surface that involved aerosol composition measurements restricted to $PM_{2.5}$, the aircraft measured $PM_{1.0}$. Nitric acid (HNO_3 (g)) was also measured from the NSF C-130 during this mission by chemical ionization mass spectrometry [*Crounse et al.*, 2006].

3.2 Model Description

The ISORROPIA-II [*Nenes et al.*, 1998; *Fountoukis and Nenes*, 2007] thermodynamic equilibrium model was used to simulate the thermodynamic partitioning of NO_3^-. The model uses inputs of ambient temperature, relative humidity, and total concentrations (gas + particle) of inorganic species to predict the equilibrium state of each species along with the aerosol water concentration. Application of the model in Mexico City during the MILAGRO study produced predictions that agreed with measured concentrations within 20% [*Fountoukis et al.*, 2007].

A box model was constructed to investigate the processes affecting WSOC and NO_3^- concentrations. From *Seinfeld and Pandis* [1998], the governing equation for an Eulerian box model with a well-mixed and expanding boundary layer is

$$\frac{dc_i}{dt} = \frac{1}{H(t)} Q_i + R_i - \frac{1}{H(t)} S_i + \frac{u}{\Delta x}(c_i^0 - c_i) + \frac{1}{H(t)} \frac{dH}{dt}(c_i^a - c_i) \qquad \text{Equation 3.1}$$

where c_i is the species *i* concentration, c_i^0 is the species *i* background concentration, c_i^a is the species *i* concentration aloft, Q_i is the emission rate, R_i is the chemical production rate, S_i is the loss rate, u is the wind speed (with constant Δx direction), and $H(t)$ is the boundary layer (BL) height. Direct measurements of BL height data were taken from *Shaw et al*. [2007]. Though BL height data were not available on 3/29, consistencies in meteorological parameters and pollutant profiles (Figure 3.1) suggest that the BL growth on 3/29 was similar to 3/27 and 3/28. A conservative tracer, water vapor, was used to estimate dilution from BL growth on 3/29 by using the aloft water vapor mixing ratio measured by the C-130. The mean uncertainty in the box model results, due to uncertainty in BL height measurements and in the measured pollutant concentrations, was estimated to be ~35%.

3.3 Results

3.3.1 NH_4NO_3 Formation

NH_4^+ and NO_3^- were highly correlated ($R^2 = 0.82$) during the three days investigated and dominated the inorganic $PM_{2.5}$ fraction, accounting for an average of 57% of measured inorganic mass (sum of chloride, nitrite, nitrate, sulfate, sodium, ammonium, calcium, and magnesium). Concentrations of both species increased rapidly with increasing solar radiation starting at approximately 07:30 (Central Standard Time, CST, UTC – 6h) (Figure 3.1), suggesting photochemical aerosol formation.

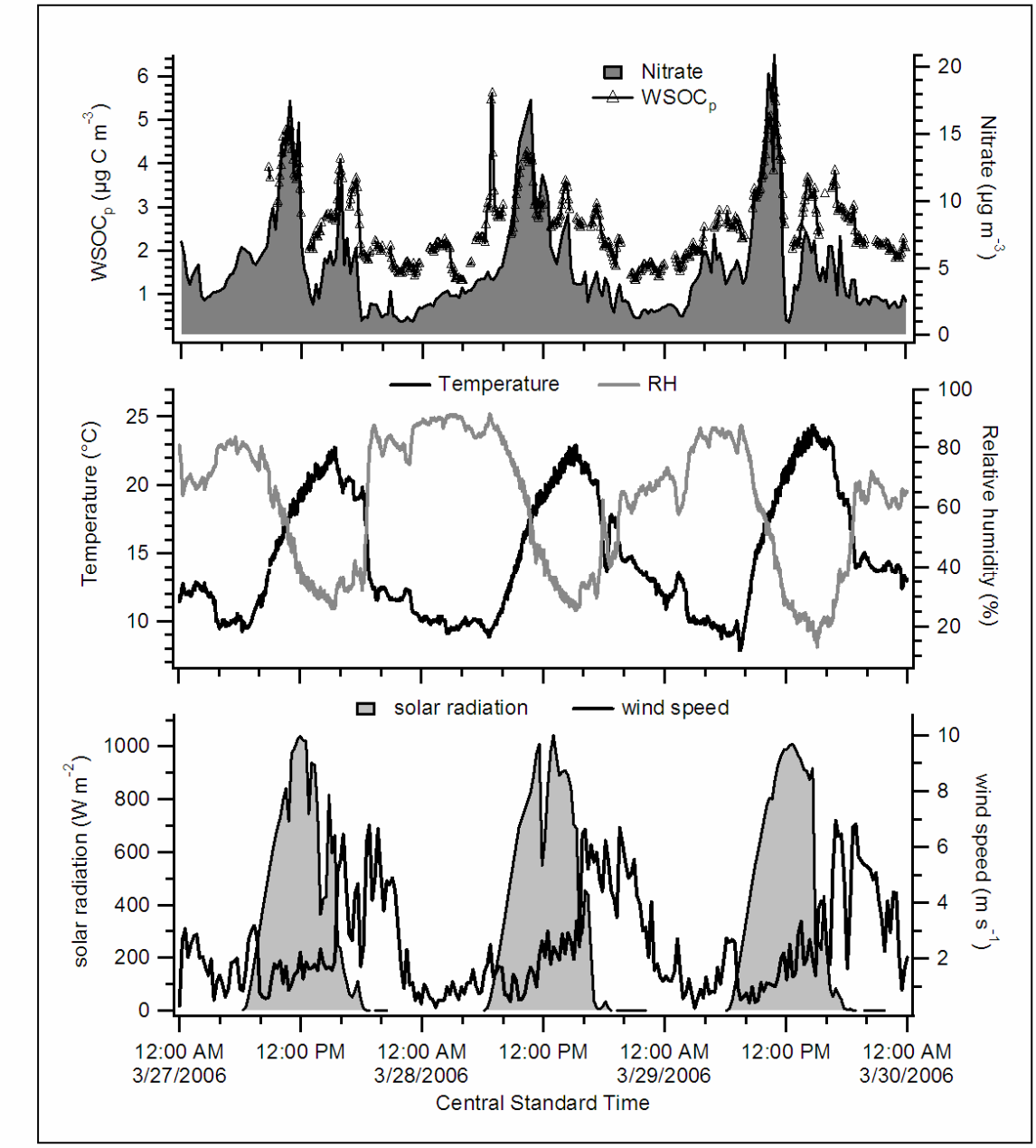

Figure 3.1 Time series of measured NO_3^-, $WSOC_p$, solar radiation, temperature, wind speed, and RH for March 27-29. Concentrations of NO_3^- and $WSOC_p$ began to rise shortly after sunrise and model results (not shown) indicate that approximately 75% of the morning concentration increases were due to secondary aerosol formation.

The NO_3^- concentration reached its daily maximum near 11:00 of 18.6 µg m^{-3}, an increase of 13.9 µg m^{-3} over pre-sunrise concentrations. The box model was applied to

investigate the contribution of secondary nitrate formation to the observed increase. The model was run for the hours 09:00 to 11:00, when BL data were available, and the results likely apply to the early morning hours as well. For the purpose of modeling NO_3^- in the morning at T1, a number of assumptions were made to simplify the model. The removal rate, S_i, was neglected because the dry deposition velocity for 0.1-2.5 μm particles (0.01 – 0.2 cm s^{-1} [*Seinfeld and Pandis*, 1998]) is not important on the timescale of several hours. Wind speeds, which generally ranged from 1-2 m s^{-1} during the period of interest (Figure 3.1), were too low to make advection an important process on the timescale of several hours, either. Each day before 11:00, ISORROPIA-II predicted that greater than 90% of total nitrate (NO_3^- + HNO_3 (g)) partitioned into the particle phase (Figure 3.2) due to thermodynamic conditions that favored the condensed phase, including low T, high RH, and excess ammonia gas (NH_3) [*Fountoukis et al*., 2007]. Thus all predicted HNO_3 (g) produced was assumed to contribute to the observed aerosol nitrate loading. The HNO_3 (g) formation rate (μg m^{-3} hr^{-1}), R_i, was calculated as k*[NO_2]*[OH], where k is the temperature-dependent kinetic rate constant [*Sander et al*., 2006], NO_2 was calculated from observations of NO, O_3, J values, and RO_2 assuming photochemical steady state, and OH was measured. After incorporating the stated assumptions, the simplified form of the model was

$$\frac{dc_i}{dt} = k \bullet [NO_2] \bullet [OH] + \frac{1}{H(t)} \frac{dH}{dt} (c_i^a - c_i) \qquad \text{Equation 3.2}$$

The model was then solved for c_i^a, the NO_3^- concentration in air entrained by the expanding BL and the two right hand terms (photochemical production and dilution) were compared. From 09:00-11:00, the BL expanded from, on average, 510 m to 1100

m. Model results indicate that approximately 75-80% of the observed nitrate concentration increase was due to secondary photochemical production (Table 3.1). By comparison to the observed NO_3^- concentration, mass conservation indicated that the average NO_3^- concentration in the entrained layer was 6.4 ug m^{-3} and was responsible for approximately 20-25% of the observed NO_3^- increase.

Table 3.1 Average box model predictions for the effects of secondary formation and entrainment on NO_3^- and $WSOC_p$ increases, and the effects of dilution and evaporation on NO_3^- and $WSOC_p$ losses. The three $WSOC_p$ columns represent aloft $WSOC_p$ concentrations of 0, 0.7, and 1.4 μg C m^{-3}, respectively (denoted in parentheses).

	Nitrate[a]	$WSOC_p(0)$[b]	$WSOC_p(0.7)$[b]	$WSOC_p(1.4)$[b]
AM concentration increase	13.9	1.9	1.9	1.9
AM aloft concentration	6.4	0	0.7	1.4
AM % increase from entrainment	23%	0%	15%	36%
AM % increase from secondary formation	77%	100%	85%	64%
Peak concentration	18.6	4.8	4.8	4.8
Noon Observed loss	15.1	2.68	2.68	2.68
Noon Dilution loss	9.1	2.34	1.99	1.65
Noon Volatility loss	6.0	0.34	0.69	1.03
Noon Volatility loss (% of total loss)	40%	13%	26%	38%
Noon Volatility loss (% of AM increase)	43%	18%	36%	54%
Noon Volatility loss (% of peak concentration)	32%	7%	14%	21%

[a]concentrations in units of μg m^{-3}
[b]concentrations in units of μg C m^{-3}

On 3/29, the C-130 flew in the vicinity (0-90 km) of T1 between the hours of 11:00 – 15:00 CST, including a pass directly over the site at 14:00. During this time, the plane flew primarily within the BL, but did sample out of the BL on several occasions. Sampling in versus out of the BL was determined by water vapor concentration, which showed rapid changes with minor altitude changes when the threshold was crossed.

During this time, the mean concentration of total nitrate (NO_3^- + HNO_3 (g)) in the 1km layer above the BL was 1.5 ± 1.3 (mean ± 1σ) μg m^{-3}. Assuming these aloft measurements are representative of what was entrained into the BL during the morning nitrate production, they suggest that the predictions of nitrate production were low, and that the contribution from photochemical production to the NO_3^- increase was perhaps as high as 90-95%.

Overall, the present results qualitatively agree with previous studies [*Salcedo et al.*, 2006; *Volkamer et al*., 2006] in the MCMA, which observed a similar morning production of HNO_3 (g) immediately followed by NH_4NO_3 formation. This morning photochemical NO_3^- production appears to be a common phenomenon in the MCMA.

3.3.2 Nitrate Loss

The NO_3^- peak was short lived, as concentrations began to drop precipitously at approximately 11:00 (Figure 3.1). Over the period between ~11:00 and ~12:45, the NO_3^- concentration decreased by an average of 15.1 μg m^{-3}, an 81% drop from the peak concentration. This decrease occurred while the HNO_3 (g) production rate (k [OH] [NO_2]) remained relatively high. Causes of this concentration decrease following the late morning maximum are hypothesized as a combination of boundary layer dilution and chemical processes (i.e., particle evaporation). Precipitation data showed that wet deposition was not important on any of the days in question. We first investigate the role of chemical processes, followed by the effects of meteorological processes on ambient concentrations.

The effect of a thermodynamic phase shift on NO_3^- was examined with ISORROPIA-II and model results are shown in Figure 3.2. Based on rising ambient temperature and decreasing relative humidity, the model predicted a rapid phase shift of NO_3^- to HNO_3 (g). NH_4NO_3 is semi-volatile and is sensitive to changes in RH and temperature (both of which directly impact aerosol water content), with higher temperature (lower RH) favoring the gas phase and lower temperature (higher RH) favoring the particle phase. (Recall that NH_3 (g) was ubiquitous at this site). It is notable that the predicted equilibrium shift coincided with the large observed decrease in NO_3^- concentration (Figure 2). ISORROPIA-II predicted an average morning aerosol water concentration maximum of 15.4 μg m^{-3}, followed by a rapid concentration decrease to 1.2 μg m^{-3} that preceded the NO_3^- concentration drop by approximately 1 hr. Given additional time for aerosol evaporation following the water loss, the timescale of this observed delay is consistent with the analysis of *Fountoukis et al*. [2007]. The observational data and model results agree well and suggest that, despite continued production of HNO_3 (g) and available NH_3 (g), changing ambient conditions produced a rapid shift in the equilibrium of the system towards the gas phase and were responsible for some fraction of the observed NO_3^- loss.

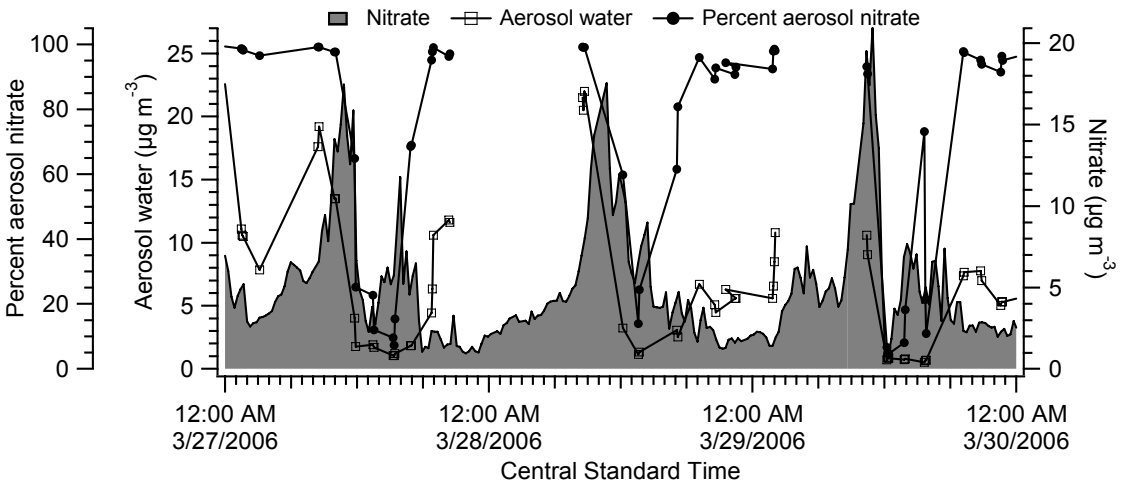

Figure 3.2 ISORROPIA-II model output (Percent aerosol nitrate and aerosol water) and measured NO_3^- for March 27-29. Based on rising morning temperature and decreasing RH, a sharp decrease in the predicted aerosol water concentration was followed by a rapid equilibrium shift in NO_3^- from the aerosol to the gas phase. This equilibrium shift likely produced at least a third of the observed nitrate concentration decrease.

Dilution must also be considered because the boundary layer underwent rapid expansion during the nitrate decrease. With two assumptions, the box model was also used to assess the relative contribution of BL dilution on the NO_3^- concentration decrease. The average NO_3^- loss, if dilution was the sole factor contributing to its decrease, was 9.1 µg m^{-3} (Table 3.1). Because of the thermodynamic shift predicted by ISORROPIA-II, the difference between the observed NO_3^- decrease (15.1 µg m^{-3}) and that predicted by dilution (9.1 ug m^{-3}) was attributed to volatility. Thus 6 µg m^{-3}, or 40%, of the concentration decrease was from particle evaporation while 60% was due to dilution. This analysis incorporated two major assumptions that set the evaporation estimate as a lower bound. First, the effect of continued HNO_3 (g) production and its conversion to NH_4NO_3 throughout this time was neglected. The second assumption was that the NO_3^- concentration aloft was neglected. Due to ISORROPIA-II predictions, we assume that

any NO_3^- entrained during this time evaporated and any HNO_3 (g) formed remained predominantly in the gas phase. Any NO_3^- in the entrained air that did not evaporate or photochemical NO_3^- formation during this time would translate to volatility losses greater than the 40% estimated by the above method, thus our estimation method is likely conservative.

It should also be noted that shortly after the concentration decrease, the NO_3^- (and $WSOC_p$) concentration increased rapidly (Figure 3.1). This smaller mid-afternoon increase is not investigated in this analysis.

3.3.3 Photochemical $WSOC_p$ Production

For the three-day analysis period, the $WSOC_p$ concentration increased an average of 1.9 μg Carbon m^{-3} (μg C m^{-3}) over the three-hour period from 08:00 to 11:00 each day and had an average peak of 4.8 μg C m^{-3} before noon (Figure 3.1). The box model was also run to assess the contribution of SOA formation to the $WSOC_p$ concentration increase, though the methodology was different from that used in the NO_3^- analysis. In this case, since the $WSOC_p$ (or SOA) chemical production rate (R_i) is unknown, the model used measured concentrations of $WSOC_p$ aloft and conservation of mass principles to predict secondary formation. The C-130 measurements on 3/29 indicate that the average $WSOC_p$ concentration in the 1km layer directly above the BL was 0.7 ± 0.7 (mean ± 1σ) μg C m^{-3}. Using the mean of measured aloft concentrations, the model predicted that ~15% of the concentration increase was due to entrainment and roughly ~85% was due to SOA formation (Table 3.1). Similar rapid morning photochemical production of SOA has been observed previously in the MCMA [*Salcedo et al*., 2006;

Volkamer et al., 2006]. Because of the relatively large variability in the aloft $WSOC_p$ concentrations, Table 3.1 also presents box model results for aloft $WSOC_p$ concentrations of 0 and 1.4 μg C m^{-3} (mean ± one standard deviation). The results indicate that the contribution from photochemical production to the morning concentration increase was in the range of 65-100%.

The $WSOC_p$ increase from SOA formation was approximately the same relative enhancement NO_3^- experienced due to secondary photochemical formation (Table 3.1). For the entire three-day period, $WSOC_p$ and NO_3^- were highly correlated ($R^2 = 0.80$), however between 08:00 and 12:45, the correlation ($R^2 = 0.88$) was even stronger (Figure 3.3). The high correlations suggest that during these periods the sources and atmospheric processes affecting both species were likely very similar. That is, the similar contributions of entrainment and secondary formation made to NO_3^- and $WSOC_p$ concentrations help explain the high correlations. Because the contributions from biomass burning were presumed to be small, it is likely that anthropogenic sources were responsible for the majority of the observed NO_3^- and $WSOC_p$. Furthermore, the strong $WSOC_p$-NO_3^- correlation is also suggestive that OH was the primary oxidation pathway in the observed SOA formation.

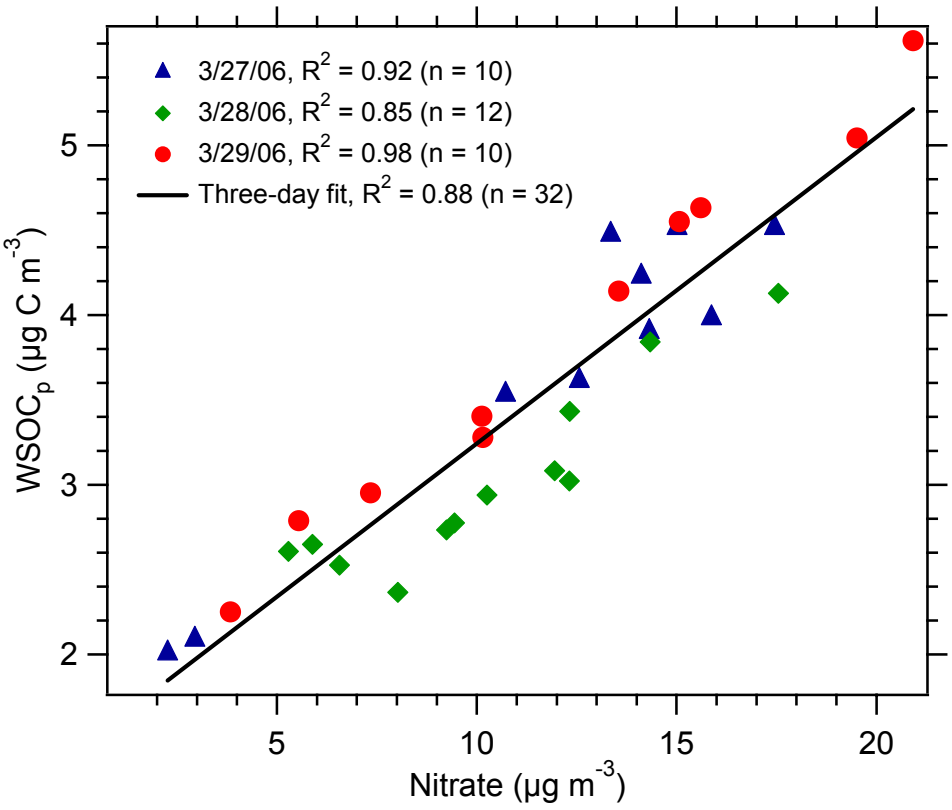

Figure 3.3 Correlations between NO_3^- and $WSOC_p$ during the hours of 08:00-12:45 on the three days of interest. The high correlation suggests similar sources and atmospheric processing of the two species.

3.3.4 $WSOC_p$ Loss

Similar to NO_3^-, the $WSOC_p$ concentration experienced a daily decrease shortly after the morning maximum. Between ~11:00 and ~12:45, the $WSOC_p$ concentration decreased an average of 2.68 µg C m^{-3}, a 56% decrease from the peak concentration. Using the average aloft $WSOC_p$ concentration (0.7 µg C m^{-3}) measured on 3/29, the box model was used to investigate $WSOC_p$ losses between 11:00 and 12:45 as well. During this time, average BL expansion was from 1100 m to 2040 m and the average $WSOC_p$ loss due to dilution was 1.99 µg C m^{-3}. $WSOC_p$ loss due to evaporation was 0.69 µg C

m^{-3}, on average, and accounted for ~25% of the observed concentration decrease. This decrease was substantial, as ~15% of $WSOC_p$ at its peak concentration (4.8 μg C m^{-3}) and ~35% of the newly formed $WSOC_p$ (1.9 μg C m^{-3}) likely volatilized (Table 3.1). Similar to the NO_3^- analysis, the production of $WSOC_p$ during the concentration decrease was ignored. Any production during this time would produce an under-prediction of the evaporation contribution to observed $WSOC_p$ losses.

Because of the high relative variation in aloft $WSOC_p$ concentrations, the box model was also run with alternate inputs (0 and 1.4 μg C m^{-3} aloft $WSOC_p$ concentrations), and the results provide an estimate of the range of $WSOC_p$ losses due to evaporation (Table 3.1). For an aloft $WSOC_p$ concentration equal to zero, the average evaporation loss was only 0.34 μg C m^{-3}. This represents less than 20% of the newly formed $WSOC_p$, and less than 10% of the peak $WSOC_p$. For an aloft $WSOC_p$ concentration = 1.4 μg C m^{-3}, the average evaporation loss was 1.03 μg C m^{-3}. This represents greater than 50% of the newly formed $WSOC_p$, and greater than 20% of the total WSOC at its peak.

3.4 Model Assumptions

Here we attempt to address and justify the major assumptions used for the modeling analyses. First, in the model assessment of NO_3^- formation, NO_2 was calculated from measurements of NO, O_3, RO_2 and J values assuming photochemical steady state. This assumption will impart added uncertainty to the estimated HNO_3 (g) formation rates, and will add uncertainty to the predictions of photochemical/entrainment contributions to concentrations. The model results predicted a higher aloft nitrate

concentration (6.4 μg m^{-3}) than that observed (1.5 μg m^{-3}), something which may be due to an under-prediction of HNO_3 (g) formation rates. If HNO_3 (g) formation rates were under predicted by this degree, the contribution of photochemical production to the morning NO_3^- increase would be greater (90-95%) than predicted levels (77%). Overall, though, both results indicate that the major factor affecting morning NO_3^- concentrations was its production through photochemical processes.

A second major assumption, necessitated by unavailable BL height, was the use of water vapor as a conservative tracer to estimate BL dilution on 3/29. Consistencies in meteorological parameters and pollutant concentrations and profiles (Figure 3.1) suggest that the BL behaved similarly on 3/27, 3/28, and 3/29. Using 4480 ppm as the aloft mixing ratio based on the C-130 observations made on 3/29, the water vapor tracer method predicted dilution values on 3/27 and 3/28 that were within 20% of those observed. This suggests that the use of water vapor to estimate dilution on 3/29 was reasonable.

Finally, the modeling of WSOC was based on aircraft measurements above the BL to determine an aloft WSOC concentration. The major assumptions in this analysis were 1) that the aircraft measurements were representative of the air entrained during BL expansion, 2) that measurements on 3/29 were representative of conditions on 3/27 and 3/28, and 3) that the WSOC in the entrained air was not volatile. First, the aloft water vapor mixing ratio used to estimate dilution on 3/29 came from measurements on the same flight, and during the same times that the aloft WSOC determinations were made. As discussed, using these water vapor values, the dilution on 3/27 and 3/28 were predicted within 20% of observed values. This suggests that the aircraft measurements

above the BL on 3/29 were representative of air that was entrained due to BL expansion on all three days. The aircraft measurements were also in fair agreement with the surface measurements during BL sampling. For approximately 40 minutes in the mid-afternoon (13:46-14:23, CST), the C-130 made measurements within the BL that included passage over T1. During this time, the ratio of mean NO_3^-, SO_4^{2-}, and WSOC concentrations measured via PILS on the C-130 to mean concentrations on the ground were 0.52, 1.01, and 0.79, respectively. Additionally, as has been stated previously, the meteorology and pollutants (magnitude of concentrations and diurnal patterns) were remarkably similar on all three days (Figure 1). Because of this, the concentrations of species mixing down with BL expansion were likely similar on each day.

The properties of WSOC in air entrained with BL expansion also add uncertainty to the model results. *Kalberer et al*. [2004] found that the volatility of chamber-generated SOA decreased significantly with time. It is likely that WSOC above the BL was aged, and thus was less volatile than the WSOC formed in the morning at the surface. If the entrained WSOC was completely volatile (or if the WSOC concentration in the entraining air was zero), then the box model results indicate that WSOC losses due to evaporation (0.34 μg C m^{-3}, average) would be roughly half (0.69 μg C m^{-3}, average) of that predicted with aloft (and non-volatile) WSOC concentration of 0.7 μg C m^{-3}. This implies a baseline case of only ~10% loss due to volatility (or only ~ 18% of the morning WSOC concentration increase), however the likelihood that either the WSOC concentration aloft was zero or the WSOC aloft was 100% volatile are both very low.

3.5 Conclusions

These findings provide insight into the semi-volatile nature of ambient SOA, an area in which knowledge is currently limited. Specifically, the results suggest that, on average, a meaningful fraction of the observed newly formed (1-3 hrs old) $WSOC_p$ mass possessed similar semi-volatile properties to NH_4NO_3 at the T and RH recorded here (Figure 3.1), though NO_3^- evaporation losses by this analysis were about 50% greater (evaporation caused 40% of total NO_3^- loss, 26% of total WSOC loss) than those of $WSOC_p$ (Table 3.1). This implies that, similar to NH_4NO_3, the loss of aerosol water affected WSOC as well. In contrast, a study by *Loeffler et al*. [2006] found that when aqueous particles containing glyoxal and methylglyoxal were evaporated, there was minimal loss of particulate organic mass due to oligomer formation. However, other studies report on a fairly volatile SOA or total organic aerosol. *Grieshop et al*. [2007] found the partitioning of fresh biogenic SOA generated in a smog chamber to be reversible when subjected to isothermal dilution, and *Wilson et al*. [2006] found the semi-volatile character of a large fraction of the organic aerosol (primary plus secondary) to be similar to that of NH_4NO_3 in filter sampling performed in both urban and rural locations. Finally, additional airborne measurements made over the sampling sites during MILAGRO have been used to investigate the production of SOA and NO_3^- by changes in concentrations with respect to CO as plumes were advected away from the urban region [*Kleinman et al.*, 2008]. They found that NO_3^- and SOA production differed; SOA was still produced relative to CO when net NO_3^- production had apparently stopped. They concluded that this was due to the more semi-volatile nature of NO_3^-, compared to SOA. Overall, the results provide novel insight into the semi-volatile nature of fresh,

anthropogenic, ground-level SOA, however their translation to other environments requires further examination.

Chapter 4

Sources and Formation of WSOC in Atlanta

In the summer of 2007, bulk measurements of water-soluble organic carbon compounds were made in the gas ($WSOC_g$) and particle ($WSOC_p$) phases. The measurements were conducted from 11 May – 19 September on the roof of the Ford Environmental Science & Technology (ES&T) building on the Georgia Institute of Technology campus in Atlanta, Georgia. In addition to $WSOC_p$ and $WSOC_g$, measurements included gas-phase formic acid, acetic acid, and oxalic acid, particulate organic carbon (OC), and meteorological parameters. All of the measurement methods are detailed in Chapter 2. Inlets were approximately 50 m above the ground. This chapter presents an overview of the WSOC results. During the month of May, intense wildfires burning in large areas of northern Florida and southern Georgia periodically influenced the air quality in Atlanta. Four such episodes were recorded from the ES&T roof, and these results are discussed in Section 4.4. Unless explicitly stated, the data presented in the remainder of this chapter do not include these biomass burning episodes.

4.1 $WSOC_p$

For the entire summer, $WSOC_p$ was in the range of 0.2 - 12.1 μg C m^{-3} and had an average concentration of 3.3 ± 1.8 μg C m^{-3} (mean ± 1σ, for n = 19051). The median $WSOC_p$ concentration was 2.9 μg C m^{-3}. $WSOC_p$ was highly correlated with OC (R^2 = 0.73) and the slope (0.70 μg C/μg C) indicates that a high fraction of the OC was likely

secondary (Figure 4.1). There was an observed temperature dependence of $WSOC_p$, which is examined in detail in Chapter 6.

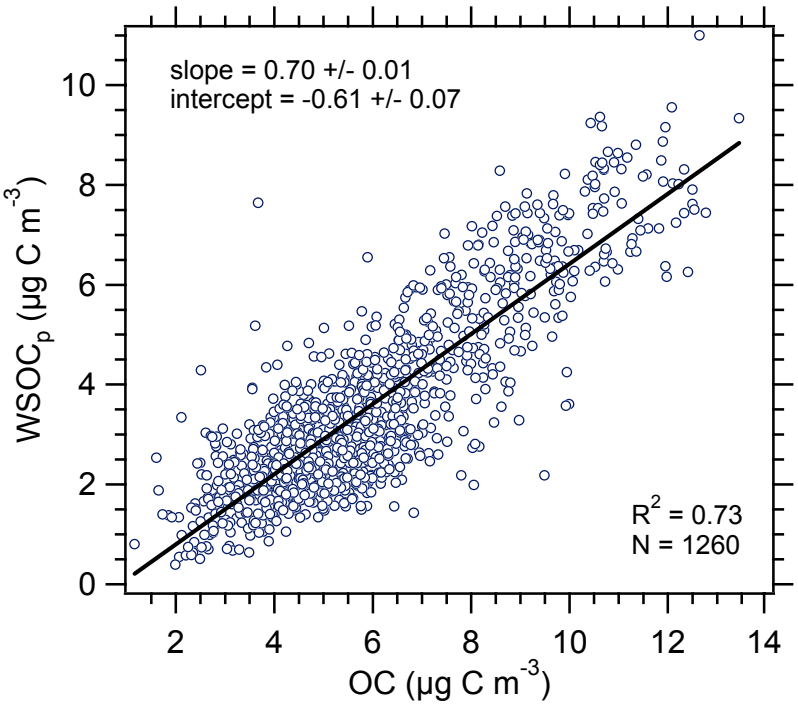

Figure 4.1 Scatter plot of $WSOC_p$ verse OC. The six-minute measurements of $WSOC_p$ were merged onto the 45-minute sample times of the OC measurement to make the comparison.

The data indicate a higher water-soluble fraction of the total OC in Atlanta than in other urban environments where simultaneous $WSOC_p$ and OC measurements were made. In St. Louis, *Sullivan et al*. [2004] observed mean $WSOC_p$/OC ratios of 0.61-0.64 during the summer and 0.31 during the fall. *Miyazaki et al*. [2006] observed mean $WSOC_p$/OC ratios of 0.35, 0.37, and 0.19 in Tokyo during the summer, fall, and winter, respectively. In the Po Valley, Italy, mean $WSOC_p$/OC ratios ranged from 0.38 in the winter to 0.50 in the summer [*Decesari et al.*, 2001]. The higher $WSOC_p$/OC ratios observed in Atlanta could indicate a source effect (i.e., the high proportion of biogenic

emissions in Atlanta), or enhanced photochemical processing compared with the other study areas. Due to the high population in Atlanta, and the extensive use of motor vehicles in and around the city, it is not likely that this effect was due to lower primary OC emissions, compared to the other study areas.

4.2 $WSOC_g$

The range of $WSOC_g$ concentrations observed for the entire summer (n = 12299) was 1.1 – 73.1 μg C m^{-3}, and mean and median $WSOC_g$ concentrations were 13.7 μg C m^{-3} and 11.8 μg C m^{-3}, respectively. While the $WSOC_g$ measurement was made for the entire summer, from September 5-20, the mist chamber samples were also analyzed for gas-phase formic, acetic, and oxalic acid. Gas phase oxalic acid concentrations were quite low throughout the two-week period; oxalic acid concentrations were above LOD (0.08 μg m^{-3}) for less than 5% of measurements. On the other hand, formic and acetic acid were present at measurable concentrations for the entire two weeks. This difference between oxalic acid and formic/acetic acid has been observed in previous studies [e.g., *Chebbi and Carlier*, 1996] and was expected, given the extreme differences in their vapor pressures. On a carbon mass basis, acetic acid concentrations were typically higher than those of formic acid (slope of acetic acid/formic acid = 1.65 μg C/μg C), but the slope of their mixing ratios was nearly 1:1 (acetic acid/formic acid = 1.08 ppb/ppb). The two were highly correlated (R^2 = 0.84, Figure 4.2), indicating similar sources.

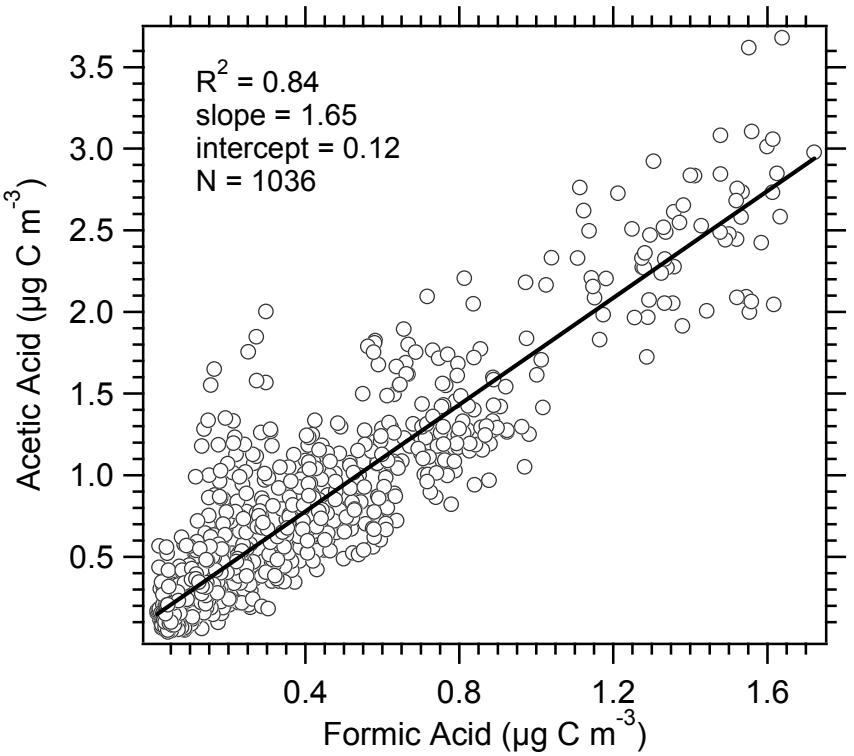

Figure 4.2 Scatter plot of gas-phase acetic acid verse formic acid for the period September 5-20.

This result is consistent with previous studies which have observed a similar high correlation between formic and acetic acid [e.g., *Khwaja*, 1995]. Figure 4.3 shows a time series of $WSOC_g$ and formic + acetic acids and in general, the two tracked relatively well ($R^2 = 0.57$, Figure 4.4).

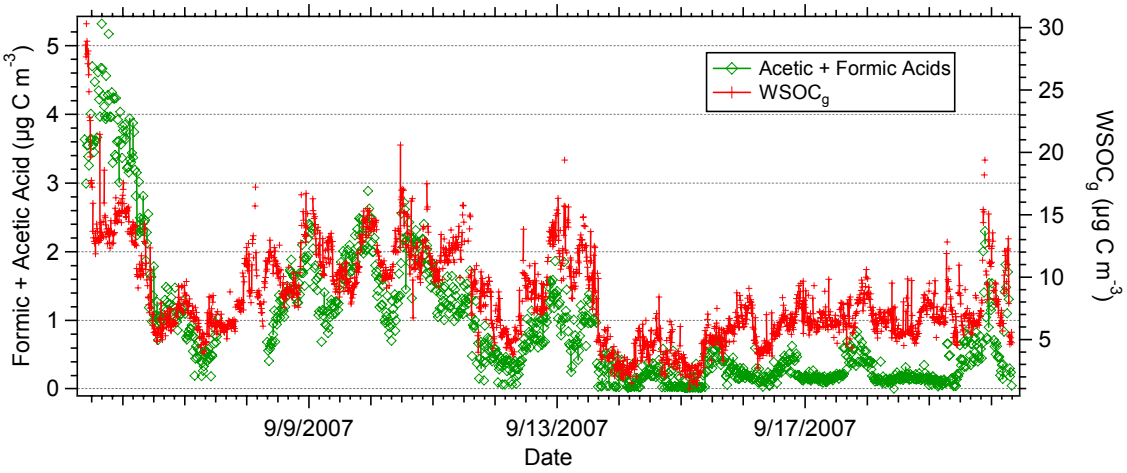

Figure 4.3 Time series of Formic + Acetic acids (left axis) and $WSOC_g$ (right axis) for the September 5-20 period.

On a carbon mass basis, formic and acetic acid together accounted for a significant fraction of the $WSOC_g$ mass. This fraction varied, but was, on average, 20% for the two-week measurement period (Figure 4.4). This stands in contrast to the chemical composition of $WSOC_p$, where identified individual compounds typically make up much smaller percentages of the total $WSOC_p$ mass [e.g., *Yang et al.*, 2005]. It is noteworthy, however, that ambient studies have found concentrations of formic and acetic acid to be the highest among all gas-phase carboxylic acids [*Chebbi and Carlier*, 1996]. In general, formic and acetic acid both showed a positive correlation with temperature, similar to that of $WSOC_g$ (discussed in detail in Chapter 6).

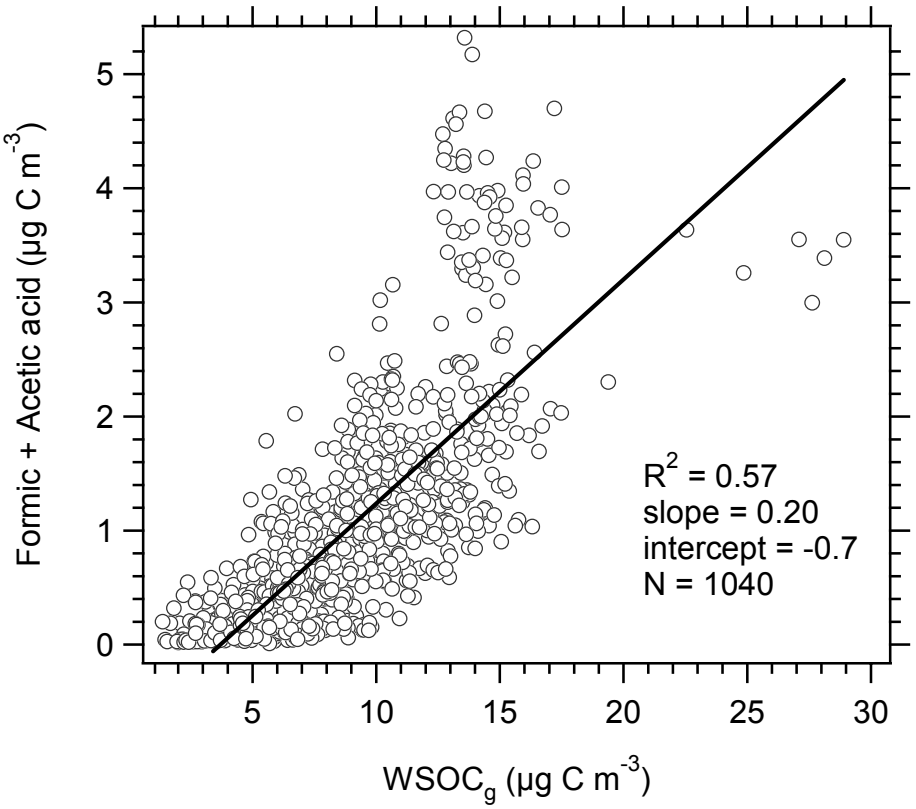

Figure 4.4 Scatter plot of gas-phase Formic + Acetic acid verse $WSOC_g$ for the September 5-20 period.

4.3 $WSOC_p$ verse $WSOC_g$

Overall, $WSOC_p$ and $WSOC_g$ were correlated during the summer, though there was a large amount of scatter in the data (Figure 4.5). Using a Deming regression analysis that minimizes the distance between the observed data and the fitted line in both the x and y directions, a slope of 0.242 and an intercept of 0.266 µg C m^{-3} were observed in the $WSOC_p$ vs. $WSOC_g$ plot.

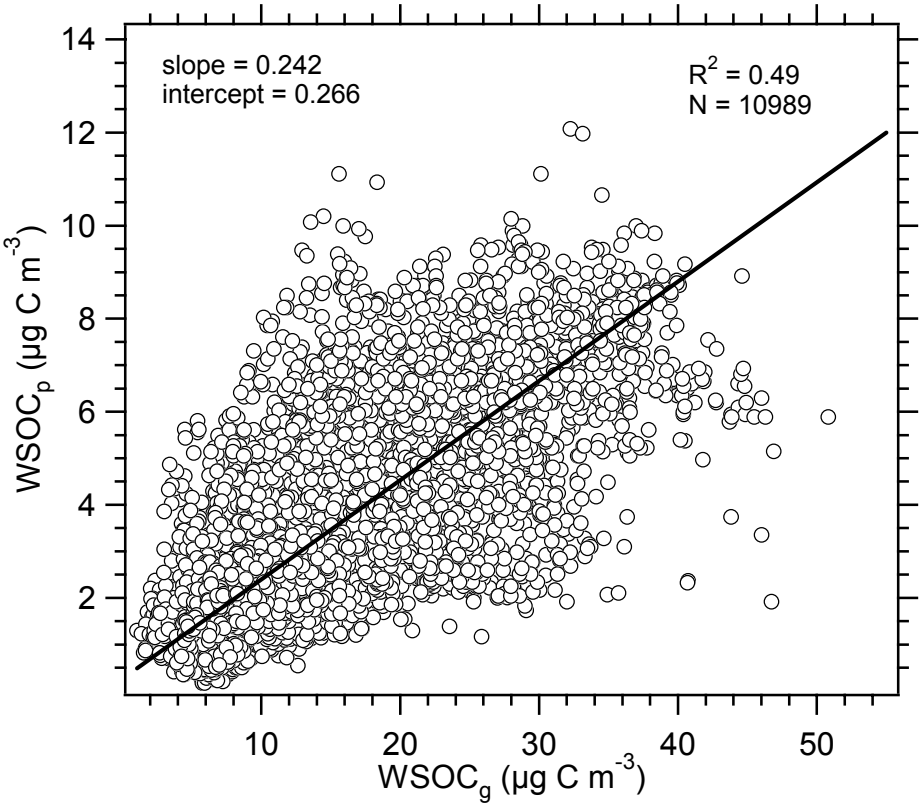

Figure 4.5 Scatter plot of $WSOC_p$ verse $WSOC_g$ for the entire summer data set.

Because $WSOC_p$ and $WSOC_g$ have oxygenated functional groups, it is expected that both have high contributions from secondary processes. In Atlanta, particle and gas-phase WSOC may come predominantly from biogenic VOCs, since they dominate the carbon emissions budget [Environmental Protection Agency, National Emissions Inventory; *Guenther et al*., 1994]. Since $WSOC_p$ and $WSOC_g$ likely share a major source (biogenic VOCs), and since both are predominantly secondary, the correlation between the two is not surprising. The large amount of scatter in the data may indicate differences that include their formation mechanisms and their atmospheric lifetimes.

The average diurnal trends of $WSOC_p$ and $WSOC_g$ are shown in Figure 4.6. Each data point corresponds to the summer-averaged data for the following hour (i.e., the data point at 05:00 represents the average data between 05:00 and 06:00). $WSOC_p$ reached an average daily maximum of 3.8 μg C m^{-3} at 14:00 (local time). This followed a steady increase in concentration from a morning minimum of 3.1 μg C m^{-3} at 06:00. Following the afternoon concentration maximum, the average $WSOC_p$ concentration decreased until it reached an average level of 3.2 μg C m^{-3} at 20:00. Between 20:00 and 06:00, the $WSOC_p$ concentration was relatively flat, as it varied only between 3.1-3.3 μg C m^{-3}. Between the hours of 06:00 and 20:00 the diurnal profiles of $WSOC_p$ and $WSOC_g$ were highly similar. The average $WSOC_g$ peak concentration also occurred at 14:00 (14.5 μg C m^{-3}) in between minima at 06:00 (12.4 μg C m^{-3}) and 19:00 (12.3 μg C m^{-3}). The mid-day increases in $WSOC_p$ and $WSOC_g$ concentrations suggests photochemical formation but the relatively modest enhancement (~20%) over pre-sunrise concentrations also suggests a substantial regional WSOC background and a relatively long lifetime of both bulk species.

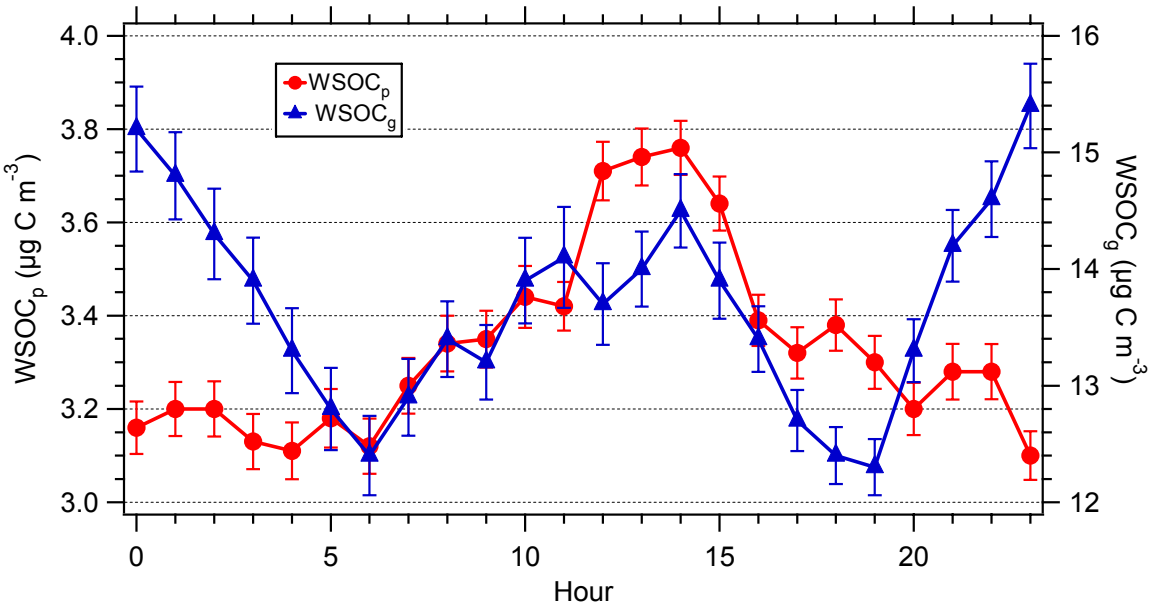

Figure 4.6 Average diurnal profiles for $WSOC_p$ and $WSOC_g$. The vertical bars on each data point represent the standard error (standard deviation/$\sqrt{N}$).

Unlike $WSOC_p$ however, the $WSOC_g$ concentration increased at night and had another maximum (15.4 µg C m^{-3}) at 23:00. On a mass basis, the major biogenic emissions in the Atlanta area are isoprene, emitted primarily by oak, and monoterpenes, which are emitted primarily by pine [*Guenther et al.*, 1994]. Emissions of isoprene from oak are positively correlated with photosynthetically active radiation [*Tingey et al.*, 1979; *Loreto and Sharkey*, 1993], while emissions of monoterpenes from pine are generally driven by temperature [*Guenther et al.*, 1993]. There have been, however, multiple field studies that observed maximum monoterpene emissions from pine to occur in the middle of the night, with minimum emissions occurring during the day [e.g., *Simon et al.*, 1994; *Hakola et al.*, 2000; *Janson et al.*, 2001]. Smog chamber experiments have demonstrated SOA formation from monoterpenes in the absence of UV from reactions initiated by ozone (O_3, called ozonolysis reactions) [e.g., *Hoffmann et al.*, 1997] and the nitrate radical (NO_3) [e.g., *Griffin et al.*, 1999]. Since monoterpenes are not soluble in water

[*Sander*, 1999], the midnight peak in $WSOC_g$ suggests oxidative reactions were occurring at night, however, the lack of a nighttime peak in the $WSOC_p$ concentration suggests that these oxidation reactions did not produce appreciable organic aerosol. Smog chamber studies by *Hallquist et al*. [1999] observed significantly lower SOA yields from the reactions of NO_3 with α–pinene, compared to reactions of NO_3 with either β–pinene, Δ^3-carene, or limonene. Additionally, nighttime chamber studies by *Griffin et al*. [1999] observed significantly lower SOA yields from the ozonolysis of β –pinene than either the ozonolysis of α–pinene or the photooxidation of β –pinene. All of this suggests that a nighttime source and reaction mechanism(s) that produces $WSOC_g$, yet little $WSOC_p$, is plausible. Although the diurnal profile did not show a nighttime peak, there was evidence for the nighttime production of $WSOC_p$. In Chapter 6, an enhancement in the partitioning of WSOC to the particle phase at RH greater than 70% is discussed. The increase in $WSOC_p$ concentrations at high RH was significant and was observed both at night and during the day. Because this phenomenon was RH-dependent, and was not specific to the time of day, the average diurnal profile of $WSOC_p$ did not show a nighttime peak.

The average diurnal profile of formic + acetic acid was similar to that of $WSOC_g$ (Figure 4.7). The formic + acetic acid concentration reached a maximum (1.2 μg C m^{-3}) near midnight, after which it declined to a minimum (0.6 μg C m^{-3}) near 06:00. With the onset of sunrise, the concentration increased steadily and peaked at 1.3 μg C m^{-3} at 14:00. Unlike $WSOC_g$, though, the concentration of formic + acetic acid remained at an elevated level throughout the afternoon and evening. Though the formic + acetic acid data only constituted a two-week period, the average diurnal profile of $WSOC_g$ during those two

weeks was consistent with that for the entire summer, suggesting that the formic + acetic acid profile was representative of the summer as well.

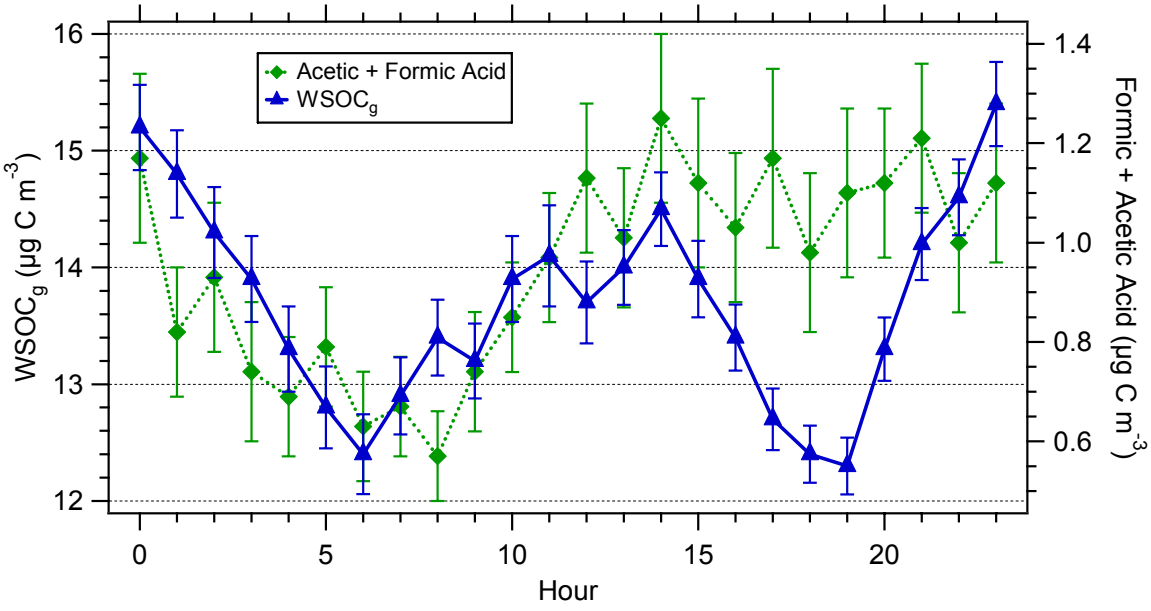

Figure 4.7 Average diurnal profiles for Formic + Acetic Acid and $WSOC_g$. The vertical bars on each data point represent the standard error (standard deviation/√N).

That the overall correlation between $WSOC_g$ and formic + acetic acid ($R^2 = 0.57$) was only moderately strong, and given the weak correlation between their average diurnal profiles ($R^2 = 0.12$, not shown), the data suggests that formic and acetic acid are not representative of the whole $WSOC_g$, though they accounted for 20% of $WSOC_g$ on a carbon mass basis. This also suggests that the partitioning behavior of WSOC may have been different from that of these light organic acids, though this question should be investigated in detail in the future.

4.4 Biomass Burning Events

From April-June, 2007, wildfires burned over 5.5E5 acres in and around the Okefenokee Swamp in southern Georgia and northern Florida [Georgia Forestry Commission, http://www.gfc.state.ga.us/]. Smoke from these fires periodically impacted Atlanta's air quality, and four such episodes were recorded on the ES&T roof. Concentrations of $WSOC_g$ in the biomass burning (BB) events were high (up to ~60 μg C m^{-3}) and were approximately equal to the highest $WSOC_g$ concentrations observed throughout the rest of the summer. For all non-BB data, the average of the top 1% of $WSOC_g$ concentrations was 41.6 μg C m^{-3}, and the highest single $WSOC_g$ concentration observed was 73.2 μg C m^{-3}. By contrast, $WSOC_p$ concentrations in the BB events were significantly higher than any ambient concentrations observed throughout the remainder of the summer. In all BB events, the $WSOC_p$ concentration reached at least 18.4 μg C m^{-3}, and in one event (5/22/07), the $WSOC_p$ concentration exceeded 50 μg C m^{-3} (Table 4.1). For non-BB data, the average of the top 1% of $WSOC_p$ concentrations was 9.3 μg C m^{-3}, and the highest single $WSOC_p$ concentration observed was 12.1 μg C m^{-3}.

Table 4.1 Summary of biomass burning events sampled on the roof of the ES&T Building during summer, 2007.

Event Date	Duration (Hr)	Maximum $WSOC_p$ (μg C m^{-3})	Maximum $WSOC_g$ (μg C m^{-3})	$WSOC_p$/ $WSOC_g$
5/16/2007	7	18.4	22.5	1.19
5/22/2007	11	53.9	64.2	0.89
5/27/2007	7.5	28.5	56.5	0.66
5/31/2007	2.5	20.5	61.7	0.90

The average $WSOC_p/WSOC_g$ ratios within each event (Table 4.1) were significantly higher than the average ratio (0.27 ± 0.12; mean ± 1σ) for the remainder of the summer.

The BB events ranged from 2.5-11 hours in length (Table 4.1) and were all marked by a very sharp onset and a much slower dissipation. Figure 4.8A shows the 5/22/2007 event and shows how rapidly WSOC concentrations could rise at the onset of events. In a period of less than 1 hour (04:06-05:00), the $WSOC_p$ concentration increased from 2.8 to 54.1 μg C m^{-3}, while the $WSOC_g$ concentration increased from 15.6 to 62.4 μg C m^{-3} over approximately the same time. $WSOC_p$ and $WSOC_g$ had strong correlations within each BB event (Figure 4.8B), and for the combined BB data ($R^2 = 0.83$, not shown).

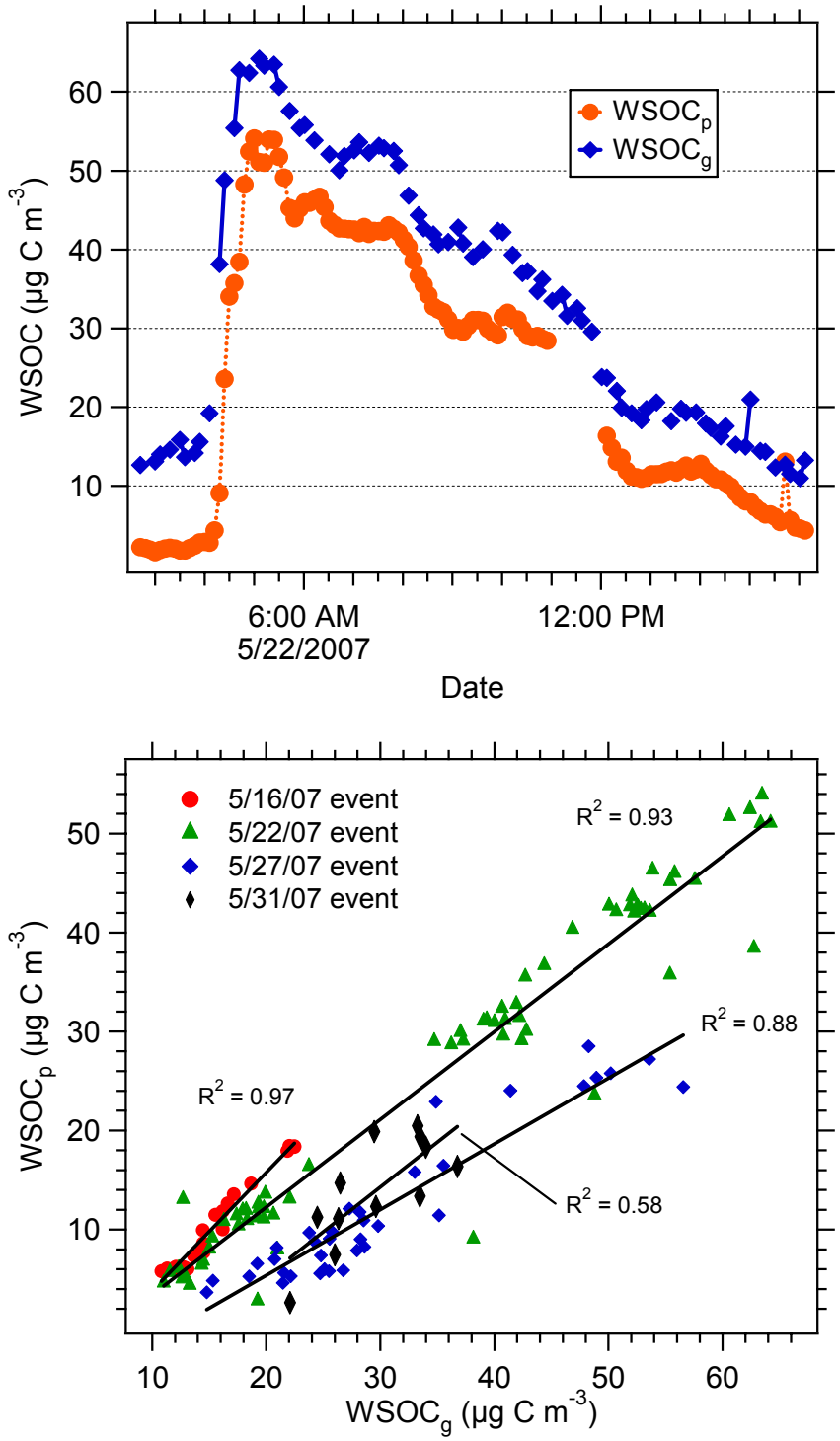

Figure 4.8 Time series of $WSOC_p$ and $WSOC_g$ concentrations for the biomass burning event sampled on 5/22/2007 (A), and $WSOC_p$-$WSOC_g$ correlations for all four biomass burning events (B).

Figure 4.8 illustrates another feature unique to the biomass burning events; relative to the $WSOC_g$ concentration, $WSOC_p$ concentrations were much higher than for non-BB data. The average $WSOC_p$:$WSOC_g$ ratio for all non-BB data was 0.27 ± 0.12 (mean ± 1σ). For the four BB events combined, the average $WSOC_p$:$WSOC_g$ ratio was 0.60 ± 0.19 (mean ± 1σ). Biomass burning is a primary source for $WSOC_p$ [*Novakov and Corrigan*, 1996; *Narukawa et al*., 1999; *Mayol-Bracero et al*., 2002; *Sullivan et al*., 2006]. In addition to the primary $WSOC_p$, *Lee et al*. [2008] observed significant concentrations of secondary $WSOC_p$ that were attributed to biomass burning, based on chemical mass balance modeling and additional chemical characterization of the $WSOC_p$. In the summertime in Atlanta, $WSOC_p$ not influenced by biomass burning is expected to be predominantly secondary and from biogenic sources [*Weber et al.*, 2007]. Since biomass burning can produce high concentrations of primary and secondary $WSOC_p$, the large discrepancy between the $WSOC_p$:$WSOC_g$ ratios of BB events and non-BB data is thus not surprising.

4.5 Conclusions

Measurements were made in the summertime in Atlanta to characterize particulate and gas-phase WSOC. $WSOC_p$ accounted for, on average, 70% of OC, and the two were correlated ($R^2 = 0.73$). $WSOC_g$ was moderately correlated with $WSOC_p$, though $WSOC_g$ concentrations were significantly higher than those of $WSOC_p$. For two weeks in the summer, gas-phase formic, acetic, and oxalic acid were measured. Oxalic acid concentrations were rarely above the detection limit, but formic and acetic acid were

present in detectable quantities throughout the two-week period. They were correlated ($R^2 = 0.84$) and together accounted for ~20% of $WSOC_g$ on a carbon mass basis.

The summer average diurnal profiles of $WSOC_p$ and $WSOC_g$ were similar between the hours of 06:00 and 20:00 (local time). Both concentrations were at a minimum in the morning and evening, and peaked around 14:00. The behavior was suggestive of photochemical sources, though the mid-day enhancements were modest (~20%) and suggested either a significant background of both concentrations, a relatively long lifetime of each species, or both. The average nighttime profiles of $WSOC_p$ and $WSOC_g$ were quite different, though. The $WSOC_p$ concentration remained relatively flat throughout the night while the $WSOC_g$ concentration peaked at approximately 23:00. The magnitude of this nighttime $WSOC_g$ peak was equal to the mid-day peak, and it suggests a nighttime biogenic VOC source that is consistent with observations from multiple ambient studies. Though the nighttime $WSOC_g$ enhancement was substantial, a nighttime peak in $WSOC_p$ was not observed. This suggests a reaction pathway that leads to oxygenated, yet volatile, products. Qualitatively, similar pathways have been observed in smog chamber experiments.

Finally, wildfires burning in southern Georgia and northern Florida influenced sampling through four distinct events at the beginning of the summer. These biomass burning events were characterized by elevated and highly correlated $WSOC_p$ and $WSOC_g$ concentrations. The maximum $WSOC_g$ concentrations were on the order of the highest ambient $WSOC_g$ concentrations observed throughout the rest of the summer. The maximum $WSOC_p$ concentrations observed in the biomass burning events were significantly higher (factor of ~2-5) than the maximum $WSOC_p$ concentrations found in

non-biomass burning air. Additionally, the $WSOC_p$:$WSOC_g$ ratios were significantly higher in the biomass burning events than they were throughout the remainder of the summer. This was attributed to the high fraction of water-soluble carbon particles emitted by the wildfires and a potentially high contribution of secondary particles from the wildfires, as well.

Chapter 5

Correlations Between Water Vapor and $WSOC_p$: a Synergistic Effect from Biogenic Emissions?

Several modeling [e.g., *Seinfeld et al*., 2001; *Pun and Seigneur*, 2007; *Chang and Pankow*, 2008] and smog chamber studies [e.g., *Edney et al.*, 2000; *Cocker et al*., 2001a, 2001b] have investigated the influence of particle-bound water on SOA formation. In general, the modeling results predict an increase in SOA formation with increased aerosol water, though the smog chamber studies did not observe an enhancement in SOA formation associated with aerosol water. Other studies suggest the enhancement of SOA by aerosol water through other means, like cloud processing [*Lim et al*., 2005], or heterogeneous reactions within fine particles [*Volkamer et al.*, 2007].

In aircraft measurements, *Peltier et al.* [2008] observed a significant water vapor-$WSOC_p$ correlation ($R^2 = 0.74$) in a plume intercepted at 3-5 km a.s.l. in the western US. This correlation was observed down wind of a region with heavy cloud coverage in an airmass with significant biogenic and anthropogenic influences. In this chapter, possible causes for periodic ground-based events in which $WSOC_p$ (SOA) and water vapor concentration were highly correlated are investigated, and the temperature-driven release of biogenic VOCs along with water-vapor is suggested as a possible cause.

5.1 The $WSOC_p$-Water Vapor Correlation

A box plot of $WSOC_p$ verse water vapor (Figure 5.1) shows that, over the range of water vapor mixing ratios observed throughout the summer, there was not a clear relationship between $WSOC_p$ and water vapor. The box plot, which was generated by

separating the data (n = 18031) into 10 equally-spaced bins according to water vapor concentration, shows median values (thick horizontal bar), 25^{th} and 75^{th} percentiles (lower and upper box bounds, respectively), and 10^{th} and 90^{th} percentiles (lower and upper whiskers, respectively) for each bin. This analysis method is a useful approach for such a large data set because it offers a better visualization of central data trends than the un-binned data, while it presents much of the data spread as well. Despite the unclear relationship between $WSOC_p$ and water vapor, there were 14 events throughout the summer in which the two were highly correlated (mean $WSOC_p$-water vapor R^2 during these events was 0.85, Table 5.1). The events were spaced throughout the summer, and occurred in four of the five months (none in May) in which measurements were made. The length of these events ranged from 10.5-45.5 hours (average = 19 h), and they accounted for ~10-15% of total sampling time (2140 hours). It is probable that even more, shorter correlation events occurred throughout the summer, but the present analysis is limited to those events that lasted at least ten hours. Because of their length, the events spanned day and night, alike, and in several events, the $WSOC_p$-water vapor correlations remained throughout an airmass change. Their frequency of occurrence and substantial length suggest that these periods could provide significant insight into ambient SOA formation in the southeastern US.

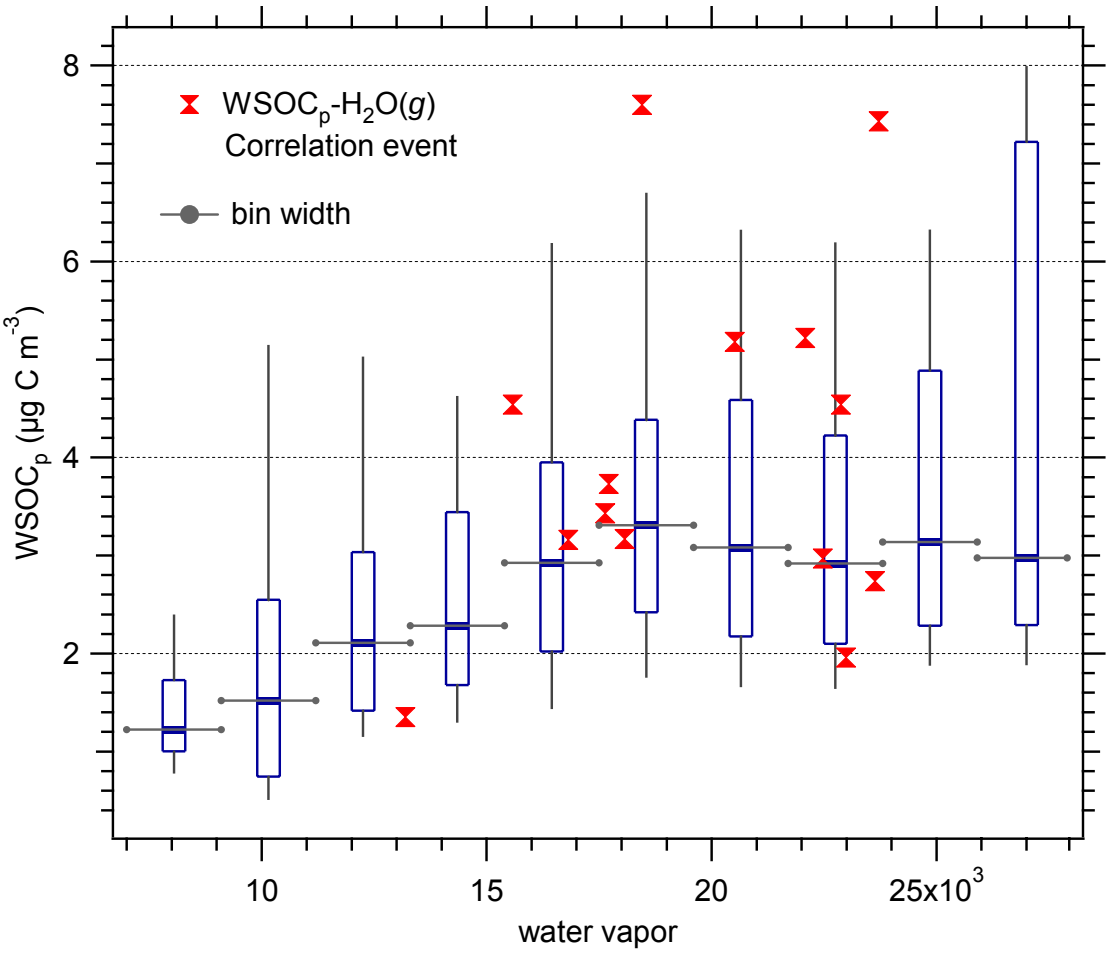

Figure 5.1 WSOC$_p$ verse water vapor for the entire summer. Also shown (markers), are the mean WSOC$_p$ concentrations and water vapor mixing ratios for the 14 events where WSOC$_p$ and water vapor where positively correlated. For the entire summer, there does not appear to be a well-defined relationship between WSOC$_p$ and water vapor, yet significant correlations between the two were observed for short periods throughout the summer.

The mean WSOC$_p$ concentration and water vapor mixing ratio for each event are also plotted in Figure 5.1. It is notable that these correlation periods were not constrained to high or low WSOC$_p$ concentrations or water vapor mixing ratios. Additionally, though there was a high correlation between WSOC$_p$ and water vapor within each event, there was no correlation between mean WSOC$_p$ concentrations and mean water vapor mixing ratios across all events. The mean WSOC$_p$ concentration in each event ranged from 1.4 –

7.6 µg C m^{-3} and the mean water vapor mixing ratio ranged from 13.2 – 23.7 x 10^3 ppm (Table 5.1). There was, likewise, a high variability of both $WSOC_p$ and water vapor concentrations within each event. For example, Figure 5.2 shows $WSOC_p$ and water vapor for the 7/12 event and shows the high variability within individual events that was routinely observed. In this event, for which the coefficient of determination (R^2) between $WSOC_p$ and water vapor was 0.85, the $WSOC_p$ concentration ranged from approximately 2 - 7 µg C m^{-3} while the water vapor mixing ratio ranged from approximately 14 - 26 x 10^3 ppm.

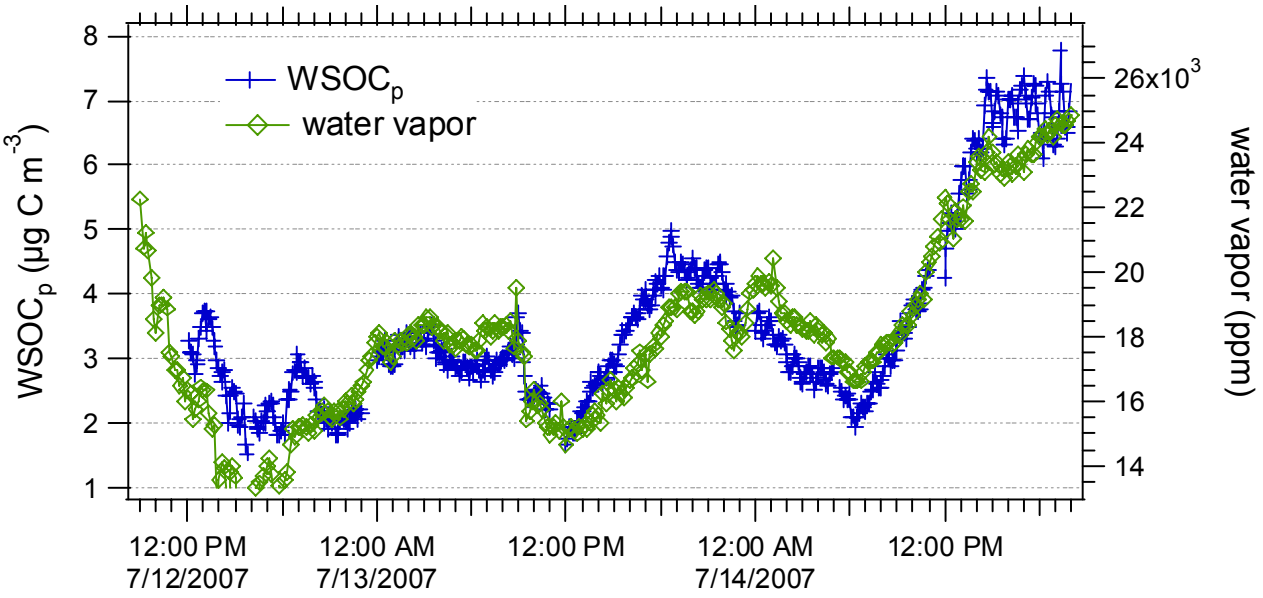

Figure 5.2 Time series of $WSOC_p$ concentration and water vapor mixing ratio for the correlation event that started on 7/12 and lasted 45.5 hours.

The correlation events were not directly related to precipitation. In the summer of 2007, Atlanta experienced severe draught conditions and had precipitation levels far-

below average, and the observed correlation events had no temporal relation with the sparse precipitation that did occur.

Water vapor, through reaction with an excited oxygen atom following ozone (O_3) photolysis, is directly involved in the primary production of the hydroxyl radical (OH) [*Eisele et al.*, 1997]. Though OH production is more sensitive to the O_3 photolysis rate, the water vapor concentration does affect OH levels as well [*Eisele et al.*, 1997]. OH is known to initiate SOA formation [e.g., *Larsen et al*., 2001], however, because it is highly reactive and because it is photochemically produced, OH concentrations decrease significantly at night, often to un-detectable levels, ($< \sim 10^5$ cm^{-3}) [*Eisele et al.*, 1997]. Only two of the 14 correlation events occurred exclusively during daylight hours. If the water vapor-OH-SOA mechanism was responsible for a $WSOC_p$-water vapor correlation, it is unlikely that this correlation would begin at night. It is also unlikely that this correlation would remain constant through daytime and nighttime periods. Seven of the observed correlation events began at night, and 12 included significant daytime and nighttime periods, suggesting that SOA formation attributed to OH, itself a product of water vapor concentrations, did not contribute significantly to the occurrence of the $WSOC_p$-water vapor correlations. Low wind speeds throughout 10 of the 14 correlation events (mean of low wind speed events = 1.5 m s^{-1}, Table 5.1) suggest that processes upwind of Atlanta did not heavily influence observations in each event either. For the four correlation events with high mean wind speeds (mean of high wind speed events = 4.4 m s^{-1}, Table 5.1), it is possible that chemistry upwind of Atlanta had an influence on observations.

Table 5.1: Start time, duration, and correlation coefficient (R^2) between $WSOC_p$ and water vapor; F_p and RH; and $WSOC_g$ and water vapor for the correlation events.

Start time[a]	Event duration (hr)	$WSOC_p$-water vapor (R^2)	F_p-RH (r)	$WSOC_g$-water vapor (R^2)
6/24/07 17:30	11.5	**0.95**	-0.85	**0.92**
6/30/07 20:30	14.5	**0.79**	0.39	0.11
7/07/07 02:30	17	**0.81**	0.43	0.36
7/07/07 20:00	15	**0.73**	**0.92**	0.27
7/12/07 20:30	45.5	**0.85**	0.41	0.01
7/18/07 18:30	16.5	**0.81**	0.35	0.03
7/21/07 19:30	12.5	**0.89**	**0.96**	0.01
7/22/07 13:30[b]	15.5	**0.92**	0.54	0.24
8/04/07 12:00	23	**0.92**	0.01	**0.72**
8/07/07 08:30	10.5	**0.82**	0.6	0.02
8/14/07 15:00	16	**0.87**	-0.86	**0.80**
8/19/07 01:30[b]	19.5	**0.84**	**0.77**	0.39
9/05/07 06:30[b]	12	**0.81**	0.53	**0.77**
9/15/07 12:00[b]	35	**0.85**	0.43	0.09
Average:	19	0.85	0.33	0.34

[a]Eastern standard time
[b]High wind speed correlation event

5.1.1 $WSOC_p$-H_2O(g) Correlation: SOA Formation and Particle Water

One hypothesis for the observed correlations between $WSOC_p$ and water vapor is that the formation of SOA is related to particle-bound water. Results in Chapter 3 and Chapter 6 have shown a link between particle-bound water and $WSOC_p$. In Mexico City, $WSOC_p$ exhibited similar behavior to aerosol nitrate, which through a thermodynamic model was shown to be directly related to aerosol water content (See Chapter 3 for complete details). The volatilization of a significant fraction (~35%) of newly formed $WSOC_p$ and nitrate shortly followed the evaporation of aerosol water, and the processes were related. In Atlanta, the partitioning of WSOC from the gas to the particle phase ($WSOC_p/WSOC_g + WSOC_p$) was increased at RH > ~70% and was attributed to the uptake of water by particles (See Chapter 6 for complete details). The RH effect on partitioning resulted in median $WSOC_p$ (i.e., SOA) concentrations above 70% RH that

were between 0.3-0.9 μg C m^{-3} higher than those predicted by WSOC partitioning behavior below 70% RH. These findings suggest that water associated with fine particles could have an important role in SOA formation that is not usually considered. It could also help explain the observed periods of high $WSOC_p$-water vapor correlation.

F_p represents the fraction of total WSOC in the particulate phase ($WSOC_p$ / $WSOC_p$ + $WSOC_g$). Because the findings in Chapters 3 and 6 suggest that aerosol water can influence WSOC partitioning, it is instructive to look at the relationship between F_p and RH during the correlation events. If the correlation of $WSOC_p$ and water vapor is related to water uptake by particles, then a positive relationship between F_p and RH may at times also be expected (most notably, when RH exceeds 70%). In three of the 14 events, there was a strong positive correlation between F_p and RH (Table 1). In 9 of the 14 events, the F_p -RH correlation was low ($r < 0.6$) and in two events, F_p and RH were negatively correlated. The strong correlation between F_p and RH in only three events suggests that a water uptake effect may have contributed to the $WSOC_p$-water vapor correlations, but that other factors likely contributed as well. Results presented in Chapter 6 identify $WSOC_p$ concentrations and NO_x concentrations as two factors that, in addition to RH, significantly impacted F_p.

The lack of a correlation between F_p and RH in some events could also be due to SOA formation that occurred sometime earlier and under higher RH conditions than those observed at the measurement site. If the SOA enhancements due to water uptake were largely non-reversible (i.e., if a significant fraction of the SOA formed due to water uptake remained after water evaporation), then $WSOC_p$ formed from this effect sometime prior to the measurement could retain a positive correlation with water vapor, while F_p

and RH retained no relation at all, depending on ambient RH at the time that measurements were made.

5.1.2 $WSOC_p$-$H_2O(g)$ Correlation: Co-Emission of SOA Precursor VOCs and Water Vapor

An alternative or additional hypothesis to explain the $WSOC_p$-water vapor correlation events is that water vapor and biogenic SOA precursors were co-emitted. $WSOC_p$ in Atlanta is predominantly secondary and biogenic [*Weber et al.*, 2007]. Water vapor is primary, and its major sources in the atmosphere are evaporation from oceanic and from terrestrial sources [*Brubaker et al.*, 2001]. Though evaporation from oceans is a major source of global water vapor, there did not appear to be a general source region effect (i.e., Gulf of Mexico or Atlantic Ocean regions) or a general circulation effect associated with the correlation events. Back trajectories were run for several points in each event and showed no consistent trends in air mass source region or trajectory shape, indicating that regional sources near Atlanta likely had the heaviest influence on the correlation events (Figure 5.3). Another major source of atmospheric water vapor is the evaporation of water from soils (evaporation) and vegetation (transpiration) [*Brubaker et al.*, 1993], known collectively as evapotranspiration. Evapotranspiration can be substantial, even producing the majority of precipitation in many continental areas [*Makarieva and Gorshkov*, 2007]. Additionally, the contribution of transpiration to the water vapor column will be highest near the surface [*Bosilovich*, 2002].

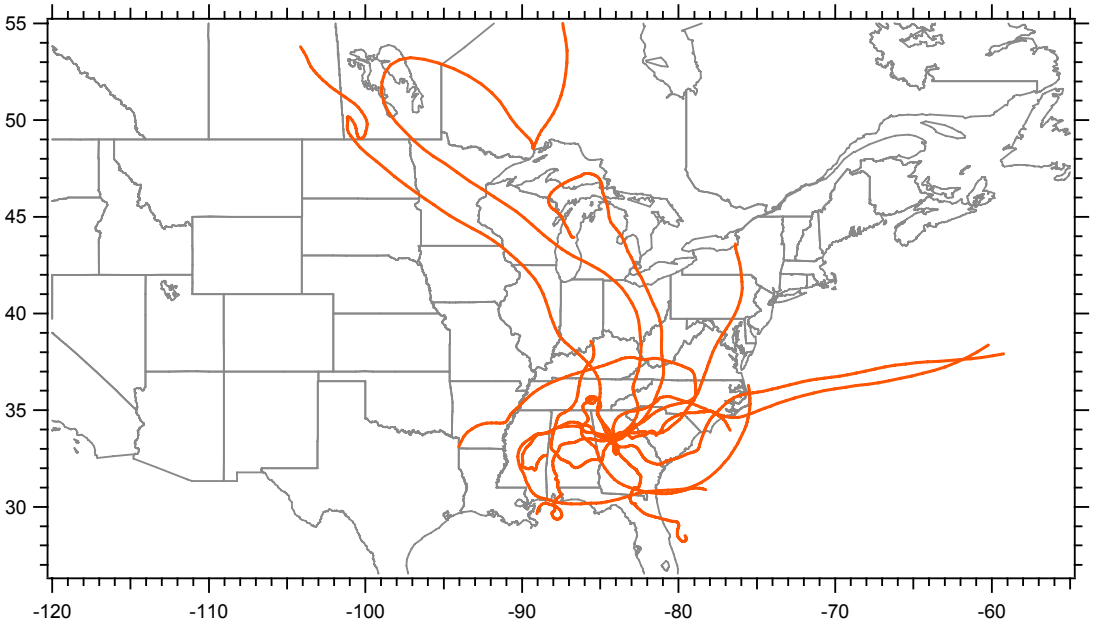

Figure 5.3 Five-day back trajectories for the events in which a high correlation between $WSOC_p$ and water vapor was observed.

Many factors influence transpiration, including temperature and solar radiation [*Kuchment et al*., 2006]. Temperature and solar radiation are also among the most important factors that affect biogenic VOC emissions [*Tingey et al*., 1979; *Tingey et al*., 1980]. Thus, the co-emission of water vapor and biogenic SOA precursors in similar proportions to each other could explain the correlation events. Major biogenic VOCs (isoprene, terpenes) are not water soluble. Rather, the oxidation of these compounds can lead to secondary products (gases + particles) that are water-soluble. Thus, if the co-emission of water vapor and biogenic VOCs was responsible for the correlation events, then a similar correlation between water vapor and $WSOC_g$ may also be expected. In four of the 14 correlation events, a significant positive correlation between water vapor and $WSOC_g$ was observed (Table 5.1). This may suggest that the co-emission of biogenic VOCs and water vapor from vegetation was at least partly responsible for the

observed correlations. The lack of a $WSOC_g$-water vapor correlation does not, however, disprove the co-emission hypothesis. It is possible that both gas and particle WSOC were initially correlated with water vapor within an airmass but, through aging processes, only the correlation with $WSOC_p$ was retained.

Temperature was highly correlated with median concentrations of both $WSOC_p$ ($R^2 = 0.91$) and $WSOC_g$ ($R^2 = 0.96$), further supporting the link between biogenic emissions and WSOC formation. Because $WSOC_p$ in Atlanta is highly biogenic and secondary in nature [*Weber et al.*, 2007], the likely reason for the positive correlation with temperature was some combination of increased photochemistry and increased biogenic VOC emissions with temperature (See Chapter 6 for more discussion of the Temperature-WSOC relationship).

Overall, the evidence suggests multiple factors contributed to the correlation events, and the co-emission of water vapor and biogenic VOCs, and an enhancement in SOA due to water uptake were the two most probable. The observations presented lead to the intriguing possibility of a synergistic role of temperature-driven emissions of biogenic VOCs and water-vapor on SOA production. Biogenic VOCs (e.g., isoprene, monoterpenes) can be oxidized to compounds that partition to the liquid phase. Higher water vapor concentrations, co-emitted with biogenic VOCs, can enhance partitioning to the liquid phase under certain atmospheric conditions (high water vapor concentration and lower T, producing high RH).

5.2 $WSOC_p$ and Combustion Emissions

Although water is released in stoichiometric proportion to carbon in efficient fossil fuel combustion, it is not likely that this mechanism had any bearing on the observed correlation events, either. In Atlanta, even using conservative (high) estimates of gasoline and diesel fuel consumption, the contribution of mobile sources to the water vapor budget is negligible (ambient water vapor concentrations are at least 3 orders of magnitude higher than can be accounted for solely from mobile combustion sources). This is somewhat paradoxical, though, because there was an observed relationship between $WSOC_p$ and EC. For the entire study, median $WSOC_p$ concentrations were correlated ($R^2 = 0.93$) with mean binned EC concentrations (Figure 5.4).

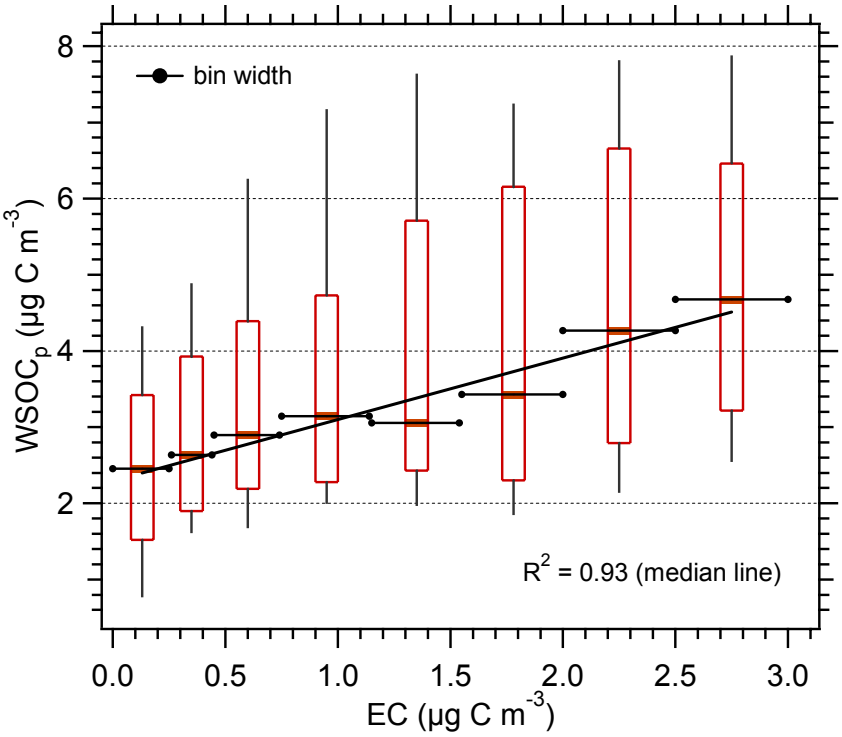

Figure 5.4 $WSOC_p$ verse EC for the entire summer. Despite the secondary nature of $WSOC_p$ and the primary nature of EC, median $WSOC_p$ concentrations show a positive correlation with EC. The P-value of the ANOVA analysis (0.0047) indicates that the correlation is statistically significant at the 99% confidence interval.

This relationship was surprising, given that $WSOC_p$, which is predominantly secondary, was far more spatially homogeneous in Atlanta than primarily-emitted EC [*Weber et al.*, 2007]. Part of the explanation for the $WSOC_p$-EC correlation may be meteorology, but that is not likely the sole explanation. Unlike $WSOC_p$, which did show a correlation with temperature, EC did not show any relationship with temperature (R^2 = 0.02, not shown). This behavior was not surprising, given that EC is primary. Concentrations of both $WSOC_p$ and EC showed negative correlations with wind speed (Figure 5a, b), though their behaviors were quite different. Median $WSOC_p$ concentrations decreased slowly with wind speed across the full wind speed range observed. From a mean bin wind speed of 0.05 to 1.1 m s^{-1}, the median $WSOC_p$ concentration decreased by 4% (from 3.20 to 3.08 μg C m^{-3}). Median EC concentrations decreased much more rapidly with wind speed. From a mean bin wind speed of 0.05 to 1.1 m s^{-1}, the median EC concentration decreased by 46% (from 1.08 to 0.58 μg C m^{-3}). Consistent with the findings of *Weber et al.* [2007], these results suggest a regional source for $WSOC_p$ compared to a local source for EC. The contribution of primary anthropogenic emissions to $WSOC_p$ is expected to be small [*Miyazaki et al.*, 2006] and likely contributed little to the $WSOC_p$-EC correlation.

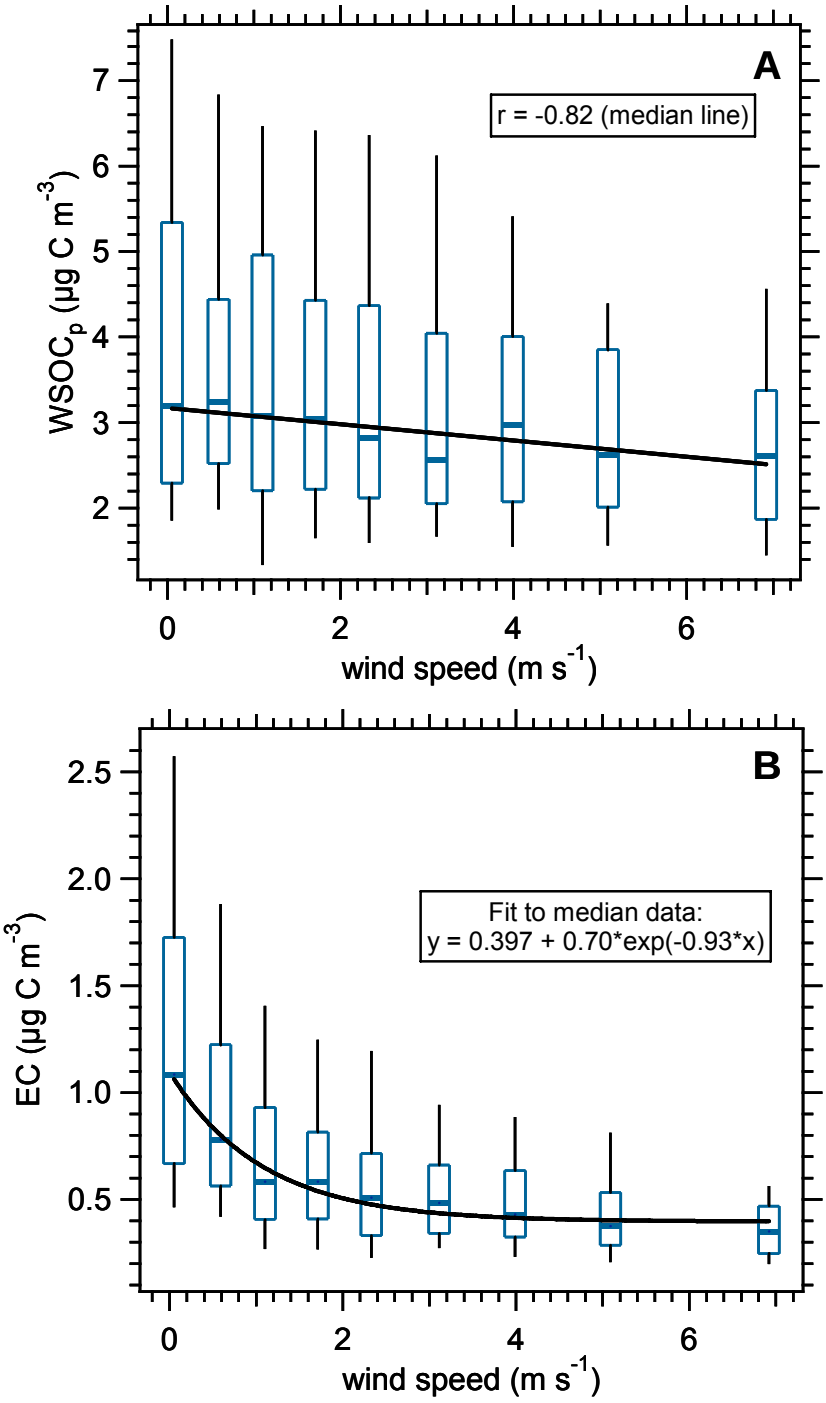

Figure 5.5 $WSOC_p$ verse wind speed (A) and EC verse wind speed (B), for data binned according to wind speed. EC concentrations decreased much more rapidly than $WSOC_p$ with increasing wind speed, indicating the heavier local influence on EC and regional influence on $WSOC_p$.

Although it is likely that their relationships with wind speed were a major cause of the $WSOC_p$-EC correlation (i.e., they are not independent variables), it is possible that other factors contributed as well. Chamber studies of biogenic SOA formation by *Lee et al.* [2004] observed significantly higher partitioning coefficients for multiple compounds in the presence of primary diesel particles above that predicted by theory. *Ervens et al.* [2008] suggest that biogenic SOA yields from cloud processing are highly influenced by NO_x levels. *Sullivan et al.* [2006] and *Weber et al*. [2007] have shown high correlations between $WSOC_p$ and carbon monoxide (CO) in plumes advecting away from urban regions, typically an indication of anthropogenic mobile emissions (in these studies biomass burning contributions were negligible, based on acetonitrile concentrations). They also found similar $\Delta WSOC_p/\Delta CO$ ratios in two areas (Atlanta, New York) with biogenic VOC levels that differed by 1-2 orders of magnitude. These studies all suggest that biogenic SOA formation can have a link to anthropogenic emissions. Thus, it is possible that the $WSOC_p$-EC correlation we observed could agree with these previous findings and suggest that in an urban environment, biogenic SOA is in some way controlled or affected by anthropogenic emissions. For example, anthropogenic emissions may be linked to this process by contributing gas or liquid phase oxidants or compounds (e.g., NO_x) that favor the gas phase production of water soluble SVOCs over other oxidized compounds, thereby enhancing water-soluble SOA production of biogenic emissions. This may be one factor, along with the temperature-dependent co-emission of water vapor and SOA precursor-VOCs by vegetation that leads to SOA production in southeastern United States.

5.3 Conclusions

Ground-based measurements of meteorological parameters, $WSOC_g$, and $WSOC_p$ were carried out in Atlanta, Georgia, from May – September 2007. Fourteen separate events were observed throughout the summer in which $WSOC_p$ and water vapor concentrations were highly correlated (average $WSOC_p$-water vapor r = 0.92), however, for the entire summer, no well-defined relationship existed between the two. The correlation events, which lasted an average of 19 hours, were characterized by both high and low $WSOC_p$ and water vapor concentrations. Several hypotheses for the correlation were explored, including heterogeneous liquid phase SOA formation and the co-emission of biogenic VOCs and water vapor. The data provide supporting evidence for contributions from both, and suggest the possibility of a synergistic effect between the co-emission of water vapor and VOCs from biogenic sources on SOA formation. Median $WSOC_p$ concentrations were also correlated with elemental carbon (EC), though this correlation extended over the entire summer. Despite the emission of water vapor from anthropogenic mobile sources and the $WSOC_p$-EC correlation, mobile sources were not considered a potential cause for the $WSOC_p$-water vapor correlations due to their low contribution to the water vapor budget. Meteorology could perhaps have influenced the $WSOC_p$-EC correlation, but other factors are implicated as well. Overall, the results suggest that the temperature-dependent co-emission of water vapor and SOA precursor-VOCs by vegetation may be an important process contributing to SOA in some environments.

Chapter 6

Gas/Particle Partitioning of WSOC in Atlanta

Current models tend to under-predict secondary organic aerosol (SOA) concentrations by a significant degree [*de Gouw et al.*, 2005]. The source of this negative model bias is highly uncertain. Explanations include unidentified SOA-producing VOCs [*Goldstein and Galbally*, 2007] and differing SOA formation mechanisms such as heterogeneous chemical reaction in clouds [*Lim et al*., 2005] or smaller haze particles [*Volkamer et al.*, 2007].

The gas/particle partitioning of organic compounds is central to the understanding of secondary organic aerosol formation. A major pathway for SOA formation is through the oxidation of hydrocarbons in the gas phase to form less volatile products. These semi-volatile products can condense and establish equilibrium between the gas and particle phase, even at levels below their saturation vapor pressures [*Pankow*, 1994a].

The partitioning coefficient, K_p, is a common parameter used to describe equilibrium gas/particle partitioning of semi-volatile organic compounds and is represented by the equation

$$K_p = \frac{C_p / M_o}{C_g} = \frac{760\ RT\ f_{om}}{10^6 MW_{om}\ \zeta\ p_i^\circ} \qquad \text{Equation 6.1}$$

where K_p has units of $m^3\ ug^{-1}$, C_p is the compound's particle-phase concentration, M_o is the mass concentration of the absorbing organic phase (including water), and C_g is the compound's gas-phase concentration. K_p can also be predicted from fundamental

properties, where R is the ideal gas constant, T is temperature, f_{om} is the organic fraction of total particulate mass, MW_{om} is the average molecular weight of the absorbing organic (and aqueous) phase, ζ is the particle-phase activity coefficient, and p_i° is the saturation vapor pressure [*Pankow*, 1994b]. In the context of this model, *Seinfeld et al.* [2001] investigated the influence of water uptake on the terms, MW_{om} and ζ. Because the molecular weight of water is significantly lower than that of any aerosol-phase organic compounds, MW_{om} will be decreased (K_p increased) with any particulate water uptake. The impact of water uptake on ζ depends on the hydrophilic character of each partitioning compound. Water will decrease ζ (increase K_p) of strongly hydrophilic compounds while it will increase ζ (decrease K_p) of strongly hydrophobic compounds. Though water uptake can have competing effects on ζ and MW_{om}, *Seinfeld et al.* [2001] found, for all five SOA systems that were modeled, increasing SOA mass with increasing RH (for $0 \leq RH \leq 80\%$).

In smog chamber studies, *Cocker et al*. [2001a] found no difference in SOA yields from the photooxidation of m-xylene or 1,3,5-trimethylbenzene with the addition of aqueous inorganic seed particles, compared to yields in the presence of dry inorganic seed, or in the absence of seed particles. *Cocker et al*. [2001b] also found a decrease in the SOA yields of α–pinene/O_3 systems when wet inorganic seed particles were present, compared to either dry inorganic seed or no seed particles present. Additionally, *Edney et al*. [2000] found no enhancement in SOA yields from toluene due to the presence of liquid water in smog chamber experiments.

Conversely, *Pun and Seigneur* [2007] showed the extreme sensitivity that certain modeled SOA systems have to liquid water content. For example, modeled SOA yields

from benzene were a factor of 3-4 higher when liquid water concentrations were 10 μg m^{-3} compared to 1 μg m^{-3}. *Chang and Pankow* [2008] propose a modified equilibrium gas/particle partitioning model that accounts for the RH effect on MW_{om} and ζ. Their results indicate that neglecting the RH effect can lead to predicted SOA concentrations that are a factor of two lower than model predictions that include the effect. Due to this potentially substantial shortcoming in predicted SOA concentrations, the above modeling studies suggest that this RH effect should be incorporated into model predictions of SOA [*Chang and Pankow,* 2008; *Pun and Seigneur,* 2007; and *Seinfeld et al*., 2001].

Water uptake may also affect partitioning through other SOA formation mechanisms, such as reactions of organic compounds in the aqueous phase. Many recent studies [e.g., *Kroll et al*., 2007; *Lim et al*., 2005] suggest that heterogeneous chemical reactions could result in significant SOA formation beyond that predicted by models. If aqueous-phase reactions, like hydration, metal catalysis, or reactions with the hydroxyl radical, were a significant source of SOA, then under equilibrium conditions adding liquid water could enhance particle-phase partitioning by increasing the capacity for these reactions to take place.

Using the same summer, 2007 data set used in Chapters 4 and 5, this analysis examines the impact of RH, and hence particulate liquid water, on the partitioning of ambient water soluble organic carbon (WSOC). This analysis also investigates other factors that may influence WSOC gas/particle partitioning, including temperature, organic aerosol mass, and NO_x and O_3 concentrations. Particulate organic compounds that are water-soluble ($WSOC_p$) have been established as a relevant and significant component in the atmosphere (see Chapter 4). The use of a single bulk measurement like

WSOC to quantify the wide range of chemical complexity comprising the organic aerosol has disadvantages and advantages. The disadvantage is that all information on properties and processes relating to specific compounds is lost. The advantage, however, is that a single (and relatively simple) measurement can be used to comprehensively quantify an important component of the ambient aerosol. In contrast, comprehensive characterization of the organic aerosol by single component analysis has not been possible due to chemical complexity.

This study extends the use of $WSOC_p$ to include the measurement of bulk water-soluble organic gases ($WSOC_g$) and examines the impact of several factors on the partitioning of ambient water soluble organic carbon. There are limitations with this non-chemically specific approach. In particular, if the chemical compositions of $WSOC_p$ and $WSOC_g$ were largely dissimilar and unrelated, then it is unlikely that any processes would be revealed and no visible trends in WSOC partitioning observed. However, clear trends in WSOC partitioning were observed throughout the summertime and these findings not only help characterize the formation of SOA in Atlanta but provide a means for simple parameterization of a complex process. Previous studies into the partitioning behavior of ambient organic compounds have looked at individual compounds or groups of compounds that comprise a very small fraction of OC mass. In this new approach to characterize the partitioning of organic aerosol, the trends we observe represent the behavior of a significant fraction of the ambient OC budget.

6.1 Partitioning Results

To investigate the partitioning of WSOC, we examine the parameter, F_p

$$F_p = \frac{WSOC_p}{WSOC_p + WSOC_g} \qquad \text{Equation 6.2}$$

which represents the fraction of total WSOC in the particle phase. Note that F_p is related to the particle/gas WSOC concentration ratio by

$$\frac{WSOC_p}{WSOC_g} = \frac{F_p}{1 - F_p} \qquad \text{Equation 6.3}$$

and can be related to a generic K_p by

$$\frac{WSOC_p}{WSOC_g} = K_p * M_o \qquad \text{Equation 6.4}$$

where M_o is the mass concentration of the absorbing organic + aqueous phase.

6.1.1 The F_p -Temperature Relationship

According to equilibrium gas/particle partitioning theory, temperature (T) imparts a strong effect on the gas/particle partitioning of organic compounds [*Pankow and Bidleman*, 1991]. Equation 6.1 suggests a positive linear relationship between K_p and T, however this relationship is diminished by the substantial temperature dependence of the saturation vapor pressure term, p_i°, in the denominator. The vapor pressures of organic

compounds approximately double for every 10 K temperature increase [*Seinfeld et al.*, 2001]. Thus, the temperature effect on partitioning in any ambient atmosphere will be dominated by the temperature effect on the individual compound saturation vapor pressures, with higher temperature favoring the gas-phase and lower temperature favoring the particle phase. A strong temperature effect on SOA formation was observed in chamber studies using anthropogenic (toluene, m-xylene, 1,2,4-trimethylbenzene) and biogenic (α-pinene) precursor VOCs [*Takekawa et al.*, 2003].

For our ambient measurements, Figure 6.1 shows a box plot of F_p verse temperature and indicates that there was not a well-defined relationship between F_p and temperature, and thus between $WSOC_p/WSOC_g$ and temperature.

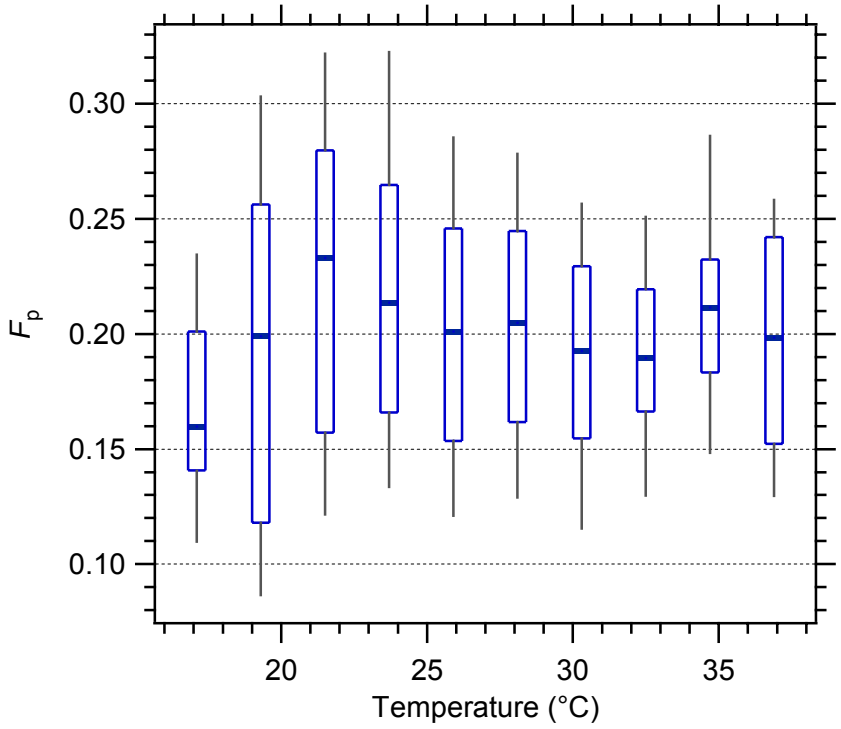

Figure 6.1 Box plot of particulate WSOC fraction, F_p, verse Temperature. The box plot was generated by segregating the data into ten equally-spaced temperature bins (average N per bin = 1040), and median values (thick horizontal bar), 25th and 75th percentiles (lower and upper box bounds, respectively), and 10th and 90th percentiles (lower and upper whiskers, respectively) for each bin are plotted.

The ambient temperature range was large enough (greater than 20°C), that any effect of temperature on WSOC partitioning should have been visible. These results appear to contradict equilibrium gas/particle partitioning theory, however, it is possible that a discernable temperature effect on partitioning was obscured by other temperature-dependent processes affecting WSOC and its precursor emissions.

Overall, median concentrations of $WSOC_p$ ($R^2 = 0.91$) and $WSOC_g$ ($R^2 = 0.97$) were highly correlated with temperature (Figure 6.2). Thus, the central tendency over the entire summer was for higher WSOC concentrations to be associated with higher temperatures. The high correlation with median concentrations accompanied with a large

amount of scatter in the overall data (evident from the spread in 10th, 25th, 75th, and 90th percentile values) implicates temperature as one of multiple factors that affected WSOC concentrations. The emissions of biogenic precursors to WSOC [*Tingey et al.*, 1980] and the photochemical formation of WSOC [*Tsigaridis et al.*, 2005] are both related to temperature. The positive effect of temperature was likely due to the role of photochemistry in WSOC formation and/or increased emissions of biogenic precursors with warmer conditions.

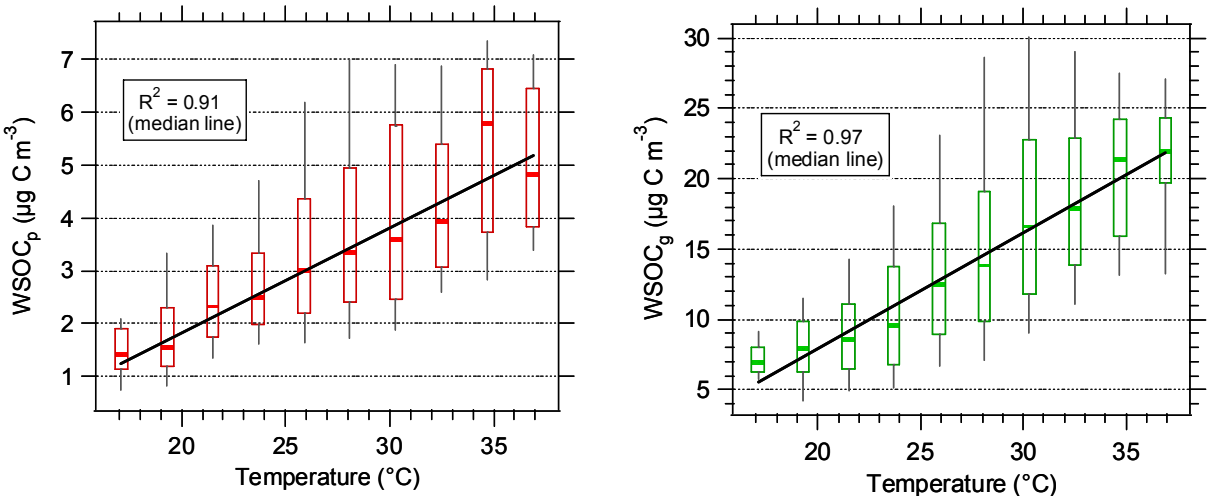

Figure 6.2 Box plots of $WSOC_p$ (A) and $WSOC_g$ (B) verse Temperature. The plots show median values (thick horizontal bar), 25th and 75th percentiles (lower and upper box bounds, respectively), and 10th and 90th percentiles (lower and upper whiskers, respectively) for each bin. For the $WSOC_p$-T plot (A), the average N per bin = 1803, and for the $WSOC_g$-T plot, the average N per bin = 1165.

It is possible that a temperature effect on WSOC gas/particle partitioning did exist, but was not visible due to the relationships $WSOC_p$ and $WSOC_g$ exhibited with temperature (Figure 6.2). The slopes of the median $WSOC_p$-T and the median $WSOC_g$-T correlation lines were 0.199 µg C/m^3/°C and 0.821 µg C/m^3/°C, respectively. If background concentrations of $WSOC_p$ and $WSOC_g$ are both assumed zero, then, using the median

relationships, a nominal temperature change would produce a constant F_p value of 0.195, which compares closely with the mean F_p for the entire study (0.203). This supports the view that a temperature-partitioning effect was obscured and highlights the dynamic nature of the ambient system in which measurements were made. Specifically, an increase in temperature led to additional inputs of WSOC (particle and gas) into the system that made a true determination of a specific temperature effect on partitioning ambiguous. This difficulty with ambient sampling underscores the need to pair ambient measurements with controlled laboratory experiments that can isolate experimental variables.

6.1.2 The F_p-Organic Carbon Concentration Relationship

Equation 6.1, along with extensive chamber experimental results [*Odum et al.*, 1996], also suggests that the mass concentration of the absorbing organic phase, M_o, will impact equilibrium gas/particle partitioning. The relationship suggests that, at a given temperature, a higher M_o will lead to a higher fraction of a partitioning compound in the particle phase due to a greater capacity (i.e., surface area or volume) of absorbing medium for the partitioning of SVOCs. The total OC concentration was used because of the strong dependence of SOA yields and partitioning on the total concentration (by mass) of organic aerosol in smog chamber studies [*Odum et al.*, 1996], and the high predictive capabilities of this method when used for subsequent smog chamber experiments of SOA formation from complex VOC mixtures [*Odum et al.*, 1997]. For these reasons, this formulation has been widely applied to air quality models, but these data suggest this may not be appropriate in all environments. Figure 6.3 shows a box plot

of F_p verse OC mass and suggests that, for the entire summer, an F_p-M_o (i.e., F_p-OC) relationship did not exist.

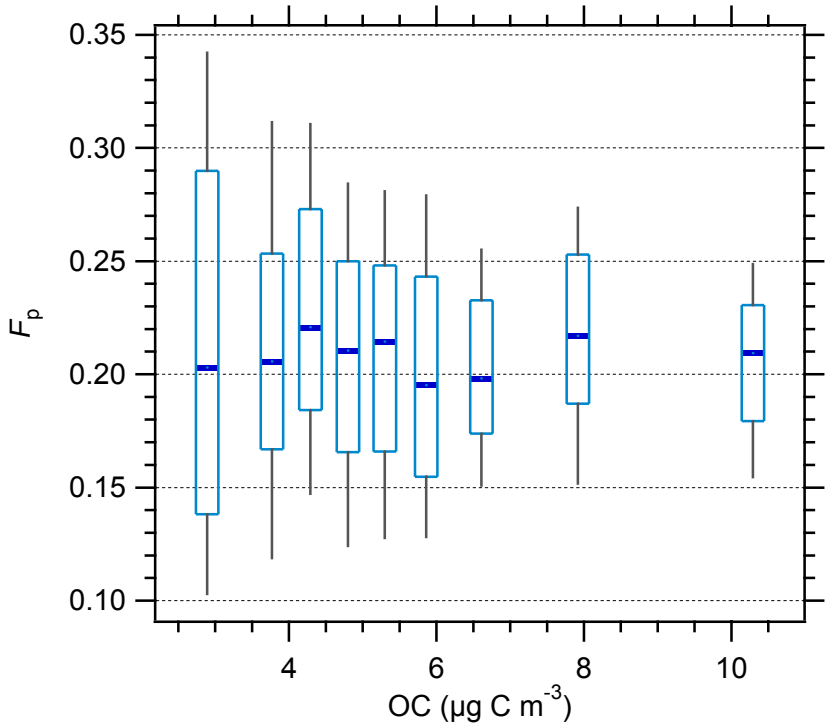

Figure 6.3 Box plot of particulate WSOC fraction, F_p, verse OC concentrations. The plots show median values (thick horizontal bar), 25th and 75th percentiles (lower and upper box bounds, respectively), and 10th and 90th percentiles (lower and upper whiskers, respectively) for each bin (average N per bin = 139).

Following the traditional line of thinking on SOA formation, because F_p describes the partitioning of only water-soluble carbon compounds, $WSOC_p$ may be a more appropriate partitioning medium than OC due to the higher chemical similarities between $WSOC_p$ and $WSOC_g$ compared to similarities between OC and $WSOC_g$. This greater similarity arises because $WSOC_p$, and presumably $WSOC_g$, are predominantly secondary, while OC is comprised of significant fractions of both secondary and primary components. Alternatively, heterogeneous reactions involving $WSOC_p$ would also be expected to

make investigating F_p relative to $WSOC_p$ a more appropriate parameter than OC. Figure 6.4 shows F_p as a function of the $WSOC_p$ concentration, and shows an observable relationship between F_p and $WSOC_p$, compared to no relationship between F_p and OC (Figure 6.3).

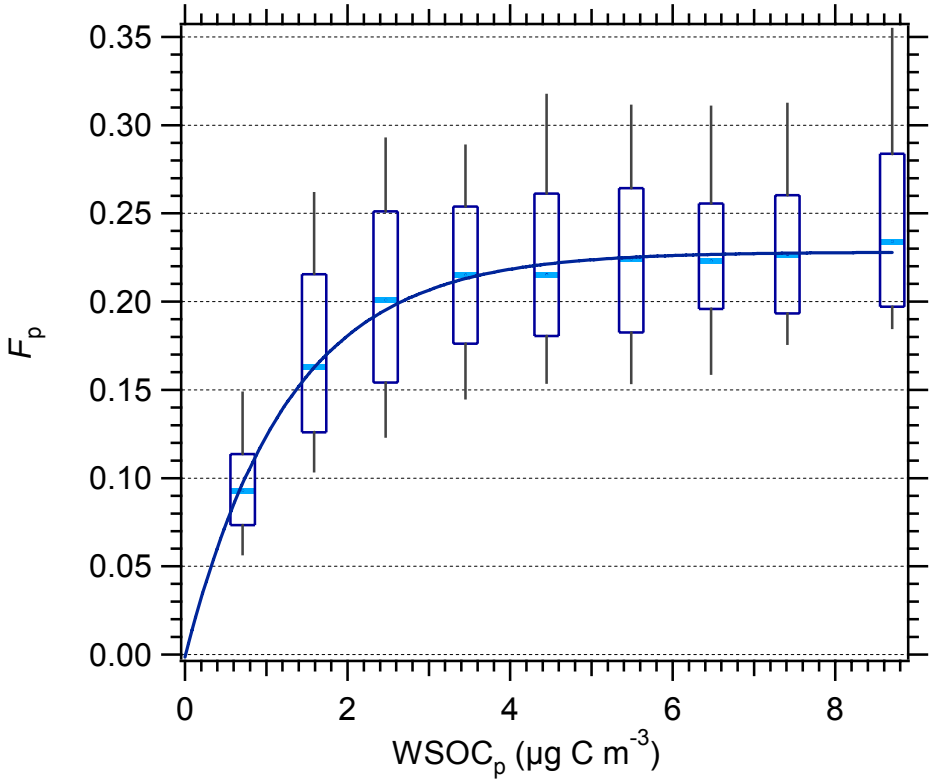

Figure 6.4 Box plot of particulate WSOC fraction, F_p, verse $WSOC_p$ concentrations. The plots show median values (thick horizontal bar), 25th and 75th percentiles (lower and upper box bounds, respectively), and 10th and 90th percentiles (lower and upper whiskers, respectively) for each bin (average N per bin = 1220).

Using $WSOC_p$ concentrations as the mass of the absorbing organic phase, the plot of F_p verse $WSOC_p$ (Figure 6.4) does suggest a relationship between gas/particle partitioning and existing organic aerosol mass. However, a dependence is only seen for $WSOC_p$ concentrations below ~4 µg C m^{-3}. In this region, higher $WSOC_p$ concentrations are

associated with a higher fraction of total WSOC partitioned in the particle phase. This relationship appears to diminish and end at $WSOC_p$ above ~4 μg C m^{-3}. It is unknown if this transition at roughly 4 μg C m^{-3} is unique to the Atlanta atmosphere or if it represents a more general process. Because the magnitude of $WSOC_g$ is much larger than $WSOC_p$ (Equation 1), it is likely that the relationship depicted in Figure 8b results from the partitioning process, and is not an artifact of the F_p calculation.

Since F_p and $WSOC_p$ are related by Equation 6.2, a relationship between the two is not surprising. There is the possibility that the behavior of Figure 6.4 was an artifact of the F_p-$WSOC_p$ dependence. Because $WSOC_p$ and $WSOC_g$ also had an observed dependence (Figure 4.5), this relationship is central to determining whether the observed F_p -$WSOC_p$ behavior was real or was an artifact. When using the Deming fit for relating $WSOC_p$ and $WSOC_g$ (slope = 0.242, intercept = 0.266), plotting F_p in this manner results in a completely different curve from the one that was observed. A similar curve is only obtained when there is a significant (< ~-0.4 μg C m^{-3}) negative y-intercept. The data does not suggest that this is the case (a positive y-intercept was observed for the Deming regression and for a standard least-squares linear regression), but the possibility should be acknowledged. A similar mathematical dependence exists in the *Odum et al*. [1996] results, where the Yield, which itself is calculated as the organic aerosol mass (M_o) formed divided by the total amount of VOC reacted, is positively related to M_o. In the unlikely event that the curve in Figure 8b was an artifact of a mathematical relationship (Equation 6.3), though the data suggests an effect of $WSOC_p$ on WSOC partitioning, then it would signify no relationship between WSOC partitioning and organic aerosol mass concentration (either OC or $WSOC_p$).

The general trends in data and fit of Figure 6.4 are similar to the smog chamber SOA Yield-M_o relationship found by *Odum et al*. [1996], where in that case M_o was OC mass formed in the chamber. A key difference between the ambient F_p -$WSOC_p$ trend and that of the chamber Yield-OM is that the F_p-$WSOC_p$ dependence appears to end at some point, whereas the Yield-OM dependence for chamber data always shows some OM effect.

The differences between the F_p-$WSOC_p$ trend and that of F_p-OC may be due to composition differences between the two systems and may suggest that the chemical nature of the absorbing organic phase is a meaningful parameter to the partitioning process. Indeed, *Seinfeld et al*. [2001] found a similar effect with water uptake; partitioning of hydrophilic compounds to the particle phase was enhanced by particulate water uptake while that for hydrophobic compounds was diminished by water uptake. Our results are also in general agreement with that of *Bowman and Karamalegos* [2002], who found a compositional effect on SOA mass concentrations in model simulations based on the affinity between partitioning SVOCs and the absorbing organic phase (i.e., due to the effect of the composition-dependent activity coefficient, ζ, on K_p). In a heterogeneous SOA formation chamber experiment, *Volkamer et al*. [2008] found a relationship between the gas/particle partitioning of C_2H_2-OH products (e.g., glyoxal) and the existing organic aerosol composition.

It is of note that the differences in F_p verse $WSOC_p$ and OC were present despite a high observed correlation between $WSOC_p$ and OC (Chapter 4.1), and despite $WSOC_p$ accounting for, on average, 70% of OC. This implies that approximately 30% of OC was insoluble in water, and similarities between this water-insoluble organic carbon fraction

and the EC diurnal profiles suggest that these insoluble organic compounds (calculated as OC-$WSOC_p$) were largely primary (Figure 6.5). These primary compounds are chemically much different from $WSOC_p$, including significant differences in oxidation, functional groups, and polarity [*Saxena and Hildemann*, 1996]. This primary component of OC, and its highly different chemical character from that of WSOC, may explain the lack of an F_p dependence on OC.

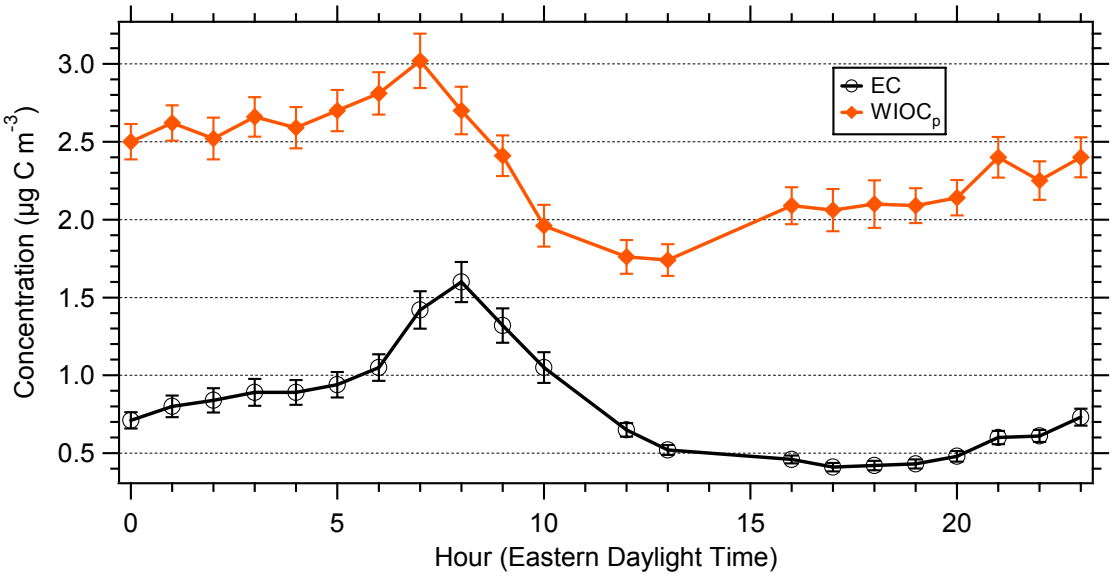

Figure 6.5 Average diurnal profiles of EC and water-insoluble OC. Water-insoluble OC was not measured directly, but was calculated as OC – $WSOC_p$.

6.1.3 The F_p -Relative Humidity Relationship

The relationship between F_p and relative humidity (RH) (Figure 6.6) shows compelling evidence for a strong RH effect on WSOC partitioning. The data showed increased particle-phase partitioning when the ambient RH was at or above 70% and, as will be shown, suggest the uptake of water by particles was responsible for this enhancement. Below 70% RH, F_p showed little variation, with a mean value of 0.190 ±

0.005 (mean ± 1σ for the five median values). At RH greater than or equal to 70%, F_p rose sharply with RH and reached a maximum of 0.305 at RH greater than or equal to 90%. This indicates that the fraction of WSOC in the particle phase increased by more than 50% at the highest RH levels, compared with that below 70%. To quantify this impact on increased SOA mass concentration, ΔF_p was calculated for each of the three bins above 70% RH. ΔF_p was defined as the difference between the bin median F_p and 0.190, the mean F_p below 70% RH. ΔF_p was multiplied by the median total WSOC concentration for each bin to provide the additional SOA concentration. Shown in Table 6.1, the partitioning shift resulted in a substantial increase in SOA mass concentrations. For the RH range of 70-79%, the SOA enhancement was 0.3 μg C m^{-3}. For 80-89% RH, the SOA enhancement was 0.6 μg C m^{-3}, and for values above 89% RH, the SOA enhancement was 0.9 μg C m^{-3}.

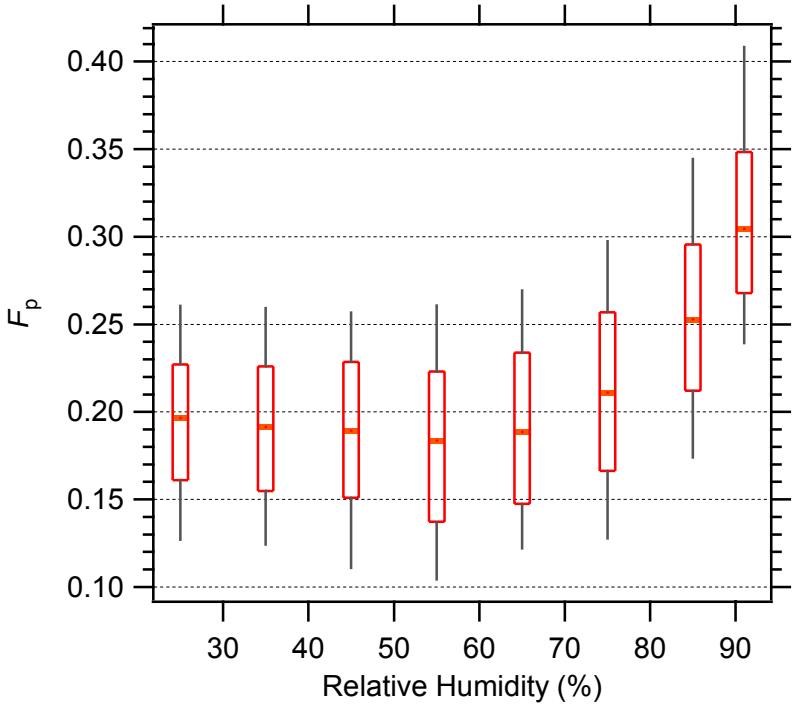

Figure 6.6 Particulate WSOC fraction, F_p, as a function of RH. The data were binned according to RH, and median (thick horizontal line), 25th and 75th percentiles (lower and upper box), and 10th and 90th percentiles (lower and upper whiskers) are shown for each bin (average N per bin = 1374).

Table 6.1 also illustrates that the median total WSOC concentration decreased as RH increased. This phenomenon was a product of the positive relationship $WSOC_p$ and $WSOC_g$ each exhibited with temperature (Figure 6.2). Because temperature and RH are inversely related, the positive correlations between temperature and both WSOC species translated into negative correlations with RH. Despite decreasing total WSOC concentrations with RH, the enhanced SOA concentrations at high RH were significant. The SOA increases at high RH levels represent values on the order of 10-25% of the mean summer $WSOC_p$ concentration. $WSOC_p$ accounted for, on average, 70% of OC, so the added SOA signifies a meaningful contribution to OC as well.

Table 6.1: Increases in F_p for RH >= 70% compared to lower RH (ΔF_p), median total WSOC ($WSOC_p$ + $WSOC_g$), and the resulting estimated SOA enhancement.

Bin mid-point RH	ΔF_p	Total WSOC[a]	SOA enhancement[a]
75%	0.021	13.4	0.3
85%	0.063	10.3	0.6
92%	0.115	7.8	0.9

[a]units of μg C m^{-3}

The distinct relationship between F_p and RH implicates aerosol water uptake as the likely cause for the observed enhancement in particle-phase partitioning. Figure 6.7, which shows the RH dependence of median F_p values, modeled aerosol liquid water concentrations, and an indirect measure of water uptake by ambient aerosol, supports this assertion. The liquid water concentration was predicted with the ISORROPIA-II thermodynamic equilibrium model [*Fountoukis and Nenes*, 2007], using mean sulfate, nitrate, and ammonium concentrations from the August 1999 Atlanta Supersite data [*Solomon et al*., 2003]. Though the model does not consider the effect of organics on water uptake, the high inorganic concentrations (sum = 14.7 μg m^{-3}) and large mass fraction of $PM_{2.5}$ suggest that the model results provide a reasonable estimate of the hygroscopic behavior of typical aerosol for the Atlanta summertime. The *Malm and Day* [2001] data represent a measure of f(RH), the enhancement in light scattering as a function of RH that is attributed to water uptake. These particular data had an inorganic/organic mass ratio of ~1, and thus in a relative sense, were compositionally similar to Atlanta aerosol as well. Their data show a flatter region below ~50% RH, compared to the model results, and are in better qualitative agreement with our observations of F_p.

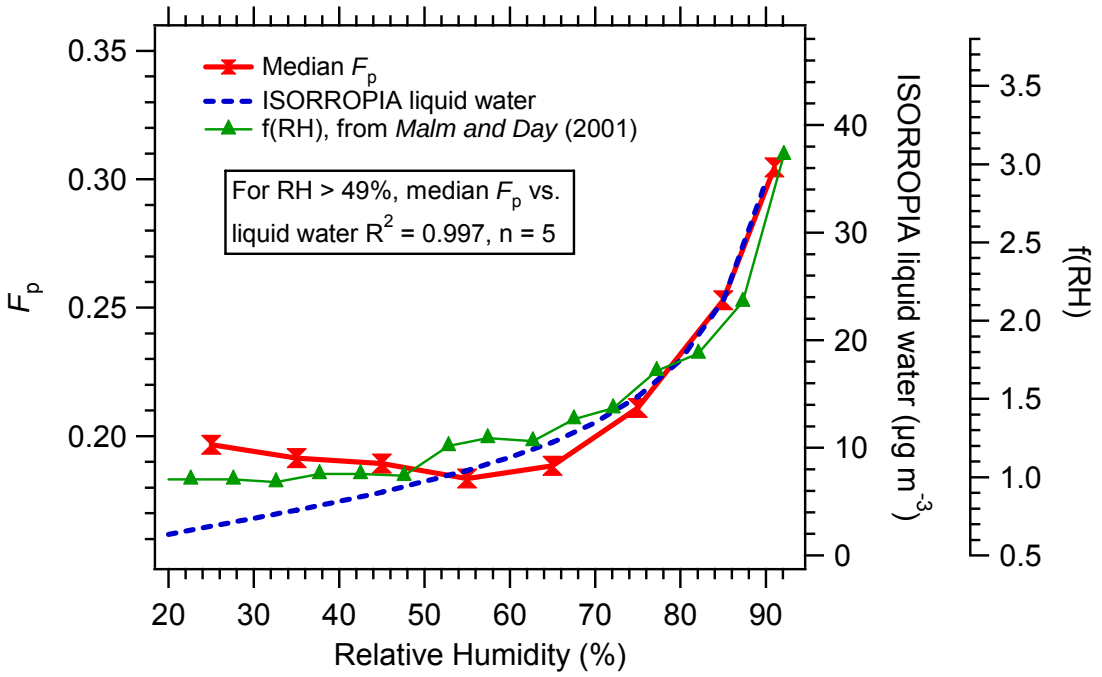

Figure 6.7 RH dependence of median particulate WSOC fraction, as well as modeled (from ISORROPIA-II) and observed (using scattering enhancement, f(RH), from *Malm and Day* (2001)) water uptake for aerosol with composition representative of that for the Atlanta summertime.

The similarities in the RH dependences of F_p, modeled aerosol water, and ambient aerosol water uptake above 55% RH in Figure 6.7 are striking. These similarities suggest that the increase in particulate condensed water with increasing RH was responsible for the observed increase in F_p. It is possible, however, that the F_p-RH relationship was actually a byproduct of a relationship between F_p and some other variable related to RH, although this seems unlikely. For example, the production of semi-volatile organic compounds (SVOCs) that partition to the aerosol phase involves the hydroxyl radical (OH) concentration, which depends on water vapor concentrations (although not RH). Consistencies in the day/night partitioning behavior of WSOC (Figure 6.10B) and the strong similarities between F_p and modeled and observed water uptake (Figure 6.7)

suggest that the F_p -RH relationship of Figure 6.6 is most directly explained by partitioning of $WSOC_g$ into particulate water. Because water uptake is largely determined by inorganic salts [*Malm and Day*, 2001], these findings suggest that inorganic aerosol have an indirect role in SOA formation. This does not, however, suggest a correlation between major inorganic components and SOA. Rather, because of persistent and appreciable inorganic salt concentrations typically present in Atlanta [*Weber et al*., 2003b], the seeds for water uptake exist nearly all of the time.

These results are consistent with our previous findings (presented in Chapter 3) that showed a link between aerosol water and both $WSOC_p$ and secondary nitrate production [*Hennigan et al*., 2008]. In that study, the formation of relatively fresh (~ 2-3 hours) $WSOC_p$ in a region of predominantly anthropogenic emissions was also likely related to aerosol water, as was nitrate, in agreement with known nitrate thermodynamic properties. In Mexico City, we found $WSOC_p$ and nitrate production in the morning during periods of high aerosol liquid water concentrations (~20 μg m^{-3}). However, changes in ambient conditions, which led to the sudden evaporation of most particle-bound water, were shortly followed by the volatilization of some fraction (~10-20%) of $WSOC_p$ and a more significant fraction of the nitrate (~30%). Though the Chapter 3 findings and the present analysis both show a link between $WSOC_p$ and aerosol water, this present study does not assess the reversibility of the observed partitioning enhancement. The question of reversible partitioning is a significant one and will be explored in future studies. Overall, though, the Atlanta and Mexico City results indicate that WSOC partitioning to liquid water occurs in urban regions dominated by biogenic or anthropogenic emissions.

Our results also qualitatively agree with the findings of *Seinfeld et al.* [2001] and *Pun and Seigneur* [2007], which demonstrated through model simulations the positive impact of particle water on SOA formation. In general, the present results disagree with the findings of *Cocker et al*. [2001a, 2001b] and *Edney et al*. [2000], who found no SOA enhancements due to particle water in smog chamber experiments. One explanation for this difference is that heterogeneous chemical reactions could have contributed to the partitioning effect observed in ambient measurements. It is possible that the enhanced particle-phase partitioning associated with water uptake in the current study was a product of additional organic reactions in the particle phase. It is likewise possible that experimental conditions (i.e., high chemical and water purity, scavenging of gas-phase OH, high aerosol loadings, O_3 concentrations, etc.) used in the smog chamber studies were not conducive to heterogeneous reactions.

The strong evidence for a WSOC partitioning dependence on liquid-water suggests a process more consistent with Henry's law-type partitioning of SVOCs to particle-water. This alone, however, also fails to describe the observations since the liquid water concentrations associated with fine particles are likely too small to simply dissolve the observed WSOC mass partitioned to fine particles. For example, the increased dissolved aerosol mass of a highly soluble and relatively abundant compound (e.g., formic acid at 5 $\mu g\ m^{-3}$) at an RH of 90% (~ 35 $\mu g\ m^{-3}$ liquid water) compared to that at 40% (~7 $\mu g\ m^{-3}$ liquid water) is ~10^{-5} $\mu g\ m^{-3}$. Aqueous phase conversion of dissolved SVOCs leading to further Henry's law partitioning to the particle phase may better account for the observed $WSOC_p/WSOC_g$ enhancements. Alternatively, larger $WSOC_g$ species may partition far more than currently thought.

6.2 Factors causing Variability in F_p

The high variability observed in the graph of F_p verse RH (Figure 6.6) also suggests that a number of additional factors influence the partitioning of WSOC compounds. Across all of the RH bins, the 10th to 90th percentile range was consistent, and averaged 0.155 ± 0.015 (mean ± 1σ). From our data set, two major factors were found; the $WSOC_p$ concentration and NO_x concentration.

6.2.1 *$WSOC_p$ Concentration and F_p Variability*

As shown above (Figs 6.3 and 6.4), F_p was not influenced by OC, but was affected by $WSOC_p$ when concentrations were below ~ 4 μg C m^{-3}. Figure 6.8 shows the relationship between mean F_p values and RH for different concentration regimes of OC (A) and $WSOC_p$ (B). When the data were sorted according to OC concentrations, there was little variation in mean F_p values plotted against RH (Figure 6.8 A) for high OC concentrations (top 35% of data, average OC = 8.2 μg C m^{-3}) compared with low OC concentrations (bottom 35% of data, average OC = 3.7 μg C m^{-3}). Of the five points plotted, only two (40% RH, and 88% RH) were statistically different at the 95% confidence interval.

When the data were sorted according to $WSOC_p$ concentrations, however, there was a substantial difference in mean F_p values plotted against RH (Figure 6.8 B) for high $WSOC_p$ concentrations (top 35% of data, average $WSOC_p$ = 5.3 μg C m^{-3}) compared with low $WSOC_p$ concentrations (bottom 35% of data, average $WSOC_p$ = 1.7 μg C m^{-3}). All of the eight points plotted were statistically different at the 99.9% confidence interval.

Note that this high verse low $WSOC_p$ range spans the transition at ~ 4 μg C m^{-3} in Figure 6.4 (i.e., the transition from a F_p -$WSOC_p$ dependence to no dependence).

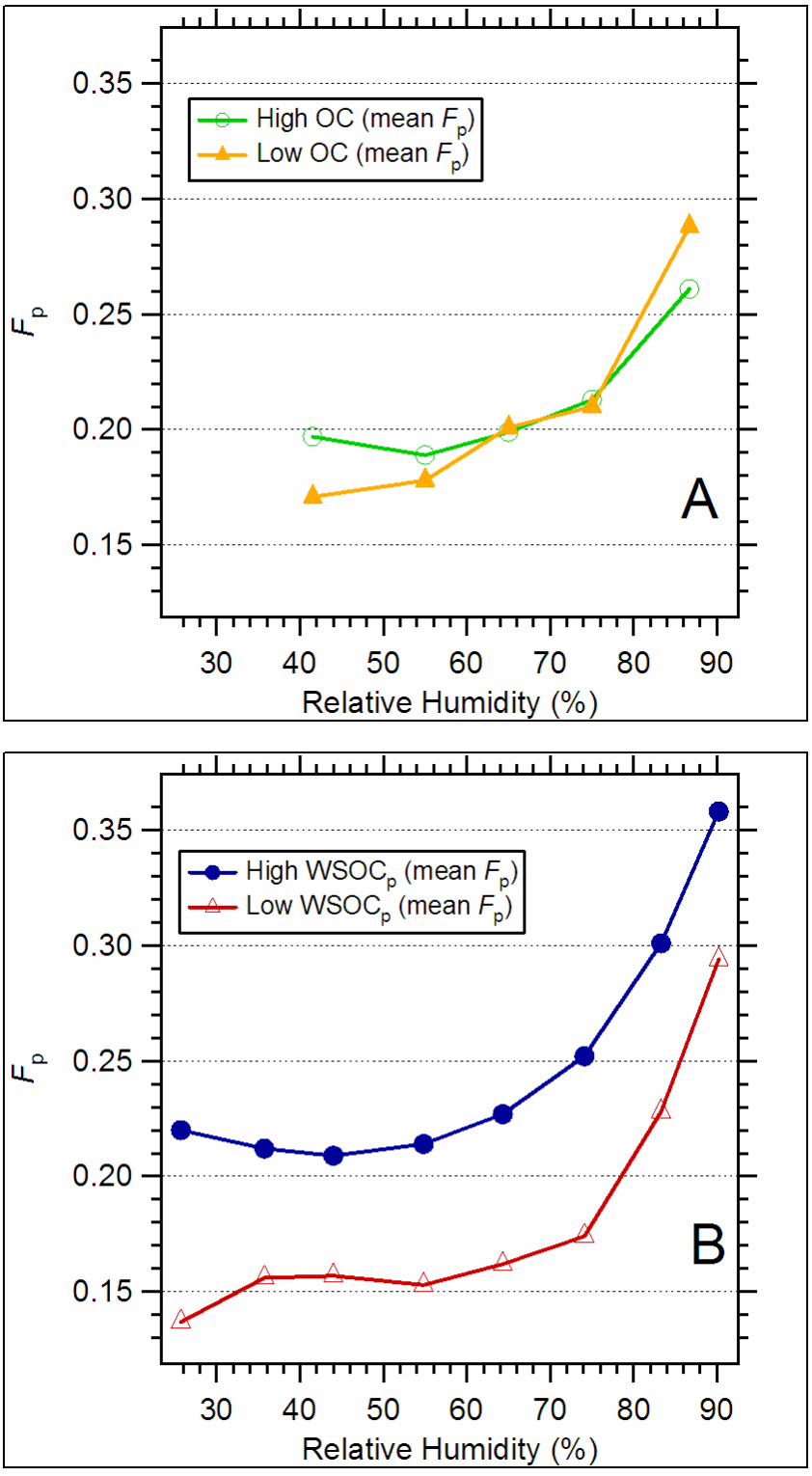

Figure 6.8 Mean F_p values verse RH for the highest (mean OC = 8.2 µg C m^{-3}) and lowest (mean OC = 3.7 µg C m^{-3}) 35% of OC concentrations (A), and for the highest (mean $WSOC_p$ = 5.3 µg C m^{-3}) and lowest (mean $WSOC_p$ = 1.7 µg C m^{-3}) 35% of $WSOC_p$ concentrations (B).

Although $WSOC_p$ and F_p were not independent, Figure 6.8b provides strong support that the $WSOC_p$ concentration did have an important effect on WSOC partitioning. This assertion is supported by the positive linear relationship between $WSOC_p$ and $WSOC_g$ (Figure 4.5). Though the data of Figure 4.5 show a large amount of scatter ($R^2 = 0.49$), in general, higher $WSOC_p$ concentrations were associated with higher $WSOC_g$ concentrations. Of the measurements corresponding to the highest 35% of $WSOC_g$ concentrations (n = 4304), approximately 70% of these data also corresponded to measurements that were within the highest 35% of $WSOC_p$ concentrations. Likewise, of the measurements corresponding to the lowest 35% of $WSOC_g$ concentrations (n = 4304), approximately 70% of these data also corresponded to measurements that were within the lowest 35% of $WSOC_p$ concentrations.

It is interesting to note that the difference in WSOC partitioning at high verses low $WSOC_p$ concentrations was approximately constant across the entire RH range. This included the highest RH levels, where particle H_2O concentrations likely far exceeded $WSOC_p$ concentrations and thus offered greater potential as an absorbing medium for partitioning gases. That F_p values at elevated RH levels remained higher for high $WSOC_p$ concentrations compared to low $WSOC_p$ concentrations provides insight into the partitioning process and suggests that, though water and organic compounds may both serve as absorbing media for partitioning SVOCs, their relative contributions may not be weighted equally.

It is apparent that both the $WSOC_p$ concentration and RH impact the gas/particle partitioning of ambient WSOC. To view the simultaneous relationship of these two parameters on F_p in a different manner from that depicted in Figure 6.8B, a plot of F_p

verse $WSOC_p$ concentration was generated for high and low RH conditions (Figure 6.9). The high RH analysis only included data with RH levels above 65% (the average RH for this analysis was 78.2%) while the low RH analysis only included data with RH levels below 50% (average RH for this analysis was 38.5%).

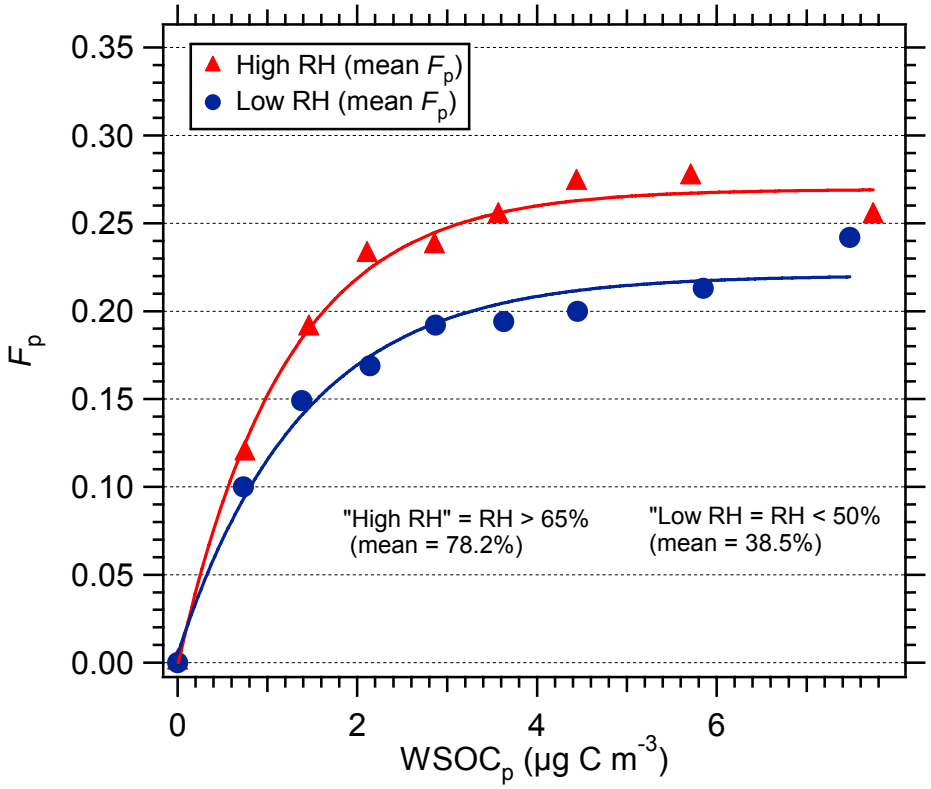

Figure 6.9 Mean F_p values as a function $WSOC_p$, segregated for high and low RH levels.

Several important features are evident from the analysis. First, for a given $WSOC_p$ concentration, higher RH levels corresponded to higher F_p values, as was discussed in detail in section 6.1.3. Additionally, the relationships between F_p and $WSOC_p$ in the high and low RH regimes were similar, supporting the previous assertions that $WSOC_p$ concentrations were an important factor in WSOC partitioning. This was even true at the

highest RH levels, where liquid water concentrations were likely substantially higher than those of $WSOC_p$. Together, this indicates that $WSOC_p$ and liquid water both be included as components of M_o for purposes of describing WSOC gas/particle partitioning. This agrees with theory, in which water and organic compounds together make up the mass of the absorbing organic phase [*Seinfeld and Pankow*, 2003], though their relative contributions as absorbing media may not be equal.

The results in Figures 6.8b and 6.9 indicate that the process is similar on wet and dry particles. This has two implications. First, the role that the particle organic component (e.g., $WSOC_p$) plays in partitioning is present even when particle H_2O concentrations likely far exceeded $WSOC_p$ concentrations. This behavior would not be expected if partitioning were described solely by the partitioning coefficient, K_p. As the liquid water content of particles increases, the importance of water in the partitioning process should increase and the importance of the $WSOC_p$ concentration should diminish. This is due to the significant impact of water on the average molecular weight of the absorbing organic + aqueous phase, MW_{om}, and on the increase it would bring to the total mass of the absorbing organic + aqueous phase, M_o (Equation 6.1). For example, at RH levels above 90%, the liquid water concentration may be an order of magnitude higher than the $WSOC_p$ concentration, and would thus dictate any relationship with M_o. Our ambient results suggest that this did not occur with WSOC partitioning: at the highest RH levels, the $WSOC_p$ concentration still appears to be important (Figure 6.8b, Figure 6.9). This indicates that $WSOC_p$ and liquid water both somewhat independently contribute to WSOC gas/particle partitioning. As an example, the liquid water may affect absorption of the water-soluble gases, and the $WSOC_p$ in the particle may influence the

heterogeneous production of lower vapor pressure products. The types of heterogeneous reactions that take place in the liquid particle may account for the F_p dependence on $WSOC_p$. Secondly, because the curve for the much dryer particles (Figure 6.9) is essentially identical to the wet particles, the overall partitioning mechanism appears to be similar throughout the RH range measured: the role of water is not just confined to RH> 80% when particles rapidly absorb water and are very wet.

There is an abundance of evidence from both laboratory and ambient studies suggesting that heterogeneous chemical reactions are important. *Limbeck et al*. [2003] observed a significant increase in isoprene SOA yields in the presence of acidic seed particles compared with yields in the presence of neutral seed particles in smog chamber studies. *Kroll et al*. [2007] found systematically higher experimental SOA yields from aromatic VOCs in the presence of ammonium sulfate seed particles compared to experiments in which no seed particles were present. In experiments designed to simulate the chemistry occurring within cloud droplets, *Altieri et al*. [2008] observed the formation of oligomers from methylglyoxal. *Volkamer et al*. [2008] observed SOA formation from acetylene in smog chamber experiments and attributed this to the formation of glyoxal and its subsequent uptake and reaction in particles. The results of *Volkamer et al*. [2008] included a linear correlation between SOA yields and aerosol liquid water concentrations, and an apparent effect of the existing organic aerosol composition on SOA yields as well, both very similar to our findings. These represent a small sampling of experimental studies in which heterogeneous reactions were observed. There have been numerous ambient studies which have identified macromolecular organic compounds, or oligomers, as components of organic aerosol [e.g., *Kalberer et al*.,

2006; *Denkenberger et al*., 2007]. It is highly unlikely that oligomer formation occurs through gas-phase processes, thus their presence in ambient particles confirms the occurrence of particle-phase reactions as well.

The combined findings presented in this Chapter make a strong case that the traditional SOA theory based solely on the K_p formulation (Equation 6.1) is not a suitable predictor of SOA in Atlanta. In traditional SOA partitioning theory, there is a strong relationship between K_p (i.e., F_p) and OC [e.g., *Odum et al.*, 1996] that was not seen in our ambient data. A relationship was observed between F_p and $WSOC_p$, though it differed from the relationships observed in chamber studies. K_p theory predicts a strong effect of water on partitioning, and indeed, a strong F_p-RH effect was seen in the ambient results. However, K_p theory also predicts that as H_2O is increased to levels significantly higher than $WSOC_p$ (or OC), the importance of $WSOC_p$ in the partitioning process should be diminished. This phenomenon was not observed in the ambient data either, as the $WSOC_p$ concentration remained an important factor for WSOC gas/particle partitioning even at the highest RH levels. A mechanism that incorporates both the absorption of SVOCs to fine particle water and the reaction of organic compounds in the aqueous phase may better represent the partitioning that occurs in the Atlanta summer. Further ambient studies are required to investigate whether or not the findings presented here are similar in other locations. Additional studies are also needed to provide insight into the specific SVOCs that are involved and to identify possible heterogeneous chemical mechanisms that may be prominent in ambient SOA formation.

6.2.2 NO_x Concentration and F_p Variability

In addition to the $WSOC_p$ concentration and relative humidity, which were shown in previous sections to influence WSOC gas/particle partitioning, it is likely that the NO_x concentration impacted F_p as well. A box plot of F_p verse RH was constructed after sorting the data according to NO_x concentrations, and median values are plotted for the high NO_x and low NO_x data (Figure 6.10A). The average NO_x concentration for the high NO_x data was 0.033 ± 0.023 ppm (mean ± 1σ) while that for the low NO_x data was 0.006 ± 0.002 ppm (mean ± 1σ). Below 80% RH, low NO_x conditions were associated with higher values of F_p (mean = 0.208), while high NO_x conditions were associated with lower values of F_p (mean = 0.180). Overall, the mean F_p difference (0.028) below 80% RH was statistically significant at the 99.9% confidence interval (t = 7.793 from student's t-test, df = 1046). Multiplying this ΔF_p by the mean total WSOC concentration below 80% RH (18.58 μg C m^{-3}) yields a $WSOC_p$ enhancement of 0.52 μg C m^{-3} from this difference. The difference in F_p values between high NO_x and low NO_x regimes (0.028) may appear small, despite its statistical significance. However, in the context of ambient concentrations, where the mean $WSOC_p$ concentration for the entire summer was 3.3 μg C m^{-3}, this difference was significant. It is also worth noting that the absolute difference in concentrations between the high and low NO_x regimes (0.027 ppm) was actually quite small, especially in relation to the full range of NO_x concentrations (0.001 – 0.378 ppm) observed throughout the summer and in relation to NO_x concentrations typically used in smog chamber studies. Based on these analyses, though, it is likely that a larger variance in NO_x concentrations would produce a larger difference in observations of F_p.

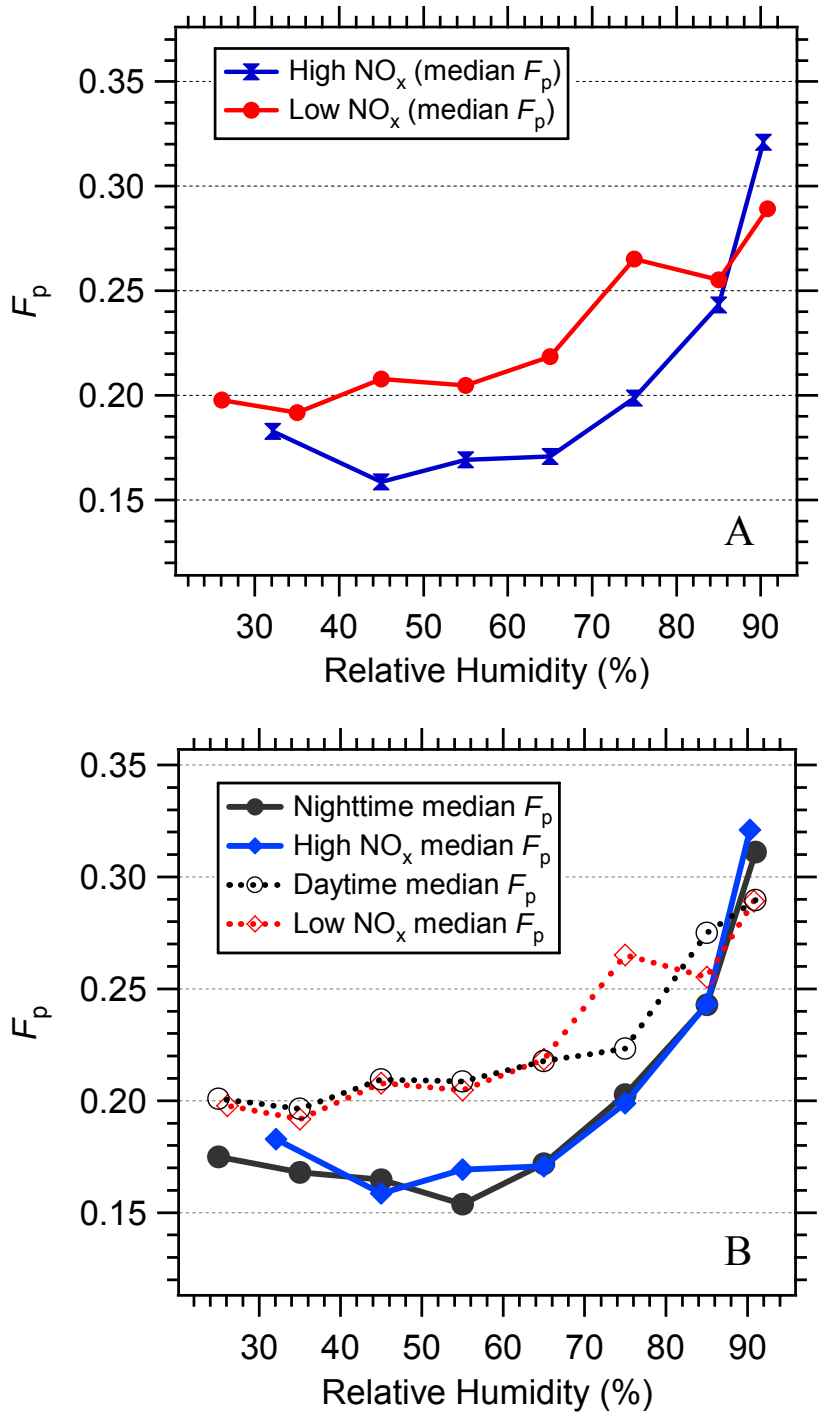

Figure 6.10 Median F_p verse RH for data sorted by NO_x concentration (A). Data represent the highest and lowest 35% of NO_x concentrations. The data from (A) are also plotted with daytime and nighttime median F_p values (B) and indicate that the diurnal variability may have been caused by differences in NO_x concentrations.

The difference in WSOC partitioning with NO_x concentrations could explain the F_p differences observed between the nighttime and the daytime, where generally more WSOC was partitioned in the particle phase during the day than at night (Figure 6.10B). Though the mean Total WSOC concentration was higher at night (17.1 μg C m^{-3}) than during the day (16.8 μg C m^{-3}), this phenomenon resulted in a mean daytime $WSOC_p$ concentration (3.5 μg C m^{-3}) that was approximately 10% higher than the mean nighttime concentration (3.2 μg C m^{-3}).

Though it is possible that the partitioning differences observed between the day and night were not caused by differences in NO_x concentrations, but by some other factor with a strong diurnal signature like OH, the evidence for a NO_x effect was compelling. Median F_p values had a strong negative linear correlation (r = -0.97) to NO_x concentrations (Figure 6.11) and a comparison between weekend and weekday data revealed no difference in F_p values. OH concentrations are also not expected to vary significantly on weekdays verse weekends, but mean weekday NO_x concentrations were only marginally higher (0.017 ppm compared to 0.013 ppm) than mean weekend NO_x concentrations, so this analysis was inconclusive. When only daytime data was considered, the mean F_p value corresponding to the top 15% of NO_x concentrations was statistically different at the 99.5% C.I. from the mean F_p value for the bottom 15% of NO_x concentrations (t = 3.111 from student's t-test, df = 264). This was also the case for nighttime only data (t = 4.676 from student's t-test, df = 335) and it supports the existence of a NO_x effect on F_p versus a confounding effect, such as oxidant (OH, O_3) concentration.

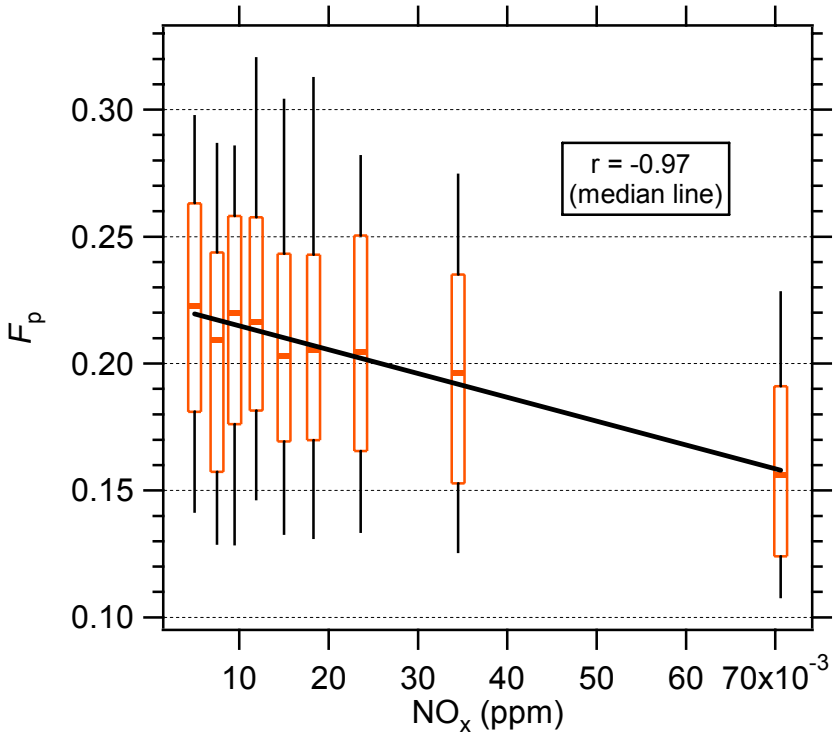

Figure 6.11 Particulate WSOC fraction, F_p, as a function of NO_x concentrations. The data were binned according to NO_x concentrations and median (thick horizontal line), 25th and 75th percentiles (lower and upper box), and 10th and 90th percentiles (lower and upper whiskers) are shown for each bin (average N per bin = 197).

Numerous smog chamber experiments have been conducted to examine the effect of NO_x on SOA formation and the results provide insight into the variations in F_p observed here. In general, SOA yields from the reaction of hydrocarbons with ten or fewer carbon atoms are significantly higher at low NO_x concentrations compared to high NO_x concentrations [*Kroll and Seinfeld*, 2008]. These small hydrocarbons include isoprene [*Kroll et al*., 2006; *Pandis et al*., 1991] and monoterpenes [*Presto et al*., 2005; *Ng et al*., 2007], biogenic species with high emission rates in the Southeast [*Guenther et al*., 1994]. Conversely, SOA yields from the reaction of larger hydrocarbons are, in general, highest at high NO_x levels [*Kroll and Seinfeld*, 2008]. The NO_x effect on SOA

yields is due to its substantial influence on the oxidant initiating SOA formation (i.e., hydroxyl radical, nitrate radical, or ozone) and on the fate of the RO_2 and RO radicals [*Kroll and Seinfeld*, 2008]. In general, reaction of smaller VOCs in the presence of higher NO_x concentrations leads to the formation of higher volatility products (e.g., fragmentation and formation of short aldehydes) compared to smaller VOC reactions in low NO_x conditions that produce lower volatility products (e.g., hydroperoxides and acids from reaction of $RO_2 + HO_2$). Because isoprene and monoterpenes are expected to be the major SOA precursors in the southeastern U.S., the observed relationship between F_p and NO_x is qualitatively consistent with the smog chamber studies which observed a similar phenomenon. For this to be true, though, it implies a physical similarity between aerosol yield in smog chamber experiments and our measurement of F_p in the ambient atmosphere. SOA yield, *Y*, is often described by the expression

$$Y = \frac{M_{soa}}{\Delta ROG} \qquad \text{Equation 6.5}$$

where M_{soa} is the mass of secondary organic aerosol formed and ΔROG is the total amount of parent VOC reacted. ΔROG can be considered the sum $M_{soa} + VOC'$, where *VOC'* is a gas-phase oxidation product of the parent VOC. In the expression for F_p (Equation 6.2), the numerator is $WSOC_p$, which is predominantly secondary and is analogous to M_{soa}, while the denominator is $WSOC_p + WSOC_g$, which is analogous to ΔROG. An obvious difference between the two parameters is that smog chamber SOA yields are derived from the reaction of a known, and oftentimes single VOC, while $WSOC_p$ and $WSOC_g$ may be formed from multiple and different VOCs.

The smog chamber results imply that the NO_x effect on F_p may not be due to its impact on gas/particle partitioning of WSOC, but rather on the oxidation of VOCs to form SVOCs and this relationship to SOA yield (see Section 6.3 below). This seems to be a more plausible explanation, since the gas/particle partitioning process should not depend on NO_x, while yield has been shown in numerous smog chamber studies to depend highly on yield.

It is noteworthy that a NO_x effect on F_p was not observed at RH levels above 80%; mean high NO_x F_p values were not statistically different from mean low NO_x F_p values in this RH range ($t = 0.357$ from student's t-test, $df = 244$). The convergence of the high and low NO_x F_p data can perhaps be explained with the findings of *Ervens et al*. [2008], who found that SOA yields of isoprene oxidation products were significantly higher at elevated NO_x concentrations. This was attributed to the preferential formation of carbonyl compounds in the gas phase under higher NO_x that were then taken up into cloud droplets and reacted further to form non-volatile organics. Thus it appears as if competition between the two SOA formation mechanisms, one 'dry' and one 'wet', produced this transition regime where both equally impacted WSOC formation.

These results could have important implications for the control strategies of O_3 and $PM_{2.5}$, criteria pollutants which annually exceed EPA attainment limits in Atlanta [http://www.epa.gov/oar/oaqps/greenbk/]. Atlanta is a NO_x-limited environment, which suggests NO_x reductions may be the most effective means of controlling O_3 concentrations. The present results indicate that attempting to mitigate excessive O_3 concentrations through NO_x reductions could produce the unwanted effect of an increase

in $PM_{2.5}$ mass concentrations. This potential feedback to NO_x control is significant and should be examined in more detail.

6.2.3 Other Influences on F_p

In contrast to NO_x, ozone (O_3) concentrations did not appear to impact WSOC partitioning at all (Figure 6.12). The mean F_p at O_3 concentrations above 70 ppb (0.211) was not statistically different from the mean F_p at O_3 concentrations below 20 ppb (0.214) (t = 0.454 from student's t-test, df = 689).

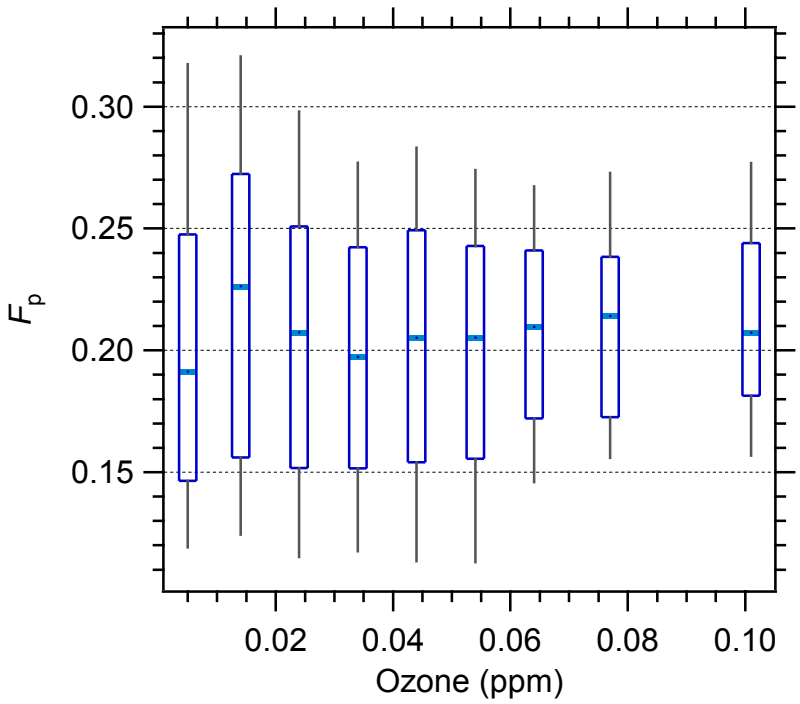

Figure 6.12 Particulate WSOC fraction, F_p, as a function of ozone concentrations. The data were binned according to ozone concentrations and median (thick horizontal line), 25th and 75th percentiles (lower and upper box), and 10th and 90th percentiles (lower and upper whiskers) are shown for each bin (average N per bin = 198).

Though there was more variability in F_p at lower O_3 concentrations, overall the central trend in F_p was flat across the entire range of O_3 concentrations encountered in the study. This result was somewhat surprising, given that high aerosol yields from O_3 reactions with biogenic VOCs have been observed in smog chamber studies [e.g., *Griffin et al.*, 1999]. $WSOC_p$ and $WSOC_g$ both exhibited non-linear relationships with O_3 (Figure 6.13) that suggest it was not primarily involved in the formation of either species. $WSOC_p$ and $WSOC_g$ concentrations were flat for O_3 concentrations below 60 ppb, while they both increased significantly at O_3 concentrations above 60 ppb. The enhancements in WSOC concentrations at elevated O_3 levels were not likely caused by some influence of O_3 on WSOC formation, though. There is not a physical significance to the 60 ppb O_3 concentration below which no WSOC would form and above which significant WSOC would form, as is shown in Figure 6.13. Rather, the enhancements were likely a product of all three components experiencing afternoon concentration maxima due to photochemical production that peaked at approximately the same time. It is possible, though, that O_3 was prominently involved in VOC oxidation but that O_3 was abundant, and VOCs limiting, in O_3-VOC reactions and thus little dependence was seen between F_p and O_3. In contrast to Atlanta, observations of SOA in Mexico City were highly correlated to O_3 concentrations (and NO_2) [*Herndon et al.*, 2008], highlighting differences between the two locations. When an analysis of F_p verse O_3 was performed for daytime only and nighttime only periods (not shown), the result was similar to the overall analysis (Figure 6.12) in that no F_p dependences on O_3 were observed.

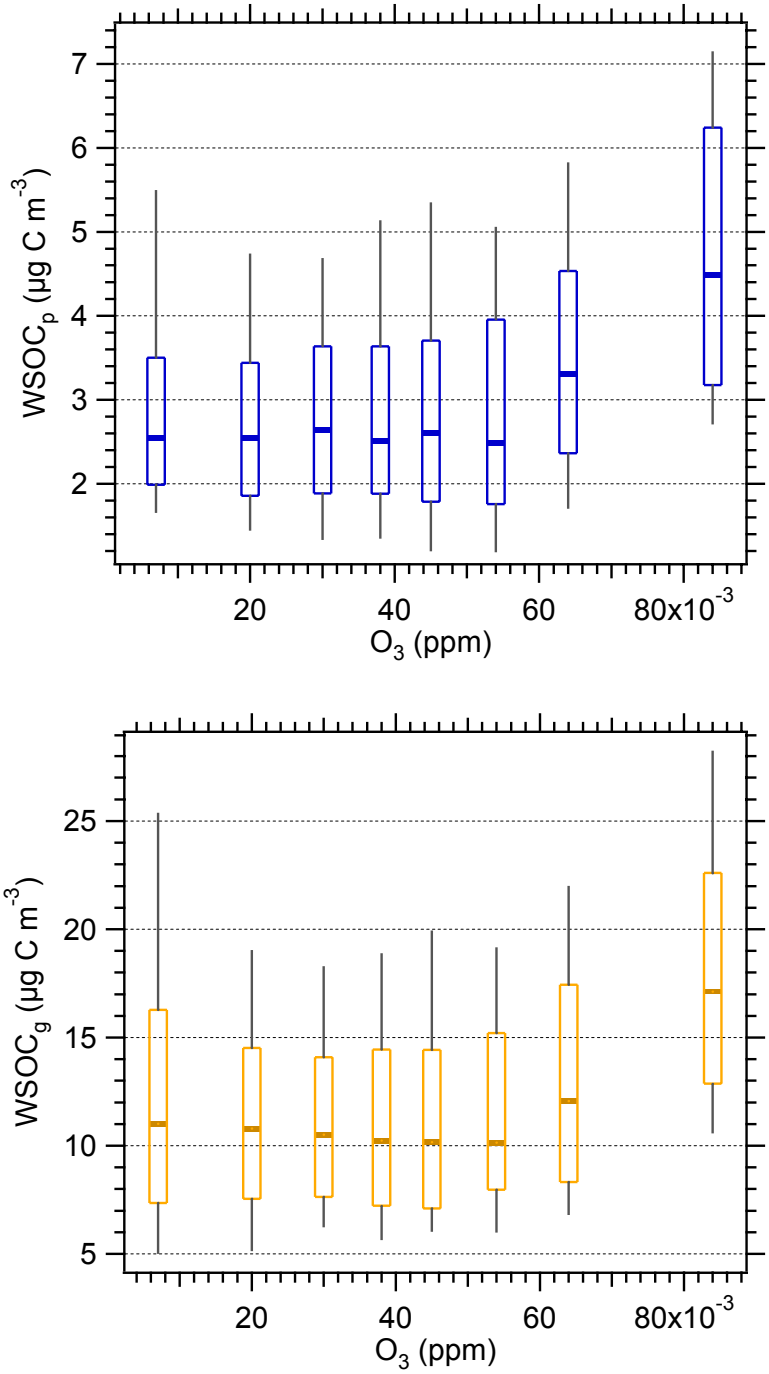

Figure 6.13 Concentrations of $WSOC_p$ (A) and $WSOC_g$ (B) as a function of the O_3 concentration.

6.3 Yield and Gas/Particle Partitioning of SOA

In previous discussions in this chapter, comparisons were made between the parameter F_p and both gas/particle partitioning and SOA yield. For primary organic aerosol, it is easy to conceptualize gas/particle partitioning as an isolated equilibrium process that behaves according to thermodynamic principles (Figure 6.14). For example, after the direct emission of polycyclic aromatic hydrocarbons (PAHs) from combustion sources, individual PAHs then establish (and maintain) equilibrium between the gas and particle phases according to a temperature-dependent partitioning coefficient [*Liang and Pankow*, 1996]. In the formation of SOA, gas/particle partitioning and aerosol yield are closely related. VOCs undergo oxidation to form SVOCs, which may then partly condense (i.e., partition) into the particle phase according to thermodynamic equilibrium (Figure 6.14). The oxidation step(s) which forms the SVOCs and the subsequent partitioning of the SVOCs between the gas and particle phases are two separate processes that both have an enormous impact on SOA yield. For example, the NO_x concentration has been shown through a high number of smog chamber experiments to impart a significant impact on SOA yields [*Kroll and Seinfeld*, 2008]. This is due to the role of NO_x in determining the chemical products of VOC oxidation (hence the volatility of the product SVOCs), not due to the role of NO_x in the partitioning process, itself. Though the effect is visible in the form of a NO_x relationship with F_p, our findings are consistent with experimental smog chamber results. On the other hand, a factor that impacts the gas/particle partitioning of SVOCs will, by default, impact aerosol yield as well. For example, compelling evidence for an RH effect on WSOC gas/particle partitioning was

presented in Section 6.1.3. In Figure 6.14, the aerosol yield from a parent VOC may be expressed as

$$Y = \frac{SOA}{SOA + SVOCs}. \qquad \text{Equation 6.6}$$

since $SOA + SVOCs$ represents the total amount of VOC reacted (equal to ΔROG in equation 6.5). Thus, by affecting the gas/particle partitioning towards the particle phase, RH may also have an increasing effect on yield by increasing SOA and decreasing $SVOCs$. In this way, the parameter F_p is related to both Y and gas/particle partitioning, as well.

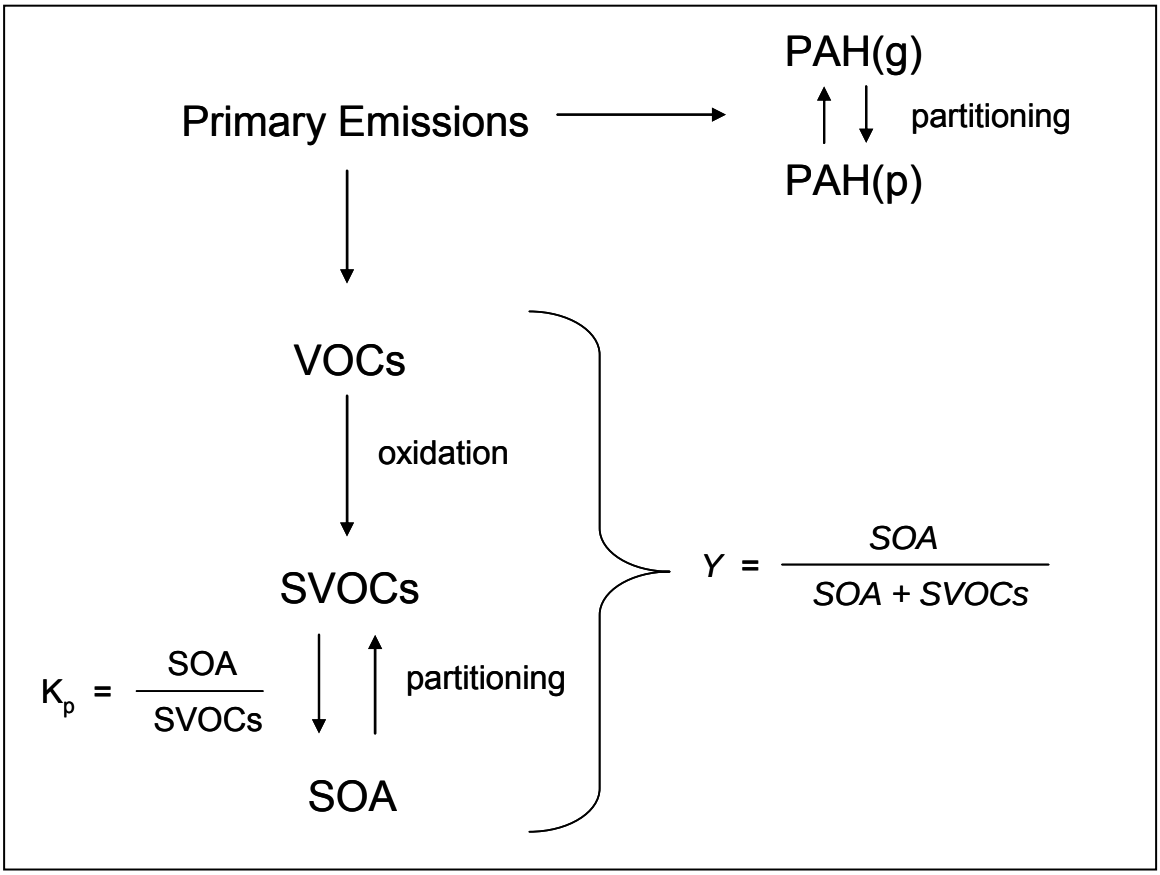

Figure 6.14 Simple schematic of the emission and gas/particle partitioning of primary compounds, and the emission of VOCs followed by reaction to form SVOCs and subsequent gas/particle partitioning of these secondary compounds.

6.4 Conclusions

Overall, the present results provide a detailed characterization of SOA partitioning in the summertime in Atlanta, a large urban center with substantial biogenic VOC emissions. Partitioning, analyzed through the fraction of total WSOC in the particle phase, F_p, was found to have no dependence on temperature, though this was likely due to the emissions of precursor VOCs and the formation of WSOC (in the gas and particle phase), which both could have temperature dependences. F_p was related to NO_x concentrations, with higher NO_x levels corresponding to lower values of F_p. This was not likely related to the partitioning process, though, but could be attributed to the effect of NO_x on the product distribution in VOC oxidation. F_p was shown to have a very strong dependence on relative humidity at RH levels above 70% due to the uptake of liquid water by fine particles. The current chapter also shows a strong partitioning dependence on the existing $WSOC_p$ concentration, but not on the OC concentration, possibly indicating a necessity or preference in chemical similarity between partitioning SVOCs and the absorbing aerosol phase, or the role of heterogeneous chemistry in SOA formation (or both). The relationship between F_p and $WSOC_p$ was present even at the highest RH levels, when the liquid water concentration was likely far greater than the $WSOC_p$ concentration. Collectively, the results implicate liquid-phase heterogeneous chemical reactions as a major SOA formation process in the ambient atmosphere and are in many ways remarkably similar to the recently reported chamber results of *Volkamer et al.* [2008].

The $WSOC_p$ results give evidence that the $WSOC_p$ measurement incorporated most, if not all, of the SOA in Atlanta. To our knowledge, this represents the first

detailed characterization of SOA formation processes based on ambient data. Previous studies have described the gas/particle partitioning of the total SOA within a smog chamber, and previous ambient studies have reported on the partitioning of individual compounds. The results provide important insight into SOA formation and the gas/particle partitioning process beyond the current scientific understanding. Specifically, fine-particle water and heterogeneous chemical reactions may be a significant, and possibly the single most important mechanism for SOA formation in summertime Atlanta. This mechanism may also play a significant role in other locations [e.g., *Hennigan et al.*, 2008c], and may explain the systematic and large under-prediction of SOA by most models.

Chapter 7

Future Work

The research for this thesis has produced significant findings, though many subsequent questions have come out of this work, as well.

A significant relationship was observed between the gas/particle partitioning of WSOC and the ambient relative humidity (RH). WSOC partitioning to the particle phase was enhanced at elevated (>70%) RH and the evidence very strongly pointed to the uptake of particle water as the cause for this enhancement. This was suggestive of a process similar to Henry's Law partitioning, but calculations showed that the amount of liquid water associated with fine particles was too small to simply dissolve the amount of soluble gas-phase species to account for the increase in SOA mass. Partitioning based strictly on a Henry's Law process is reversible, and though the calculations suggest that it was not this process alone that was responsible for the enhancement in partitioning to the particle phase, the question of reversible partitioning should be examined through experimental means. Specifically, side-by-side comparisons between two $WSOC_p$ measurements, one with the sample stream un-modified and one passed through a dryer to evaporate particle water prior to PILS-WSOC analysis, could help to answer this question.

The enhancement in partitioning to the particle phase at elevated RH was attributed to the uptake of liquid water by particles. This was due to strong similarities between the partitioning parameter, F_p, and both liquid water concentrations predicted by

the ISORROPIA-II model [*Fountoukis and Nenes*, 2007] and a measure of the scattering enhancement of ambient particles as a function of RH [*Malm and Day*, 2001]. The relationship between F_p and liquid water could be verified, however, if simultaneous measurements of F_p and particulate inorganic ionic components were conducted. Using inputs of particulate inorganic ionic concentrations and ambient temperature and RH, the ISORROPIA-II model calculates the particle liquid water content based on known thermodynamic properties. This also may help explain some of the variability seen in WSOC partitioning at a given RH as differing inorganic ionic concentrations will produce different liquid water concentrations for the same temperature and RH conditions.

The measurements of F_p were conducted in the late spring and throughout the entire summer, from 11 May – 20 September, 2007. Thus, we have provided a detailed characterization of WSOC partitioning in the Atlanta summer. The partitioning behavior of WSOC should also be investigated in the other seasons, when emissions and physical and chemical processes differ from those of summer. Studies [e.g., *Decesari et al*., 2001; *Sullivan et al*., 2004; *Miyazaki et al*., 2006] have shown large differences in $WSOC_p$ trends between summer and winter or fall seasons. WSOC partitioning may show substantial differences between seasons, as well, and could provide additional insight into the factors controlling the partitioning process. Additionally, any temporal comparison should include the entire spring season that contains the onset and duration of the leaf-growing period (i.e., the period of intense biomass production). There were events throughout the summer in which the correlation of $WSOC_p$ and water vapor concentrations were quite high. One viable hypothesis to explain the correlations was

that water vapor and biogenic VOCs were co-emitted in similar proportions, leading to concentrations that tracked one another for extended periods of time. High rates of primary production by trees or the production of a dense forest canopy are accompanied by high rates of water evaporation from trees [*Baldocchi and Meyers*, 1998]. Thus, it would be instructive to conduct measurements of $WSOC_p$ and water vapor during the growing season to contrast this period to the summertime.

From September 5-20, measurements of gas-phase formic, acetic, and oxalic acid were made in addition to the measurements of WSOC, OC, EC, and meteorological parameters. The results showed that formic and acetic acid together accounted for approximately 20% of $WSOC_g$ on a carbon mass basis. It would be informative to make measurements of $WSOC_g$ and $WSOC_p$ concurrently with gas and particle-phase formic and acetic acid. The characterization of WSOC partitioning was, by definition, chemically non-specific. In measuring the partitioning of individual compounds known to be abundant, a comparison can be made to the overall behavior of WSOC. This would enhance the overall understanding of WSOC partitioning and would provide some clarity to the question of Henry's Law partitioning, since formic and acetic acid are highly soluble, but also relatively volatile species. In addition to simultaneous gas and particle measurements of the carboxylic acids, gas and particle measurements of a compound like glyoxal, which may participate in heterogeneous reactions, would add to this analysis.

For the investigation of WSOC partitioning, all measurements were made on the Georgia Institute of Technology Campus, located near the center of Atlanta. Atlanta is a large urban area that has heavy influences from anthropogenic and biogenic emission sources. In Atlanta, $WSOC_p$ in the summertime is predominantly biogenic in origin

[*Weber et al*., 2007]. It would thus be interesting to investigate WSOC partitioning in an urban location dominated by anthropogenic emissions (e.g., Los Angeles or Mexico City). In Atlanta, the NO_x concentration appears to impact F_p, with lower NO_x concentrations favoring higher values of F_p. Comparisons of WSOC partitioning between central Atlanta and a rural site near Atlanta may also provide insight into the partitioning behavior WSOC and further our understanding of the F_p -NO_x relationship.

Chapter 8

Conclusions

Secondary organic aerosol is an important component of the earth's atmosphere. It is ubiquitous and often accounts for a significant fraction of the total aerosol mass loading. The potential impacts of SOA are related to its impacts on human health, and its direct and indirect effects on climate. A significant increase in our current understanding of SOA is required if its full impact on humans and the environment is to be realized. Recognizing that particulate water-soluble organic carbon is a significant component of SOA, this thesis examines several important factors of SOA including its sources, formation, volatility, and partitioning.

This work first investigates the formation and volatility of SOA in the Mexico City Metropolitan Area. Ambient measurements were made approximately 30 km downwind of the city center, in an area and three-day time period dominated by anthropogenic emissions. The mornings of the analysis period were characterized by intense photochemical formation of SOA, which was similar to photochemical nitrate formation. The strong similarities observed between nitrate and SOA suggest that SOA was predominantly from anthropogenic sources and that the hydroxyl radical was primarily responsible for initiating SOA formation. The morning peaks of both nitrate and SOA were immediately followed by sharp concentration decreases. Box model results indicate that dilution from an expanding boundary layer was the major cause (~60%) for these mid-day concentration decreases, however, other factors likely contributed as well. Results from the ISORROPIA-II thermodynamic equilibrium model

suggest that aerosol evaporation also contributed significantly (~40%) to the nitrate concentration decrease. This was due to changing environmental conditions (increasing temperature and decreasing relative humidity) that shifted the equilibrium from primarily in the particle phase (aerosol ammonium nitrate) to the gas phase (nitric acid + ammonia).

Box model calculations show that dilution alone (~60-90% of SOA decrease due to dilution) was also insufficient to account for all of the observed SOA decrease and it is likely that some fraction (~10-40%) volatilized as well. It is thus likely that particle-bound water played a role in the formation/evaporation of SOA in Mexico City. It was shown, through the aerosol equilibrium model results, to strongly impact the behavior of nitrate. In the morning, when photochemical formation occurred, the aerosol water concentration was high. Shortly (~30-60 min) before the nitrate evaporation occurred, the changing ambient conditions led to rapid evaporation of most particle-bound water. The strong similarities between SOA and nitrate behaviors suggest that the physical and chemical processes affecting them were largely the same, and that the significant evaporation of liquid water influenced the SOA evaporation, as well.

Through simultaneous measurements of water-soluble organic carbon in the particle and gas ($WSOC_g$) phases, the partitioning of WSOC was investigated in Atlanta, an area that stands in contrast to Mexico City by the dominance of biogenic VOC emissions over those from anthropogenic sources. An extensive data set was collected, as measurements were conducted from 11 May – 20 September, 2007 at a sampling rate of ~10 minutes for the WSOC methods, and 1 hour for the OC and EC methods.

Since the $WSOC_g$ measurement has been made only sparingly in urban areas, and never in Atlanta, a characterization of $WSOC_g$ was first performed. For two weeks in September, measurements of formic acid, acetic acid, and oxalic acid were made in the gas phase, in addition to the bulk $WSOC_g$. Oxalic acid was rarely present above the detection limit (0.08 μg m^{-3}), but formic and acetic acid were both abundant and were highly correlated. They were also correlated with $WSOC_g$ and together accounted for approximately 20% of $WSOC_g$ on a carbon mass basis. The diurnal signature of $WSOC_g$ was similar to that of $WSOC_p$ during the daytime, as they both increased in the morning and early afternoon, peaked around 14:00, and then decreased in the late afternoon and early evening. This behavior was strongly suggestive of photochemical production of WSOC in the gas and particle phases, though the magnitude of each enhancement also suggests high regional backgrounds for $WSOC_p$ and $WSOC_g$ as well. Unlike the diurnal profile of $WSOC_p$, which remained relatively flat throughout the night and early morning, the diurnal profile of $WSOC_g$ also showed a nighttime enhancement with a peak occurring at approximately midnight. The magnitude of this peak was as large as the mid-day peak and suggests a significant nighttime source of $WSOC_g$, perhaps from nighttime monoterpene emissions and subsequent reaction with O_3 or the nitrate radical.

In five separate events in May, emissions from wildfires burning in southern Georgia and northern Florida heavily impacted the ground-level air quality in Atlanta. The highest ambient concentrations for $WSOC_p$ and among the highest $WSOC_g$ concentrations were recorded within these events. $WSOC_g$ accounted for a lower fraction of the total WSOC in these events, compared with the remainder of the summer where the influence from biomass burning was presumably small. The relatively lower

contribution to total WSOC made by $WSOC_g$ was likely due to high concentrations of primary and secondary $WSOC_p$ from the burning emissions.

Two factors were identified as the most important parameters affecting the partitioning of WSOC; relative humidity, and the $WSOC_p$ concentration. The NO_x concentration also impacted the fraction of WSOC in the particle phase (F_p), however this was not likely due to an effect on the physical partitioning process. At relative humidity levels below 70%, F_p was approximately constant. At relative humidity levels above 70%, the fraction of WSOC in the particle phase increased exponentially with increasing RH. At the highest RH levels ($\geq$ 90%), the fraction of WSOC in the particle phase was approximately 50% higher than that below 70% RH. This enhancement in particle phase partitioning led to median increases in $WSOC_p$ concentrations ranging from 0.3-0.9 μg C m^{-3}, a meaningful enhancement in relation to typical ambient concentrations. The curve of median aerosol WSOC fraction verse RH showed remarkable consistencies with two independent measures of aerosol water. First, the ISORROPIA-II model was used to predict aerosol water concentrations, using the average inorganic concentrations from the Atlanta Supersite in August, 1999 as the aerosol composition. Second, water uptake by particles was approximated using a light scattering enhancement in relation to a "dry" light scattering, with a particle composition that was typical for the Atlanta summertime. Both measures of water uptake matched the median F_p values as a function of RH, and this provided strong evidence that the enhanced particle phase partitioning was due to water uptake. The behavior was observed during the day and night alike, and exists as a potentially significant source of SOA that is generally not considered.

The $WSOC_p$ concentration was another factor that influenced WSOC partitioning. Partitioning theory predicts that the mass of the absorbing organic aerosol will impact partitioning, with higher mass concentrations representing a greater capacity to absorb partitioning species and leading to more SOA. This theory is supported by multiple smog chamber experiments which observed higher SOA yields at higher organic aerosol loadings. This work was in general agreement with theory and with the smog chamber results, as WSOC partitioning exhibited a dependence on the $WSOC_p$ concentration. The dependence was strongest at the lowest concentrations of $WSOC_p$, but was relatively flat at $WSOC_p$ concentrations above 4 μg C m^{-3}. Overall, this was suggestive of a relatively non-volatile total WSOC. Despite the strong dependence of WSOC partitioning on the $WSOC_p$ concentration, and despite a high correlation ($R^2 = 0.73$) between $WSOC_p$ and OC, a relationship was not observed between F_p and OC. This suggests that chemical similarities between the partitioning compounds and the absorbing medium are important.

In addition to RH and $WSOC_p$ concentrations, NO_x concentrations had an apparent impact on F_p as well, though this was not likely due to an effect of NO_x on the gas/particle partitioning of WSOC. Median F_p values were negatively correlated ($r = -0.97$) with NO_x concentrations, as lower NO_x concentrations corresponded to a higher fraction of WSOC in the particle phase. Smog chamber studies have observed higher aerosol yields at lower NO_x concentrations from parent VOCs containing ten or fewer carbon atoms. Thus, it is likely that the NO_x relationship with F_p was due to its impact on SVOC formation rather than its role in WSOC partitioning. This is consistent with the emissions inventory in the southeastern U.S., where biogenic emissions of isoprene and

monoterpenes (which contain five and ten C atoms, respectively) far exceed emissions of other VOCs.

The gas/particle partitioning of WSOC did not appear to be impacted by temperature. This was particularly surprising since equilibrium theory predicts a strong temperature effect from the strong temperature dependence of compound saturation vapor pressures. Over the temperature range encountered throughout the summer (> 20 °C), the change in saturation vapor pressures of organic components should have produced a visible effect on WSOC partitioning. This effect may have been masked by the behaviors of $WSOC_p$ and $WSOC_g$, which both showed positive linear correlations with temperature. This effect was likely due to increased secondary gas and particle production from increased photochemical activity, and from increased WSOC precursor VOC emissions (e.g., isoprene) increasing with increasing temperature.

Aerosol liquid water was shown to be an important factor in SOA formation in both Mexico City and Atlanta. These relationships may have been related to periodic events in Atlanta in which a high correlation (average $R^2 = 0.85$) was observed between $WSOC_p$ and water vapor. The events were routinely observed and lasted an average of 19 hours, indicating their potential importance in inferring SOA sources and/or formation. The correlation was surprising, given that $WSOC_p$ is in the particle phase and is predominantly secondary while water vapor is in the gas phase and is primary. Though combustion of fossil fuels (e.g., by transportation sources) emits both water vapor and VOCs that can form SOA, this was not a source of the $WSOC_p$-water vapor correlations, since the contribution these emissions make to the water vapor budget is negligible. This was somewhat paradoxical since a correlation between $WSOC_p$ and EC was observed.

This $WSOC_p$-EC correlation was likely related to previous studies which observed a relationship between biogenic SOA formation and anthropogenic emissions. Two factors were identified as the probable causes for the observed $WSOC_p$-H_2O(v) correlation events. First, an enhancement in SOA formation due to aerosol water uptake was one likely cause. In several of the correlation events, F_p was also correlated with RH, likely due to the water uptake effect on SOA previously discussed. The other likely cause for the events was the co-emission of VOCs and water vapor from biogenic sources. In several of the correlation events, water vapor was also correlated with $WSOC_g$. For many continental areas, water vapor emitted by vegetation (transpiration) is the dominant source of atmospheric water vapor. Additionally, water vapor from terrestrial sources will constitute a greater fraction of water vapor near the surface and the factors that control transpiration and biogenic VOC emissions are highly similar. This all suggests the potential for a synergistic effect between biogenic emissions of water vapor and VOCs. The VOCs may undergo oxidation and form secondary gaseous and particle components while the water vapor co-emitted with the VOCs may enhance the partitioning of these compounds to the particle phase and may result in a significant enhancement in SOA concentrations over that if water vapor concentrations were lower.

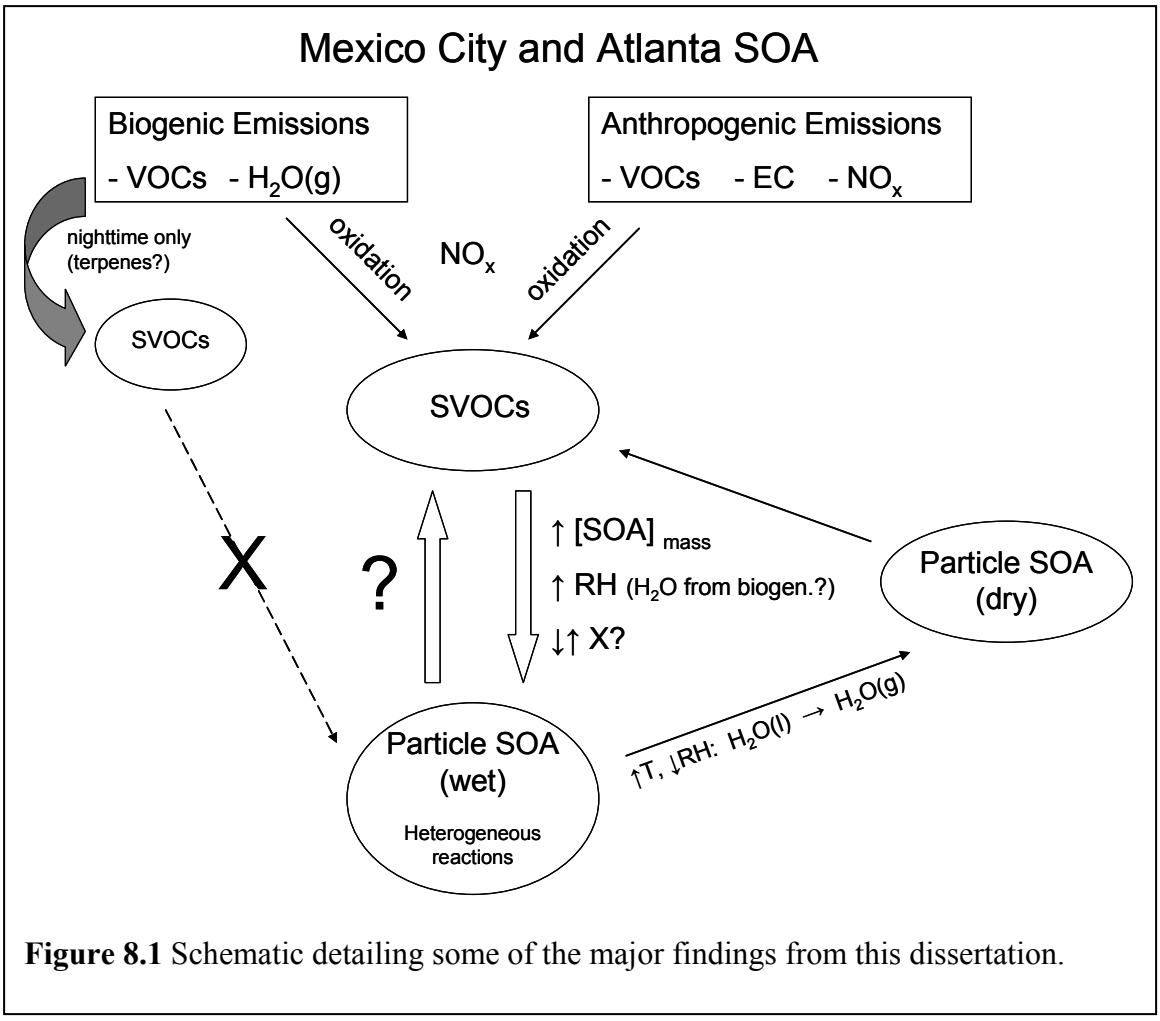

Figure 8.1 Schematic detailing some of the major findings from this dissertation.

Overall, this work presents new and significant findings on several important aspects of SOA, including its volatility, sources, formation, and partitioning. Many of the findings are summarized in the schematic presented in Figure 8.1. Significant SOA formation was observed in Mexico City and Atlanta, urban environments dominated by anthropogenic and biogenic emissions, respectively. In Atlanta, the formation and partitioning of SOA were influenced by many factors. It is likely that biogenic emissions were responsible for the majority of SOA formation in Atlanta, and the diurnal signature showed a mid-day enhancement consistent with photochemical production. But SOA

concentrations were also positively correlated to the primary anthropogenic pollutant, EC, which suggests a controlling or limiting effect that was consistent with previous studies. Confounding this, however, was a negative relationship between NO_x concentrations and the fraction of WSOC (SOA) in the particle phase. These findings were not necessarily contradictory, though, since the positive correlation with EC was one of absolute SOA concentrations while the negative correlation with NO_x was with the fraction of total WSOC in the particle phase. Other factors influencing the partitioning of WSOC included the absolute $WSOC_p$ concentration and the ambient RH. In particular, the enhancement in WSOC partitioning to the particle phase due to water uptake (RH) was significant because it represents a potentially meaningful source of SOA that is generally not considered. The evidence of vegetation as a common source of SOA and water vapor in Atlanta also was also significant. Though different analyses were performed on the SOA of Mexico City and Atlanta, the importance of particle-bound water emerged as a common finding between the two locations. In Mexico City, following rapid morning photochemical SOA production, a significant fraction of the newly formed SOA volatilized due to changing ambient conditions. This SOA volatilization occurred shortly after the evaporation of the majority of particle-bound water, and the two processes were likely related. The results are significant because the work is a product of ambient measurements, where data and analyses are especially lacking. Additionally, the measurements, which were made for an extended period of time with high time resolution, allowed for a robust characterization of the measured components.

REFERENCES

Anderson, C. H.; Dibb, J. E.; Griffin, R. J.; Hagler, G. S. W.; Bergin, M. H., Atmospheric water-soluble organic carbon measurements at Summit, Greenland. *Atmospheric Environment* **2008**, doi:10.1016/j.atmosenv.2008.03.06

Andreae, M. O.; Merlet, P., Emission of trace gases and aerosols from biomass burning. *Global Biogeochemical Cycles* **2001,** *15* (4), 955-966.

Atkinson, R.; Arey, J., Gas-phase tropospheric chemistry of biogenic volatile organic compounds: a review. *Atmospheric Environment* **2003,** *37*, S197-S219.

Atkinson, R., Atmospheric chemistry of VOCs and NOx. *Atmospheric Environment* **2000,** *34* (12-14), 2063-2101.

Atkinson, R., Gas-phase tropospheric chemistry of volatile organic compounds .1. Alkanes and alkenes. *Journal of Physical and Chemical Reference Data* **1997,** *26* (2), 215-290.

Baldocchi, D.; Meyers, T., On using eco-physiological, micrometeorological and biogeochemical theory to evaluate carbon dioxide, water vapor and trace gas fluxes over vegetation: a perspective. *Agricultural and Forest Meteorology* **1998,** *90* (1-2), 1-25.

Baltensperger, U.; Kalberer, M.; Dommen, J.; Paulsen, D.; Alfarra, M. R.; Coe, H.; Fisseha, R.; Gascho, A.; Gysel, M.; Nyeki, S.; Sax, M.; Steinbacher, M.; Prevot, A. S. H.; Sjogren, S.; Weingartner, E.; Zenobi, R., Secondary organic aerosols from anthropogenic and biogenic precursors. *Faraday Discussions* **2005,** *130*, 265-278.

Birch, M. E., Analysis of carbonaceous aerosols: interlaboratory comparison. *Analyst* **1998,** *123* (5), 851-857.

Birch, M. E.; Cary, R. A., Elemental carbon-based method for monitoring occupational exposures to particulate diesel exhaust. *Aerosol Science and Technology* **1996,** *25* (3), 221-241.

Blando, J. D.; Turpin, B. J., Secondary organic aerosol formation in cloud and fog droplets: a literature evaluation of plausibility. *Atmospheric Environment* **2000,** *34* (10), 1623-1632.

Bosilovich, M. G.; On the vertical distribution of local and remote sources of water for precipitation. Meteorology and Atmospheric Physics **2002**, 80, 31-41.

Brubaker, K. L.; Dirmeyer, P. A.; Sudradjat, A.; Levy, B. S.; Bernal, F., A 36-yr climatological description of the evaporative sources of warm-season precipitation in the Mississippi River basin. *Journal of Hydrometeorology* **2001,** 2, (6), 537-557.

Brubaker, K. L.; Entekhabi, D.; Eagleson, P. S., Estimation of continental precipitation recycling. *Journal of Climate* **1993,** 6, (6), 1077-1089.

Carlton, A. G.; Turpin, B. J.; Altieri, K. E.; Seitzinger, S.; Reff, A.; Lim, H. J.; Ervens, B., Atmospheric oxalic acid and SOA production from glyoxal: Results of aqueous photooxidation experiments. *Atmospheric Environment* **2007,** *41* (35), 7588-7602.

Chameides, W. L.; Fehsenfeld, F.; Rodgers, M. O.; Cardelino, C.; Martinez, J.; Parrish, D.; Lonneman, W.; Lawson, D. R.; Rasmussen, R. A.; Zimmerman, P.; Greenberg, J.; Middleton, P.; Wang, T., Ozone precursor relationships in the ambient atmosphere. *Journal of Geophysical Research-Atmospheres* **1992,** *97* (D5), 6037-6055.

Chameides, W. L.; Davis, D. D., Aqueous-phase source of formic acid in clouds. *Nature* **1983,** *304* (5925), 427-429.

Chang, E. I.; Pankow, J. F., Organic particulate matter formation at varying relative humidity using surrogate secondary and primary organic compounds with activity corrections in the condensed phase obtained using a method based on the Wilson equation. *Atmospheric Chemistry and Physics Discussions* **2008**, 8, 995-1039.

Charlson, R. J.; Schwartz, S. E.; Hales, J. M.; Cess, R. D.; Coakley, J. A.; Hansen, J. E.; Hofmann, D. J., Climate forcing by anthropogenic aerosols. *Science* **1992,** *255* (5043), 423-430.

Chebbi, A.; Carlier, P., Carboxylic acids in the troposphere, occurrence, sources, and sinks: A review. *Atmospheric Environment* **1996,** 30, (24), 4233-4249.

Claeys, M.; Graham, B.; Vas, G.; Wang, W.; Vermeylen, R.; Pashynska, V.; Cafmeyer, J.; Guyon, P.; Andreae, M. O.; Artaxo, P.; Maenhaut, W., Formation of secondary organic aerosols through photooxidation of isoprene. *Science* **2004,** *303* (5661), 1173-1176.

Cocker, D. R.; Clegg, S. L.; Flagan, R. C.; Seinfeld, J. H., The effect of water on gas-particle partitioning of secondary organic aerosol. Part I: alpha-pinene/ozone system. *Atmospheric Environment* **2001a,** 35, (35), 6049-6072.

Cocker, D. R.; Mader, B. T.; Kalberer, M.; Flagan, R. C.; Seinfeld, J. H., The effect of water on gas-particle partitioning of secondary organic aerosol: II. m-xylene and 1,3,5-trimethylbenzene photooxidation systems. *Atmospheric Environment* **2001b,** *35* (35), 6073-6085.

Cofer, W. R.; Edahl, R. A., A new technique for collection, concentration and determination of gaseous tropospheric formaldehyde. *Atmospheric Environment* **1986,** *20* (5), 979-984.

Crounse, J. D.; McKinney, K. A.; Kwan, A. J.; Wennberg, P. O., Measurement of gas-phase hydroperoxides by chemical ionization mass spectrometry. *Analytical Chemistry* **2006,** *78* (19), 6726-6732.

Decesari, S.; Facchini, M. C.; Matta, E.; Lettini, F.; Mircea, M.; Fuzzi, S.; Tagliavini, E.; Putaud, J. P., Chemical features and seasonal variation of fine aerosol water-soluble organic compounds in the Po Valley, Italy. *Atmospheric Environment* **2001,** 35, (21), 3691-3699.

de Gouw, J. A.; Middlebrook, A. M.; Warneke, C.; Goldan, P. D.; Kuster, W. C.; Roberts, J. M.; Fehsenfeld, F. C.; Worsnop, D. R.; Canagaratna, M. R.; Pszenny, A. A. P.; Keene, W. C.; Marchewka, M.; Bertman, S. B.; Bates, T. S., Budget of organic carbon in a polluted atmosphere: Results from the New England Air Quality Study in 2002. *Journal of Geophysical Research-Atmospheres* **2005,** *110* (D16).

Dockery, D. W.; Cunningham, J.; Damokosh, A. I.; Neas, L. M.; Spengler, J. D.; Koutrakis, P.; Ware, J. H.; Raizenne, M.; Speizer, F. E., Health effects of acid aerosols on North American children: Respiratory symptoms. *Environmental Health Perspectives* **1996,** *104* (5), 500-505.

Dockery, D. W.; Pope, C. A.; Xu, X. P.; Spengler, J. D.; Ware, J. H.; Fay, M. E.; Ferris, B. G.; Speizer, F. E., An association between air pollution and mortality in 6 United States cities. *New England Journal of Medicine* **1993,** *329* (24), 1753-1759.

Dommen, J.; Metzger, A.; Duplissy, J.; Kalberer, M.; Alfarra, M. R.; Gascho, A.; Weingartner, E.; Prevot, A. S. H.; Verheggen, B.; Baltensperger, U., Laboratory observation of oligomers in the aerosol from isoprene/NOx photooxidation. *Geophysical Research Letters* **2006,** *33* (13).

Eatough, D. J.; Wadsworth, A.; Eatough, D. A.; Crawford, J. W.; Hansen, L. D.; Lewis, E. A., A multiple-system, multichannel diffusion denuder sampler for the determination of fine-particulate organic material in the atmosphere. *Atmospheric Environment Part a-General Topics* **1993,** 27, (8), 1213-1219.

Edney, E. O.; Driscoll, D. J.; Speer, R. E.; Weathers, W. S.; Kleindienst, T. E.; Li, W.; Smith, D. F.; Fr, Impact of aerosol liquid water on secondary organic aerosol yields of irradiated toluene/propylene/NOx/(NH4)(2) SO4/air mixtures. *Atmospheric Environment* **2000,** 34, (23), 3907-3919.

Eisele, F. L.; Mount, G. H.; Tanner, D.; Jefferson, A.; Shetter, R.; Harder, J. W.; Williams, E. J., Understanding the production and interconversion of the hydroxyl radical during the Tropospheric OH Photochemistry Experiment. *Journal of Geophysical Research-Atmospheres* **1997,** 102, (D5), 6457-6465.

Environmental Protection Agency, National Emissions Inventory, www.epa.gov/ttn/chief/net/2002inventory.html

Ervens, B.; Carlton, A. G.; Turpin, B. J.; Altieri, K. E.; Kreidenweis, S. M.; Feingold, G., Secondary organic aerosol yields from cloud-processing of isoprene oxidation products. *Geophysical Research Letters* **2008,** 35, (2).

Forstner, H. J. L.; Flagan, R. C.; Seinfeld, J. H.; Xa, Molecular speciation of secondary organic aerosol from photooxidation of the higher alkenes: 1-octene and 1-decene. *Atmospheric Environment* **1997,** *31* (13), 1953-1964.

Fountoukis, C.; Nenes, A., ISORROPIA II: a computationally efficient thermodynamic equilibrium model for K+-Ca2+-Mg2+-Nh(4)(+)-Na+-SO42--NO3--Cl--H2O aerosols. *Atmospheric Chemistry and Physics* **2007,** *7* (17), 4639-4659.

Fountoukis, C., Nenes, A., Sullivan, A., Weber, R., VanReken, T., Fischer, M., Matías, E., Moya, M., Farmer, D., Cohen, R. C., Thermodynamic characterization of Mexico City aerosol during MILAGRO 2006, *Atmospheric Chemistry and Physics Discussions* **2007**, 7, 9203-9233.

Galloway, J. N.; Likens, G. E.; Keene, W. C.; Miller, J. M., The composition of precipitation in remote areas of the world. *Journal of Geophysical Research-Oceans and Atmospheres* **1982,** *87* (NC11), 8771-8786.

Gao, S.; Surratt, J. D.; Knipping, E. M.; Edgerton, E. S.; Shahgholi, M.; Seinfeld, J. H., Characterization of polar organic components in fine aerosols in the southeastern United States: Identity, origin, and evolution. *Journal of Geophysical Research-Atmospheres* **2006,** *111* (D14).

Gao, S.; Ng, N. L.; Keywood, M.; Varutbangkul, V.; Bahreini, R.; Nenes, A.; He, J. W.; Yoo, K. Y.; Beauchamp, J. L.; Hodyss, R. P.; Flagan, R. C.; Seinfeld, J. H., Particle phase acidity and oligomer formation in secondary organic aerosol. *Environmental Science & Technology* **2004,** *38* (24), 6582-6589.

Gauderman, W. J.; McConnell, R.; Gilliland, F.; London, S.; Thomas, D.; Avol, E.; Vora, H.; Berhane, K.; Rappaport, E. B.; Lurmann, F.; Margolis, H. G.; Peters, J., Association between air pollution and lung function growth in southern California children. *American Journal of Respiratory and Critical Care Medicine* **2000,** *162* (4), 1383-1390.

Georgia Forestry Commission, http://www.gfc.state.ga.us/

Goldstein, A. H.; Galbally, I. E., Known and unexplored organic constituents in the earth's atmosphere. *Environmental Science & Technology* **2007,** *41* (5), 1514-1521.

Gong, H. M.; Matsunaga, A.; Ziemann, P. J., Products and mechanism of secondary organic aerosol formation from reactions of linear alkenes with NO3 radicals. *Journal of Physical Chemistry A* **2005,** *109* (19), 4312-4324.

Graber, E. R.; Rudich, Y., Atmospheric HULIS: How humic-like are they? A comprehensive and critical review. *Atmospheric Chemistry and Physics* **2006,** *6*, 729-753.

Gray, H. A.; Cass, G. R.; Huntzicker, J. J.; Heyerdahl, E. K.; Rau, J. A., Characteristics of atmospheric organic and elemental carbon particle concentrations in Los Angeles. *Environmental Science & Technology* **1986,** 20, (6), 580-589.

Grieshop, A. P.; Donahue, N. M.; Robinson, A. L., Is the gas-particle partitioning in alpha-pinene secondary organic aerosol reversible? *Geophysical Research Letters* **2007,** *34* (14), 5.

Griffin, R. J.; Cocker, D. R.; Flagan, R. C.; Seinfeld, J. H., Organic aerosol formation from the oxidation of biogenic hydrocarbons. *Journal of Geophysical Research-Atmospheres* **1999,** 104, (D3), 3555-3567.

Guenther, A.; Hewitt, C. N.; Erickson, D.; Fall, R.; Geron, C.; Graedel, T.; Harley, P.; Klinger, L.; Lerdau, M.; McKay, W. A.; Pierce, T.; Scholes, B.; Steinbrecher, R.; Tallamraju, R.; Taylor, J.; Zimmerman, P., A global model of natural volatile organic compound emissions. *Journal of Geophysical Research-Atmospheres* **1995,** *100* (D5), 8873-8892.

Guenther, A.; Zimmerman, P.; Wildermuth, M., Natural volatile organic compound emission rate estimates for United States woodland landscapes. *Atmospheric Environment* **1994,** 28, (6), 1197-1210.

Guenther, A. B.; Zimmerman, P. R.; Harley, P. C.; Monson, R. K.; Fall, R., Isoprene and monoterpene emission rate variability – model evaluations and sensitivity analysis. *Journal of Geophysical Research-Atmospheres* **1993,** 98, (D7), 12609-12617.

Hakola, H.; Laurila, T.; Rinne, J.; Puhto, K., The ambient concentrations of biogenic hydrocarbons at a northern European, boreal site. *Atmospheric Environment* **2000,** 34, (29-30), 4971-4982.

Hallquist, M.; Wangberg, I.; Ljungstrom, E.; Barnes, I.; Becker, K. H., Aerosol and product yields from NO3 radical-initiated oxidation of selected monoterpenes. *Environmental Science & Technology* **1999,** 33, (4), 553-559.

Hansen, J.; Sato, M.; Ruedy, R.; Lacis, A.; Oinas, V., Global warming in the twenty-first century: An alternative scenario. *Proceedings of the National Academy of Sciences of the United States of America* **2000,** *97* (18), 9875-9880.

Haywood, J.; Boucher, O., Estimates of the direct and indirect radiative forcing due to tropospheric aerosols: A review. *Reviews of Geophysics* **2000,** *38* (4), 513-543.

Hennigan, C. J.; Sullivan, A. P.; Fountoukis, C. I.; Nenes, A.; Peltier, R. E.; Hecobian, A.; Vargas, O.; Case Hanks, A. T.; Huey, L. G.; Lefer, B. L.; Russell, A. G.; Weber, R. J., On the volatility and production mechanisms of newly formed nitrate and water soluble organic aerosol in Mexico City. *Atmospheric Chemistry and Physics* **2008**, 8, 3761-3768.

Hennigan, C. J.; Sandholm, S.; Kim, S.; Stickel, R. E.; Huey, L. G.; Weber, R. J., Influence of Ohio River valley emissions on fine particle sulfate measured from aircraft over large regions of the eastern United States and Canada during INTEX-NA. *Journal of Geophysical Research-Atmospheres* **2006,** *111* (D24).

Henze, D. K.; Seinfeld, J. H., Global secondary organic aerosol from isoprene oxidation. *Geophysical Research Letters* **2006,** *33* (9).

Herndon, S. C., et al., Correlation of secondary organic aerosol with odd oxygen in Mexico City, *Geophysical Research Letters* **2008**, 35, L15804, doi:10.1029/2008GL034058.

Hildemann, L. M.; Klinedinst, D. B.; Klouda, G. A.; Currie, L. A.; Cass, G. R., Sources of urban contemporary carbon aerosol. *Environmental Science & Technology* **1994,** *28* (9), 1565-1576.

Hoffmann, T.; Odum, J. R.; Bowman, F.; Collins, D.; Klockow, D.; Flagan, R. C.; Seinfeld, J. H.; Xb, Formation of organic aerosols from the oxidation of biogenic hydrocarbons. *Journal of Atmospheric Chemistry* **1997,** 26, (2), 189-222.

Iinuma, Y.; Boge, O.; Gnauk, T.; Herrmann, H., Aerosol-chamber study of the alpha-pinene/O-3 reaction: influence of particle acidity on aerosol yields and products. *Atmospheric Environment* **2004,** *38* (5), 761-773.

IPCC, 2007: Summary for Policymakers. In: *Climate Change 2007: The Physical Science Basis. Contribution of Working Group I to the Fourth Assessment Report of the Intergovernmental Panel on Climate Change* [Solomon, S., D. Qin, M. Manning, Z. Chen, M. Marquis, K.B. Averyt, M.Tignor and H.L. Miller (eds.)]. Cambridge University Press, Cambridge, New York, NY, USA.

Jang, M. S.; Kamens, R. M., Atmospheric secondary aerosol formation by heterogeneous reactions of aldehydes in the presence of a sulfuric acid aerosol catalyst. *Environmental Science & Technology* **2001,** *35* (24), 4758-4766.

Janson, R.; Rosman, K.; Karlsson, A.; Hansson, H. C., Biogenic emissions and gaseous precursors to forest aerosols. *Tellus Series B-Chemical and Physical Meteorology* **2001,** 53, (4), 423-440.

Kalberer, M.; Sax, M.; Samburova, V., Molecular size evolution of oligomers in organic aerosols collected in urban atmospheres and generated in a smog chamber. *Environmental Science & Technology* **2006,** *40* (19), 5917-5922.

Kalberer, M.; Paulsen, D.; Sax, M.; Steinbacher, M.; Dommen, J.; Prevot, A. S. H.; Fisseha, R.; Weingartner, E.; Frankevich, V.; Zenobi, R.; Baltensperger, U., Identification of polymers as major components of atmospheric organic aerosols. *Science* **2004,** *303* (5664), 1659-1662.

Kanakidou, M.; Seinfeld, J. H.; Pandis, S. N.; Barnes, I.; Dentener, F. J.; Facchini, M. C.; Van Dingenen, R.; Ervens, B.; Nenes, A.; Nielsen, C. J.; Swietlicki, E.; Putaud, J. P.; Balkanski, Y.; Fuzzi, S.; Horth, J.; Moortgat, G. K.; Winterhalter, R.; Myhre, C. E. L.; Tsigaridis, K.; Vignati, E.; Stephanou, E. G.; Wilson, J., Organic aerosol and global climate modelling: a review. *Atmospheric Chemistry and Physics* **2005,** *5*, 1053-1123.

Khwaja, H. A., Atmospheric concentrations of carboxylic acids and related compounds at a semiurban site. *Atmospheric Environment* **1995,** 29, (1), 127-139.

Kleinman, L. I.; Springston, S. R.; Daum, P. H.; Lee, Y. N.; Nunnermacker, L. J.; Senum, G. I.; Wang, J.; Weinstein-Lloyd, J.; Alexander, M. L.; Hubbe, J.; Ortega, J.; Canagaratna, M. R.; Jayne, J., The time evolution of aerosol composition over the Mexico City plateau. *Atmospheric Chemistry and Physics* **2008,** *8* (6), 1559-1575.

Kondo, Y.; Miyazaki, Y.; Takegawa, N.; Miyakawa, T.; Weber, R. J.; Jimenez, J. L.; Zhang, Q.; Worsnop, D. R., Oxygenated and water-soluble organic aerosols in Tokyo. *Journal of Geophysical Research-Atmospheres* **2007,** 112, (D1), 11.

Kroll, J. H.; Seinfeld, J. H., Chemistry of secondary organic aerosol: Formation and evolution of low-volatility organics in the atmosphere. *Atmospheric Environment* **2008,** *42* (16), 3593-3624.

Kroll, J. H.; Chan, A. W. H.; Ng, N. L.; Flagan, R. C.; Seinfeld, J. H., Reactions of semivolatile organics and their effects on secondary organic aerosol formation. *Environmental Science & Technology* **2007,** *41* (10), 3545-3550.

Kroll, J. H.; Ng, N. L.; Murphy, S. M.; Flagan, R. C.; Seinfeld, J. H., Secondary organic aerosol formation from isoprene photooxidation. *Environmental Science & Technology* **2006,** *40* (6), 1869-1877.

Kroll, J. H.; Ng, N. L.; Murphy, S. M.; Flagan, R. C.; Seinfeld, J. H., Secondary organic aerosol formation from isoprene photooxidation under high-NOx conditions. *Geophysical Research Letters* **2005,** *32* (18).

Kuchment, L. S.; Demidov, V. N.; Startseva, Z. P., Coupled modeling of the hydrological and carbon cycles in the soil-vegetation-atmosphere system. *Journal of Hydrology* **2006,** 323, (1-4), 4-21.

Larsen, B. R.; Di Bella, D.; Glasius, M.; Winterhalter, R.; Jensen, N. R.; Hjorth, J., Gas-phase OH oxidation of monoterpenes: Gaseous and particulate products. *Journal of Atmospheric Chemistry* **2001,** 38, (3), 231-276.

Lee, S.; Kim, H. K.; Yan, B.; Cobb, C. E.; Hennigan, C.; Nichols, S.; Chamber, M.; Edgerton, E. S.; Jansen, J. J.; Hu, Y. T.; Zheng, M.; Weber, R. J.; Russell, A. G., Diagnosis of aged prescribed burning plumes impacting an urban area. *Environmental Science & Technology* **2008,** 42, (5), 1438-1444.

Lee, S.; Baumann, K.; Schauer, J. J.; Sheesley, R. J.; Naeher, L. P.; Meinardi, S.; Blake, D. R.; Edgerton, E. S.; Russell, A. G.; Clements, M., Gaseous and particulate emissions from prescribed burning in Georgia. *Environmental Science & Technology* **2005,** *39* (23), 9049-9056.

Lee, S. D.; Jang, M. S.; Kamens, R. M., SOA formation from the photooxidation of alpha-pinene in the presence of freshly emitted diesel soot exhaust. *Atmospheric Environment* **2004,** *38* (16), 2597-2605.

Liang, C. K.; Pankow, J. F., Gas/particle partitioning of organic compounds to environmental tobacco smoke: Partition coefficient measurements by desorption and comparison to urban particulate material. *Environmental Science & Technology* **1996,** *30* (9), 2800-2805.

Lim, H. J.; Carlton, A. G.; Turpin, B. J., Isoprene forms secondary organic aerosol through cloud processing: Model simulations. *Environmental Science & Technology* **2005,** *39* (12), 4441-4446.

Lim, Y. B.; Ziemann, P. J., Products and mechanism of secondary organic aerosol formation from reactions of n-alkanes with OH radicals in the presence of NOx. *Environmental Science & Technology* **2005,** *39* (23), 9229-9236.

Limbeck, A.; Kulmala, M.; Puxbaum, H., Secondary organic aerosol formation in the atmosphere via heterogeneous reaction of gaseous isoprene on acidic particles. *Geophysical Research Letters* **2003,** *30* (19), 4.

Liousse, C.; Penner, J. E.; Chuang, C.; Walton, J. J.; Eddleman, H.; Cachier, H., A global three-dimensional model study of carbonaceous aerosols. *Journal of Geophysical Research-Atmospheres* **1996,** *101* (D14), 19411-19432.

Lipsky, E. M.; Robinson, A. L., Effects of dilution on fine particle mass and partitioning of semivolatile organics in diesel exhaust and wood smoke. *Environmental Science & Technology* **2006,** *40* (1), 155-162.

Loeffler, K. W.; Koehler, C. A.; Paul, N. M.; De Haan, D. O., Oligomer formation in evaporating aqueous glyoxal and methyl glyoxal solutions. *Environmental Science & Technology* **2006,** *40* (20), 6318-6323.

Lohmann, U.; Feichter, J.; Chuang, C. C.; Penner, J. E., Prediction of the number of cloud droplets in the ECHAM GCM. *Journal of Geophysical Research-Atmospheres* **1999,** *104* (D8), 9169-9198.

Loreto, F.; Sharkey, T. D., On the relationship between isoprene emission and photosynthetic metabolites under different environmental conditions. *Planta* **1993,** 189, (3), 420-424.

Ma, Y.; Weber, R. J.; Lee, Y. N.; Orsini, D. A.; Maxwell-Meier, K.; Thornton, D. C.; Bandy, A. R.; Clarke, A. D.; Blake, D. R.; Sachse, G. W.; Fuelberg, H. E.; Kiley, C. M.; Woo, J. H.; Streets, D. G.; Carmichael, G. R., Characteristics and influence of biosmoke on the fine-particle ionic composition measured in Asian outflow during the Transport and Chemical Evolution Over the Pacific (TRACE-P) experiment. *Journal of Geophysical Research-Atmospheres* **2003,** *108* (D21).

Makarieva, A. M.; Gorshkov, V. G., Biotic pump of atmospheric moisture as driver of the hydrological cycle on land. *Hydrology and Earth System Sciences* **2007,** 11, (2), 1013-1033.

Malm, W. C.; Day, D. E., Estimates of aerosol species scattering characteristics as a function of relative humidity. *Atmospheric Environment* **2001,** *35* (16), 2845-2860.

Malm, W. C.; Gebhart, K. A.; Molenar, J.; Cahill, T.; Eldred, R.; Huffman, D., Examining the relationship between atmospheric aerosols and light extinction at Mount Rainier National Park and North Cascades National Park. *Atmospheric Environment* **1994,** *28* (2), 347-360.

Marple, V. A.; Rubow, K. L.; Behm, S. M., A microorifice uniform deposit impactor (MOUDI) – description, calibration, and use. *Aerosol Science and Technology* **1991,** 14, (4), 434-446.

Mayol-Bracero, O. L.; Guyon, P.; Graham, B.; Roberts, G.; Andreae, M. O.; Decesari, S.; Facchini, M. C.; Fuzzi, S.; Artaxo, P., Water-soluble organic compounds in biomass burning aerosols over Amazonia - 2. Apportionment of the chemical composition and importance of the polyacidic fraction. *Journal of Geophysical Research-Atmospheres* **2002,** 107, (D20).

Miyazaki, Y.; Kondo, Y.; Takegawa, N.; Komazaki, Y.; Fukuda, M.; Kawamura, K.; Mochida, M.; Okuzawa, K.; Weber, R. J., Time-resolved measurements of water-soluble organic carbon in Tokyo. *Journal of Geophysical Research-Atmospheres* **2006,** *111* (D23), 12.

Narukawa, M.; Kawamura, K.; Takeuchi, N.; Nakajima, T., Distribution of dicarboxylic acids and carbon isotopic compositions in aerosols from 1997 Indonesian forest fires. *Geophysical Research Letters* **1999,** 26, (20), 3101-3104.

Ng, N. L.; Kroll, J. H.; Chan, A. W. H.; Chhabra, P. S.; Flagan, R. C.; Seinfeld, J. H., Secondary organic aerosol formation from m-xylene, toluene, and benzene. *Atmospheric Chemistry and Physics* **2007,** *7* (14), 3909-3922.

Nenes, A.; Pandis, S. N.; Pilinis, C., ISORROPIA: A new thermodynamic equilibrium model for multiphase multicomponent inorganic aerosols. *Aquatic Geochemistry* **1998,** *4* (1), 123-152.

NIOSH, Elemental Carbon (Diesel Particulate): Method 5040, in *NIOSH Manual of Analytical Methods*, edited by P. M. Eller and M. E. Cassinelli, National Institute for Occupational Safety and Health, Cincinnati, 1996.

Novakov, T.; Corrigan, C. E., Cloud condensation nucleus activity of the organic component of biomass smoke particles. *Geophysical Research Letters* **1996,** 23, (16), 2141-2144.

Odum, J. R.; Jungkamp, T. P. W.; Griffin, R. J.; Flagan, R. C.; Seinfeld, J. H., The atmospheric aerosol-forming potential of whole gasoline vapor. *Science* **1997,** *276* (5309), 96-99.

Odum, J. R.; Hoffmann, T.; Bowman, F.; Collins, D.; Flagan, R. C.; Seinfeld, J. H.; Va, Gas/particle partitioning and secondary organic aerosol yields. *Environmental Science & Technology* **1996,** *30* (8), 2580-2585.

Orsini, D. A.; Ma, Y. L.; Sullivan, A.; Sierau, B.; Baumann, K.; Weber, R. J., Refinements to the particle-into-liquid sampler (PILS) for ground and airborne measurements of water soluble aerosol composition. *Atmospheric Environment* **2003,** *37* (9-10), 1243-1259.

Pandis, S. N.; Harley, R. A.; Cass, G. R.; Seinfeld, J. H., Secondary organic aerosol formation and transport. *Atmospheric Environment Part a-General Topics* **1992,** *26* (13), 2269-2282.

Pandis, S. N.; Paulson, S. E.; Seinfeld, J. H.; Flagan, R. C., Aerosol formation in the photooxidation of isoprene and beta-pinene. *Atmospheric Environment Part a-General Topics* **1991,** *25* (5-6), 997-1008.

Pankow, J. F., An absorption model of gas-particle partitioning of organic compounds in the atmosphere. *Atmospheric Environment* **1994a,** *28* (2), 185-188.

Pankow, J. F., An absorption model of the gas aerosol partitioning involved in the formation of secondary organic aerosol. *Atmospheric Environment* **1994b,** *28* (2), 189-193.

Pankow, J. F.; Bidleman, T. F., Effects of temperature, TSP and percent nonexchangeable material in determining the gas particle partitioning of organic compounds. *Atmospheric Environment Part a-General Topics* **1991,** *25* (10), 2241-2249.

Peltier, R. E.; Hecobian, A. H.; Weber, R. J.; Stohl, A.; Atlas, E. L.; Riemer, D. D.; Blake, D. R.; Apel, E.; Campos, T.; Karl, T., Investigating the sources and atmospheric processing of fine particles from Asia and the Northwestern United States measured during INTEX B. *Atmospheric Chemistry and Physics* **2008,** *8* (6), 1835-1853.

Peltier, R. E.; Sullivan, A. P.; Weber, R. J.; Wollny, A. G.; Holloway, J. S.; Brock, C. A.; de Gouw, J. A.; Atlas, E. L., No evidence for acid-catalyzed secondary organic aerosol formation in power plant plumes over metropolitan Atlanta, Georgia. *Geophysical Research Letters* **2007a,** *34* (6).

Peltier, R. E.; Weber, R. J.; Sullivan, A. P., Investigating a liquid-based method for online organic carbon detection in atmospheric particles. *Aerosol Science and Technology* **2007b,** *41* (12), 1117-1127.

Pope, C. A., Respiratory hospital admissions associated with PM10 pollution in Utah, Salt Lake, and Cache Valleys. *Archives of Environmental Health* **1991,** *46* (2), 90-97.

Presto, A. A.; Hartz, K. E. H.; Donahue, N. M., Secondary organic aerosol production from terpene ozonolysis. 2. Effect of NOx concentration. *Environmental Science & Technology* **2005,** *39* (18), 7046-7054.

Pun, B. K.; Seigneur, C., Investigative modeling of new pathways for secondary organic aerosol formation. *Atmospheric Chemistry and Physics* **2007,** 7, (9), 2199-2216.

Robinson, A. L.; Donahue, N. M.; Shrivastava, M. K.; Weitkamp, E. A.; Sage, A. M.; Grieshop, A. P.; Lane, T. E.; Pierce, J. R.; Pandis, S. N., Rethinking organic aerosols: Semivolatile emissions and photochemical aging. *Science* **2007,** *315* (5816), 1259-1262.

Rudich, Y.; Donahue, N. M.; Mentel, T. F., Aging of organic aerosol: Bridging the gap between laboratory and field studies. *Annual Review of Physical Chemistry* **2007,** *58*, 321-352.

Ryerson, T. B.; Williams, E. J.; Fehsenfeld, F. C., An efficient photolysis system for fast-response NO2 measurements. *Journal of Geophysical Research-Atmospheres* **2000,** *105* (D21), 26447-26461.

Salcedo, D.; Onasch, T. B.; Dzepina, K.; Canagaratna, M. R.; Zhang, Q.; Huffman, J. A.; DeCarlo, P. F.; Jayne, J. T.; Mortimer, P.; Worsnop, D. R.; Kolb, C. E.; Johnson, K. S.; Zuberi, B.; Marr, L. C.; Volkamer, R.; Molina, L. T.; Molina, M. J.; Cardenas, B.; Bernabe, R. M.; Marquez, C.; Gaffney, J. S.; Marley, N. A.; Laskin, A.; Shutthanandan, V.; Xie, Y.; Brune, W.; Lesher, R.; Shirley, T.; Jimenez, J. L., Characterization of ambient aerosols in Mexico City during the MCMA-2003 campaign with Aerosol Mass Spectrometry: results from the CENICA Supersite. *Atmospheric Chemistry and Physics* **2006,** *6*, 925-946.

Samet, J. M.; Dominici, F.; Curriero, F. C.; Coursac, I.; Zeger, S. L., Fine particulate air pollution and mortality in 20 US Cities, 1987-1994. *New England Journal of Medicine* **2000,** *343* (24), 1742-1749.

Sander, S. P., Friedl, R. R., Golden, D. M., Kurylo, M. J., Moortgat, G. K., Keller-Rudek, H., Wine, P. H., Ravishankara, A. R., Kolb, C. E., Molina, M. J., Finlayson-Pitts, B. J., Huie, R. E., Orkin, V. L., Chemical kinetics and photochemical data for use in atmospheric studies, Evaluation Number 15, JPL Publication 06-2, Jet Propulsion Laboratory, Pasadena, **2006**.

Sander, R., Compilation of Henry's Law Constants for Inorganic and Organic Species of Potential Importance in Environmental Chemistry, Version 3, 1999, http://www.mpch-mainz.mpg.de/~sander/res/henry.html

Saxena, P.; Hildemann, L. M.; Un, Water-soluble organics in atmospheric particles: A critical review of the literature and application of thermodynamics to identify candidate compounds. *Journal of Atmospheric Chemistry* **1996,** 24, (1), 57-109.

Seinfeld, J. H.; Pankow, J. F., Organic atmospheric particulate material. *Annual Review of Physical Chemistry* **2003,** *54*, 121-140.

Seinfeld, J. H.; Erdakos, G. B.; Asher, W. E.; Pankow, J. F., Modeling the formation of secondary organic aerosol (SOA). 2. The predicted effects of relative humidity on aerosol formation in the alpha-pinene-, beta-pinene-, sabinene-, Delta(3)-Carene-, and cyclohexene-ozone systems. *Environmental Science & Technology* **2001,** 35, (9), 1806-1817.

Seinfeld, J. H. and S. N. Pandis, *Atmospheric Chemistry and Physics, From Air Pollution to Climate Change*, John Wiley & Sons, New York, NY, **1998**.

Shaw, W. J., Pekour, M. S., Coulter, R. L., Martin, T. J., Walters, J. T., The daytime mixing layer observed by radiosonde, profiler, and lidar during MILAGRO, *Atmospheric Chemistry and Physics Discussions* **2007***,* 7, 15025-15065.

Shetter, R. E.; Muller, M., Photolysis frequency measurements using actinic flux spectroradiometry during the PEM-Tropics mission: Instrumentation description and some results. *Journal of Geophysical Research-Atmospheres* **1999,** *104* (D5), 5647-5661.

Simon, V.; Clement, B.; Riba, M. L.; Torres, L., The LANDES experiment – Monoterpenes emitted from the maritime pine. *Journal of Geophysical Research-Atmospheres* **1994,** 99, (D8), 16501-16510.

Sjostedt, S. J.; Huey, L. G.; Tanner, D. J.; Peischl, J.; Chen, G.; Dibb, J. E.; Lefer, B.; Hutterli, M. A.; Beyersdorf, A. J.; Blake, N. J.; Blake, D. R.; Sueper, D.; Ryerson, T.; Burkhart, J.; Stohl, A., Observations of hydroxyl and the sum of peroxy radicals at Summit, Greenland during summer 2003. *Atmospheric Environment* **2007,** *41* (24), 5122-5137.

Sloane, C. S.; Watson, J.; Chow, J.; Pritchett, L.; Richards, L. W., Size-segregated fine particle measurements by chemical species and their impact on visibility impairment in Denver. *Atmospheric Environment Part a-General Topics* **1991,** *25* (5-6), 1013-1024.

Solomon, P.; Baumann, K.; Edgerton, E.; Tanner, R.; Eatough, D.; Modey, W.; Marin, H.; Savoie, D.; Natarajan, S.; Meyer, M. B.; Norris, G., Comparison of integrated samplers for mass and composition during the 1999 Atlanta Supersites project. *Journal of Geophysical Research-Atmospheres* **2003,** *108* (D7).

Song, C.; Na, K. S.; Cocker, D. R., Impact of the hydrocarbon to NOx ratio on secondary organic aerosol formation. *Environmental Science & Technology* **2005,** *39* (9), 3143-3149.

Sorooshian, A.; Ng, N. L.; Chan, A. W. H.; Feingold, G.; Flagan, R. C.; Seinfeld, J. H., Particulate organic acids and overall water-soluble aerosol composition measurements from the 2006 Gulf of Mexico Atmospheric Composition and Climate Study (GoMACCS). *Journal of Geophysical Research-Atmospheres* **2007,** *112* (D13), 16.

Spaulding, R. S.; Talbot, R. W.; Charles, M. J., Optimization of a mist chamber (cofer scrubber) for sampling water-soluble organics in air. *Environmental Science & Technology* **2002,** *36* (8), 1798-1808.

Stone, E. A.; Snyder, D. C.; Sheesley, R. J.; Sullivan, A. P.; Weber, R. J.; Schauer, J. J., Source apportionment of fine organic aerosol in Mexico City during the MILAGRO experiment 2006. *Atmospheric Chemistry and Physics* **2008,** *8* (5), 1249-1259.

Sullivan, A. P.; Peltier, R. E.; Brock, C. A.; de Gouw, J. A.; Holloway, J. S.; Warneke, C.; Wollny, A. G.; Weber, R. J., Airborne measurements of carbonaceous aerosol soluble in water over northeastern United States: Method development and an investigation into water-soluble organic carbon sources. *Journal of Geophysical Research-Atmospheres* **2006,** 111, (D23), 14.

Sullivan, A. P.; Weber, R. J., Chemical characterization of the ambient organic aerosol soluble in water: 1. Isolation of hydrophobic and hydrophilic fractions with a XAD-8 resin. *Journal of Geophysical Research-Atmospheres* **2006,** *111* (D5), 9.

Sullivan, A. P.; Weber, R. J.; Clements, A. L.; Turner, J. R.; Bae, M. S.; Schauer, J. J., A method for on-line measurement of water-soluble organic carbon in ambient aerosol particles: Results from an urban site. *Geophysical Research Letters* **2004,** 31, (13), 4.

Surratt, J. D.; Murphy, S. M.; Kroll, J. H.; Ng, N. L.; Hildebrandt, L.; Sorooshian, A.; Szmigielski, R.; Vermeylen, R.; Maenhaut, W.; Claeys, M.; Flagan, R. C.; Seinfeld, J. H., Chemical composition of secondary organic aerosol formed from the photooxidation of isoprene. *Journal of Physical Chemistry A* **2006,** *110* (31), 9665-9690.

Takekawa, H.; Minoura, H.; Yamazaki, S., Temperature dependence of secondary organic aerosol formation by photo-oxidation of hydrocarbons. *Atmospheric Environment* **2003,** *37* (24), 3413-3424.

Tingey, D. T.; Manning, M.; Grothaus, L. C.; Burns, W. F., Influence of light and temperature on monoterpene emission rates from slash pine. *Plant Physiology* **1980,** 65, (5), 797-801.

Tingey, D. T.; Manning, M.; Grothaus, L. C.; Burns, W. F., Influence of light and temperature on isoprene emission rates from live oak. *Physiologia Plantarum* **1979,** 47, (2), 112-118.

Tsigaridis, K.; Lathiere, J.; Kanakidou, M.; Hauglustaine, D. A., Naturally driven variability in the global secondary organic aerosol over a decade. *Atmospheric Chemistry and Physics* **2005,** *5*, 1891-1904.

Tsigaridis, K.; Kanakidou, M., Global modelling of secondary organic aerosol in the troposphere: a sensitivity analysis. *Atmospheric Chemistry and Physics* **2003,** *3*, 1849-1869.

Turpin, B. J.; Huntzicker, J. J., Identification of secondary organic aerosol episodes and quantitation of primary and secondary organic aerosol concentrations during SCAQS. *Atmospheric Environment* **1995,** 29, (23), 3527-3544.

Volkamer, R.; San Martini, F.; Molina, L. T.; Salcedo, D.; Jimenez, J. L.; Molina, M. J., A missing sink for gas-phase glyoxal in Mexico City: Formation of secondary organic aerosol. *Geophysical Research Letters* **2007**, 34, L19807, doi:10.1029/2007GL030752.

Volkamer, R.; Jimenez, J. L.; San Martini, F.; Dzepina, K.; Zhang, Q.; Salcedo, D.; Molina, L. T.; Worsnop, D. R.; Molina, M. J., Secondary organic aerosol formation from anthropogenic air pollution: Rapid and higher than expected. *Geophysical Research Letters* **2006,** *33* (17), 4.

Vutukuru, S.; Griffin, R. J.; Dabdub, D., Simulation and analysis of secondary organic aerosol dynamics in the South Coast Air Basin of California. *Journal of Geophysical Research-Atmospheres* **2006,** *111* (D10).

Wang, S. C.; Paulson, S. E.; Grosjean, D.; Flagan, R. C.; Seinfeld, J. H., Aerosol formation and growth in atmospheric organic NOx systems 1. Outdoor smog chamber studies of C-7 hydrocarbons and C-8 hydrocarbons. *Atmospheric Environment Part a-General Topics* **1992,** *26* (3), 403-420.

Weber, R. J.; Sullivan, A. P.; Peltier, R. E.; Russell, A.; Yan, B.; Zheng, M.; de Gouw, J.; Warneke, C.; Brock, C.; Holloway, J. S.; Atlas, E. L.; Edgerton, E., A study of secondary organic aerosol formation in the anthropogenic-influenced southeastern United States. *Journal of Geophysical Research-Atmospheres* **2007,** 112, (D13).

Weber, R.; Orsini, D.; Duan, Y.; Baumann, K.; Kiang, C. S.; Chameides, W.; Lee, Y. N.; Brechtel, F.; Klotz, P.; Jongejan, P.; ten Brink, H.; Slanina, J.; Boring, C. B.; Genfa, Z.; Dasgupta, P.; Hering, S.; Stolzenburg, M.; Dutcher, D. D.; Edgerton, E.; Hartsell, B.; Solomon, P.; Tanner, R., Intercomparison of near real time monitors of PM2.5 nitrate and sulfate at the US Environmental Protection Agency Atlanta Supersite. *Journal of Geophysical Research-Atmospheres* **2003a,** *108* (D7).

Weber, R., et al., Short-term temporal variation in PM2.5 mass and chemical composition during the Atlanta supersite experiment, 1999. *Journal of the Air & Waste Management Association* **2003b,** *53* (1), 84-91.

Weber, R. J.; Orsini, D.; Daun, Y.; Lee, Y. N.; Klotz, P. J.; Brechtel, F., A particle-into-liquid collector for rapid measurement of aerosol bulk chemical composition. *Aerosol Science and Technology* **2001,** *35* (3), 718-727.

Weitkamp, E. A.; Sage, A. M.; Pierce, J. R.; Donahue, N. M.; Robinson, A. L., Organic aerosol formation from photochemical oxidation of diesel exhaust in a smog chamber. *Environmental Science & Technology* **2007,** *41* (20), 6969-6975.

Wilson, W. E.; Grover, B. D.; Long, R. W.; Eatough, N. L.; Eatough, D. J., The measurement of fine-particulate semivolatile material in urban aerosols. *Journal of the Air & Waste Management Association* **2006,** *56* (4), 384-397.

Yang, H.; Yu, J. Z.; Ho, S. S. H.; Xu, J. H.; Wu, W. S.; Wan, C. H.; Wang, X. D.; Wang, X. R.; Wang, L. S., The chemical composition of inorganic and carbonaceous materials in PM2.5 in Nanjing, China. *Atmospheric Environment* **2005,** 39, (20), 3735-3749.

Zhang, Q.; Alfarra, M. R.; Worsnop, D. R.; Allan, J. D.; Coe, H.; Canagaratna, M. R.; Jimenez, J. L., Deconvolution and quantification of hydrocarbon-like and oxygenated organic aerosols based on aerosol mass spectrometry. *Environmental Science & Technology* **2005a,** 39, (13), 4938-4952.

Zhang, Q.; Worsnop, D. R.; Canagaratna, M. R.; Jimenez, J. L., Hydrocarbon-like and oxygenated organic aerosols in Pittsburgh: insights into sources and processes of organic aerosols. *Atmospheric Chemistry and Physics* **2005b,** 5, 3289-3311.

Zhang, Q.; Stanier, C. O.; Canagaratna, M. R.; Jayne, J. T.; Worsnop, D. R.; Pandis, S. N.; Jimenez, J. L., Insights into the chemistry of new particle formation and growth events in Pittsburgh based on aerosol mass spectrometry. *Environmental Science & Technology* **2004,** *38* (18), 4797-4809.